NASA CR-175,365

NASA-CR-175365
19840009452

A Reproduced Copy

OF

NASA CR- 175,365

Reproduced for NASA

by the

NASA **Scientific and Technical Information Facility**

LIBRARY COPY

JUL 17 1984

LANGLEY RESEARCH CENTER
LIBRARY, NASA
HAMPTON, VIRGINIA

FFNo 672 Aug 65

SEMI-ANNUAL STATUS REPORT

(Period Covered: August 1, 1983 - January 31, 1984)

JAN 1984
RECEIVED
NASA STI FACILITY
ACCESS DEPT.

A COMPREHENSIVE MODEL TO DETERMINE THE EFFECTS OF TEMPERATURE AND SPECIES FLUCTUATIONS ON REACTION RATES IN TURBULENT REACTING FLOWS*

F. Magnotti, G. Diskin, J. Matulaitis, and W. Chinitz**

* Work supported under Grant No. NAG1 - 18,
National Aeronautics and Space Administration,
Langley Research Center, High-Speed Aerodynamics Division,
Hypersonic Propulsion Branch
Hampton, VA 23665

** Principal Investigator

FEB 1984
RECEIVED
NASA STI FACILITY
ACCESS DEPT.

(NASA-CR-175365) A COMPREHENSIVE MODEL TO DETERMINE THE EFFECTS OF TEMPERATURE AND SPECIES FLUCTUATIONS ON REACTION RATES IN TURBULENT REACTION FLOWS Semiannual Status Report, 1 Aug. 1983 - 31 Jan. 1984 (Cooper

N84-17520

Unclas
G3/34 00574

N84-17520 #

I. INTRODUCTION

A number of new tasks undertaken during the semi-annual reporting period are discussed (Sections 2 and 3). A final report on the H_2-kinetics modeling work is contained herein as Section 4. Our continuing work dealing with turbulent reaction rate modeling is in Section 5. An addition to these items, two publications are in preparation:

1. Chinitz, W. and Evans, J. S., "A Model for Reaction Rates in Turbulent Reacting Flows", NASA Tech. Memorandum.

2. Chinitz, W., "Models for Calculating Reaction Rates in Turbulent Reacting Flows", paper to be presented at the 1984 JANNAF Propulsion Meeting, Feb. 7-9, 1984, New Orleans, LA.

2. ALTERNATIVE SILANE COMBUSTION MECHANISM

The use of silane (SiH_4) as an effective ignitor and flame stabilizing pilot fuel has been well documented (e.g. ref. 1). In order to better understand its behavior at the conditions encountered in the combustor of a SCRAMJET engine, and to be able to predict its behavior at conditions which cannot be readily achieved in the laboratory, a reliable chemical kinetic mechanism must be developed. The first attempt at the formulation of such a mechanism for SiH_4 is in ref. 1. It was shown subsequently (ref. 2), however, that the mechanism in ref. 1 yields predicted ignition delay times which are about five times longer than those experimentally obtained in a shock tube.

As a consequence, an alternative mechanism was developed in ref. 3 so as to obtain agreement with the experimental shock tube data. The mechanism in ref. 3 postulates that silane pyrolysis

$$SiH_4 \rightarrow SiH_2 + H_2 \qquad \text{(i)}$$

along with its direct oxidation

$$SiH_4 + O_2 \rightarrow SiH_3 + HO_2 \qquad \text{(ii)}$$

are the initiating reactions. An examination of the magnitudes of the rate constants recommended in ref. 3 indicates that reaction (i), along with the extremely rapid subsequent oxidation of SiH_2

$$SiH_2 + O_2 \rightarrow HSiO + OH, \qquad \text{(iii)}$$

are principally responsible for the disappearance of silane at SCRAMJET engine operation conditions.

An alternative mechanism has been developed wherein the reaction

$$SiH_4 + O_2 \rightarrow SiH_2O + H_2O \qquad \text{(iv)}$$

along with the hydrogen atom abstraction reaction

$$SiH_4 + M \rightarrow SiH_3 + H \qquad \text{(v)}$$

are the principal initiating reactions. Reaction (iv) is likely to be semi-global in nature, similar to the semi-global reactions in the methane mechanism in ref. 4. The complete silane oxidation mechanism postulated is in Table I. Complete details of its formulation will be presented in a forthcoming NASA Contractors Report. In this status report, we focus upon the results obtained using this mechanism.

A comparison between the shock tube data and the theoretical ignition delay times calculated using the proposed mechanism is in figs. 1 and 2. Generally, excellent agreement is obtained over the range of experimental conditions. A comparison between this mechanism and that in ref. 3 obtained for a number of SiH_4/H_2 mixtures at one atmosphere, equivalence ratios of 1.0 and 0.5, in the temperature range from 800K to 1250K, is in figs. 3 and 4. For most of the conditions examined, the proposed mechanism predicts substantially lower ignition delays. Only for the 2% SiH_4 mixture at initial temperatures exceeding about 930K does the mechanism in ref. 3 predict shorter ignition delays.

The predicted effect of equivalence ratio on ignition delay time is in fig. 5. As can be seen, in the range $0.5 \leq \phi \leq 10.0$, increasing ϕ results in reduced ignition delays. This may partially explain the empirically-observed pyroforicity of silane at one atmosphere, room temperature conditions since, under the circumstances in which this phenomenon has been observed, highly fuel-rich regions are certain to exist. The effect of decreasing the pressure to 0.5 atm is shown in fig. 6. As would be anticipated from prior chemical kinetics studies, decreasing the pressure results in increased delay times for SiH_4/H_2 mixtures down to 2% silane.

Perfectly stirred reactor calculations were carried out to assess the flame-stabilizing behavior of silane. In fig. 7, blowout limit correlations are shown for pure silane at 1.0 atm, 600K initial temperature using the proposed mechanism and that in ref. 3. As can be seen, the mechanism in Table I predicts a reduced stable flame region when compared with that in ref. 3. Both, however, exhibit the same general shape, with $(\dot{m}/V)max$ occurring at about $\phi = 2.5$, rather than at the anticipated value of $\phi = 1.0$. The reasons for this behavior, and whether or not it is in fact real, remain a matter of speculation. Experimental PSR studies would be required to help settle these matters.

Computed blowout limit correlations using the mechanism in Table I are shown in figs. 8-10 for 1.0 atm, T_o = 300K, 600K and 1200K, respectively, for 100% SiH_4, 20% SiH_4/80% H_2 and 100% H_2. The figures make clear that the principal benefits to be derived from using silane for purposes of flame stabilization are derived using larger silane concentrations in regions of high equivalence ratio. In low ϕ regions, pure hydrogen produces a larger stable flame region. Also of interest is the unusual "reversal" behavior at T_o = 1200K in which, for the 20% SiH_4/80% H_2 mixture, for example, above $\phi = 1.0$, increasing equivalence ratio permits higher values of $\dot{m}/V$. Similar behavior is observed for 100%

SiH_4 down to $\phi = 0.5$. The reality of this behavior must also await experimental PSR results.

The results in figs 8-10 are shown once again in figs. 11-13 as ϕ versus residence time. The effect of pressure on blowout limit behavior is shown in figs. 14 and 15. As expected, reducing the pressure tends to reduce the stable flame region.

Consideration of computer run times and storage limitations require the development of a global silane oxidation model. Such a model has been formulated for the mechanism in Table I. The model consists of the three reactions:

$$2\ SiH_4 + O_2 = 2\ HSiO + 3H_2 \qquad \text{(vi)}$$

$$2\ HSiO + O_2 = 2\ SiO_2 + H_2 \qquad \text{(vii)}$$

$$2\ H_2 + O_2 = 2\ H_2O \qquad \text{(viii)}$$

with the rate coefficients given by

$$k_{f,vi} = \frac{\left(0.95234\ \phi + \frac{4.4762}{\phi} - 4.4286\right)}{p^{5.644}} \cdot 10^{15}\ T^{2.30} \cdot e^{-19350/RT}$$

$$k_{f,vii} = 5.0 \times 10^{10}\ T^{2.80}\ e^{-14000/RT}$$

$$k_{f,viii} = \frac{\left(2.3829\phi + \frac{76.190}{\phi} - 3.5714\right)}{p^{1.415}} \cdot 10^{6} \left(\frac{X}{20}\right)^{0.574} \cdot T^{3.29}\ e^{-16500/RT}$$

The minimum ranges of validity of the above model are

$0.5 \leq p \leq 1.0$ atm

$0.5 \leq \phi \leq 4.0$

$2\%\ SiH_4 \leq X \leq 20\%\ SiH_4$

$800\ K \leq T_o \leq 1250K$

$800K \leq T \leq 3000K$

Typical results obtained using the global model are compared with results using the compelte mechanism in Table I in figs. 16-20. Generally, the global model tends to replicate the ignition phase extremely well. On the other hand, the final approach to equilibrium is either too rapid (figs 16 - 18,20) or too slow (fig. 19). However, previous work on global modeling (eg, ref. 5) clearly indicates the primary importance of proper replication of ignition behavior, in which case the model proposed above should yield good-to-excellent results when used in computer codes which model complex flows.

The forthcoming Contractors Report, mentioned earlier, will present additional results obtained using the mechanism in Table I, including estimates of reaction times, as well as ignition delay times.

REFERENCES FOR SECTION 2

1. Beach, H. L., Jr., Mackley, E. A., Rogers, R. C. and Chinitz, W., "Use of Silane in Scramjet Research", paper presented at the 17th JANNAF Combustion Meeting, Hampton, VA, Sept. 22-26, 1980.
2. McLain, A. G., Jackimowski, C. J. and Rogers, R.C., "Ignition of $SiH_4 - H_2 - O_2 - N_2$ Behind Reflected Shock Waves", NASA TP-2114, Feb. 1983.
3. Jackimowski, C. J. and McLain, A. G., "A Chemical Kinetic Mechanism for the Ignition of Silane/Hydrogen Mixtures", NASA TP-2129, Feb. 1983.
4. Edelman, R. B. and Harsha, P. T., "Laminar and Turbulent Gas Dynamics in Combustors - Current Status", Prog. Energy Combust. Sci., vol. 4, pp. 1-62,
5, Rogers, R. C. and Chinitz, W., "Using a Global Hydrogen-Air Combustion Model in Turbulent Reacting Flow Calculations", AIAA Journal, vol. 21, pp. 586-592, April 1983.

TABLE I

SILANE OXIDATION MECHANISM

M		SIH4	=	SIH3	+	H	2.00E+17	0.	59000.
SIH4	+	SIH3	=	2 SIH3	+	H	7.76E+11	0.	6980.
SIH4	+	02	=	SIH20	+	H20	2.00E+14	0.	19500.
SIH4	+	H	=	SIH3	+	H2	2.00E+13	0.	2650.0
SIH4	+	0	=	SIH3	+	OH	4.10E+12	0.	1580.0
SIH4	+	OH	=	SIH3	+	H20	8.64E+12	0.	95.000
SIH4	+	H02	=	SIH3	+	H202	3.00E+12	0.	5600.
SIH3	+	02	=	SIH20	+	OH	1.72E+14	0.	11430.
SIH3	+	0	=	SIH20	+	H	1.30E+14	0.	2000.
SIH3	+	OH	=	SIH20	+	H2	5.00E+12	0.	0.0
M	+	SIH20	=	HSIO	+	H	5.00E+16	0.	76600.
SIH20	+	H	=	HSIO	+	H2	3.30E+14	0.	10500.
SIH20	+	0	=	HSIO	+	OH	1.80E+13	0.	3080.
SIH20	+	OH	=	HSIO	+	H20	7.50E+12	0.	170.
SIH20	+	02	=	HSIO	+	H02	3.95E+14	0.0	29500.
SIH20	+	H02	=	HSIO	+	H202	1.00E+12	0.	8000.
M	+	HSIO	=	H	+	SIO	5.00E+14	0.	29000.
HSIO	+	H	=	SIO	+	H2	2.00E+14	0.	0.00
HSIO	+	0	=	SIO	+	OH	1.00E+14	0.	0.00
HSIO	+	OH	=	SIO	+	H20	1.00E+14	0.	0.00
HSIO	+	02	=	SIO	+	H02	1.20E+14	0.0	3795.
SIO	+	02	=	SIO2	+	0	1.00E+13	0.	6500.
SIO	+	OH	=	SIO2	+	H	4.00E+12	0.	5700.
SIO	+	0	=	SIO2	+	M	2.50E+15	0.	4370.
M	1	02	1	0	1	0	7.2E18	-1.	117908.
M	1	H2	1	H	1	H	5.5E18	-1.	103298.
M	1	H20	1	H	1	OH	5.2E21	-1.5	110000.
H		02		H02		M	2.3E15	0.	-800.
M	1	H202	1	OH	1	OH	1.2E17	0.	45500.
0		H		OH		M	7.1E18	-1.	0.
H20		0		OH		OH	5.8E13	0.	18000.
H2		OH		H20		H	2.0E13	0.	5166.
02		H		OH		0	2.2E14	0.	16800.
H2		0		OH		H	7.5E13	0.	11099.
H2		02		OH		OH	1.0E13	0.	43000.
H		H02		H2		02	2.4E13	0.	695.
H		H02		OH		OH	2.4E14	0.	1887.
H20		0		H		H02	5.8E12	.5	57000.
0		H02		OH		02	5.0E13	0.	1000.
OH		H02		02		H20	3.0E13	0.	0.
H02		H2		H		H202	7.3E12	0.	18677.
H202		H		OH		H20	3.2E14	0.	8950.
H02		OH		0		H202	5.2E10	.5	21062.
H02		H20		OH		H202	[illegible]	[illegible]	[illegible]

ORIGINAL PAGE IS
OF POOR QUALITY

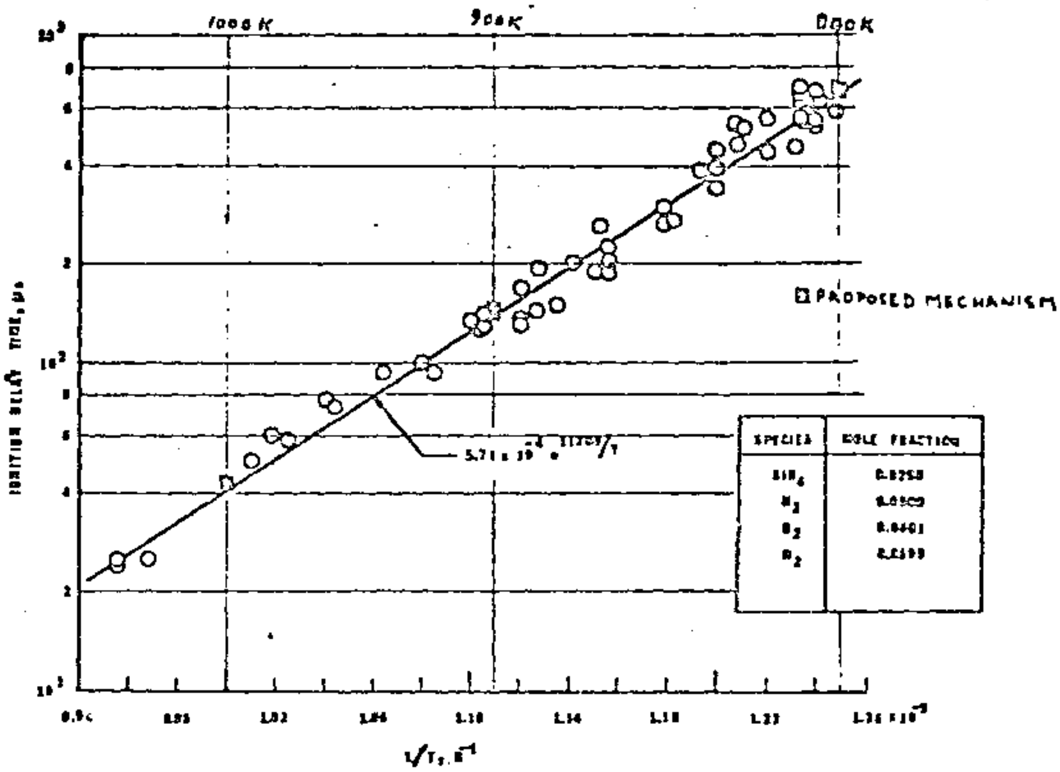

Figure 1.-, Variation of ignition delay time with reciprocal temperature for mixture I. Silane-oxygen equivalence ratio of 1.0; Pressure = 1.25 atm.

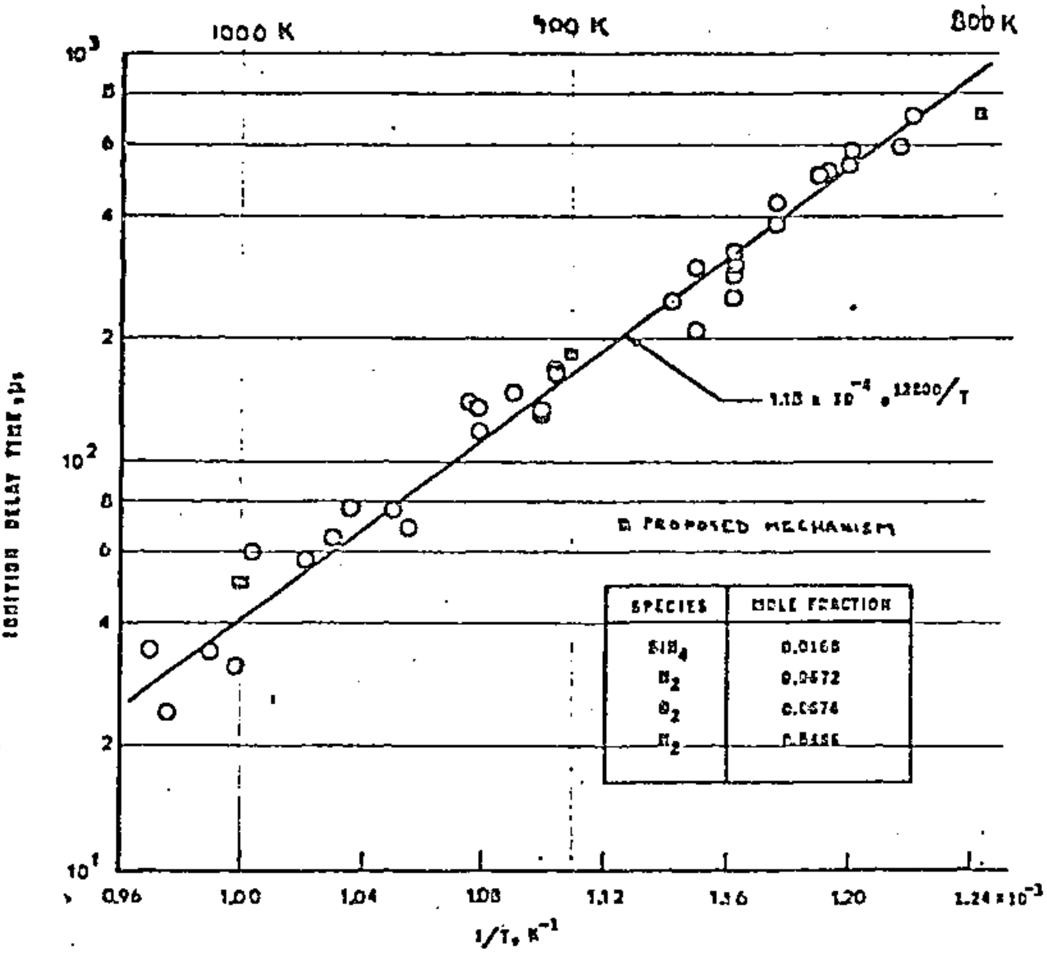

Figure 2.- Variation of ignition delay time with reciprocal temperature for mixture II. Silane-oxygen equivalence ratio of 0.5; Pressure = 1.35 atm.

Temperature for Various Silane-Hydrogen Fuel Mixtures φ = 1

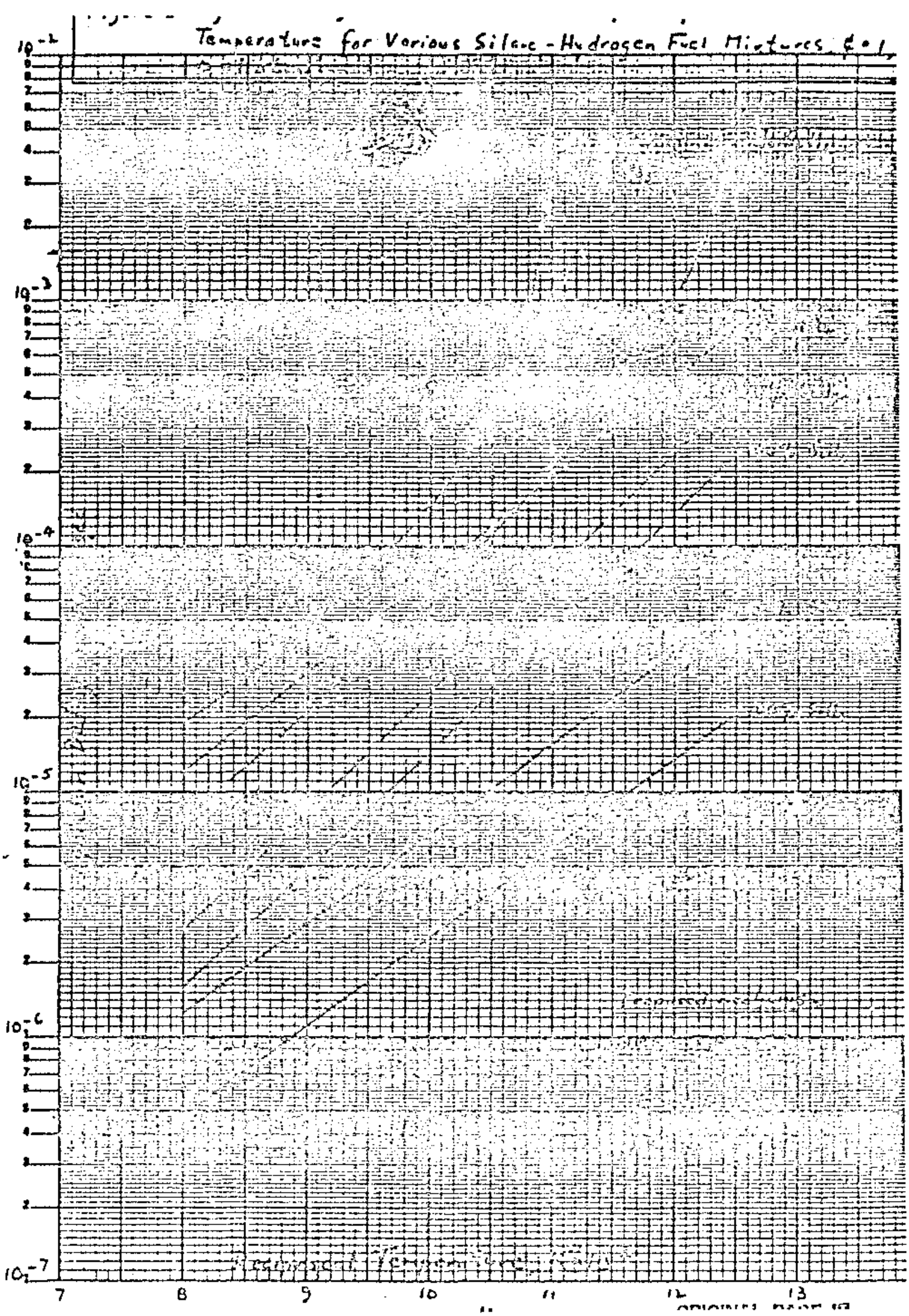

Figure [illegible]. Ignition Delay Time as a function of Reciprocal Initial Temper
for Various Silane-Hydrogen Fuel Mixtures, $\phi = 0.5$, $p = 1$ atm.

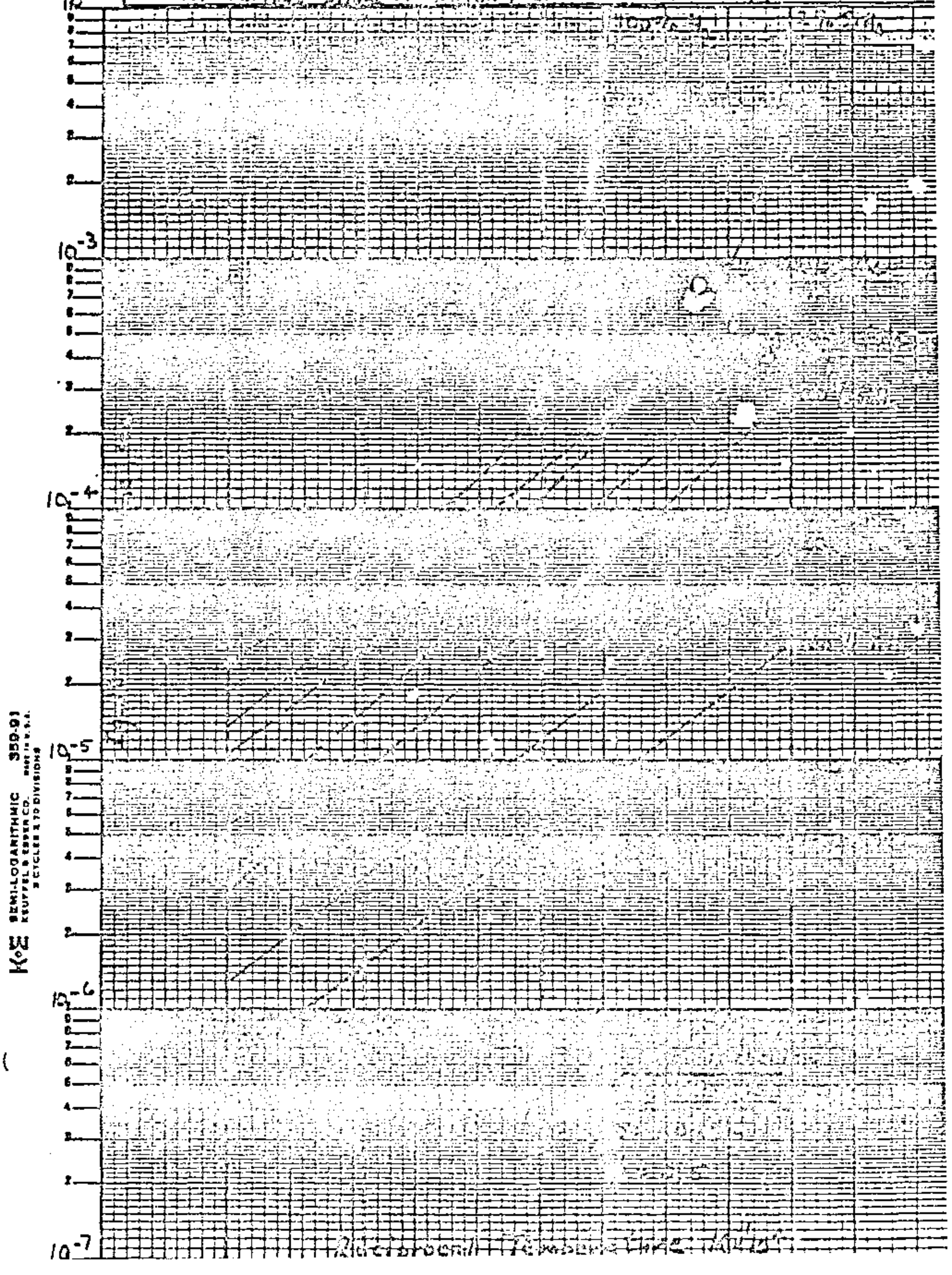

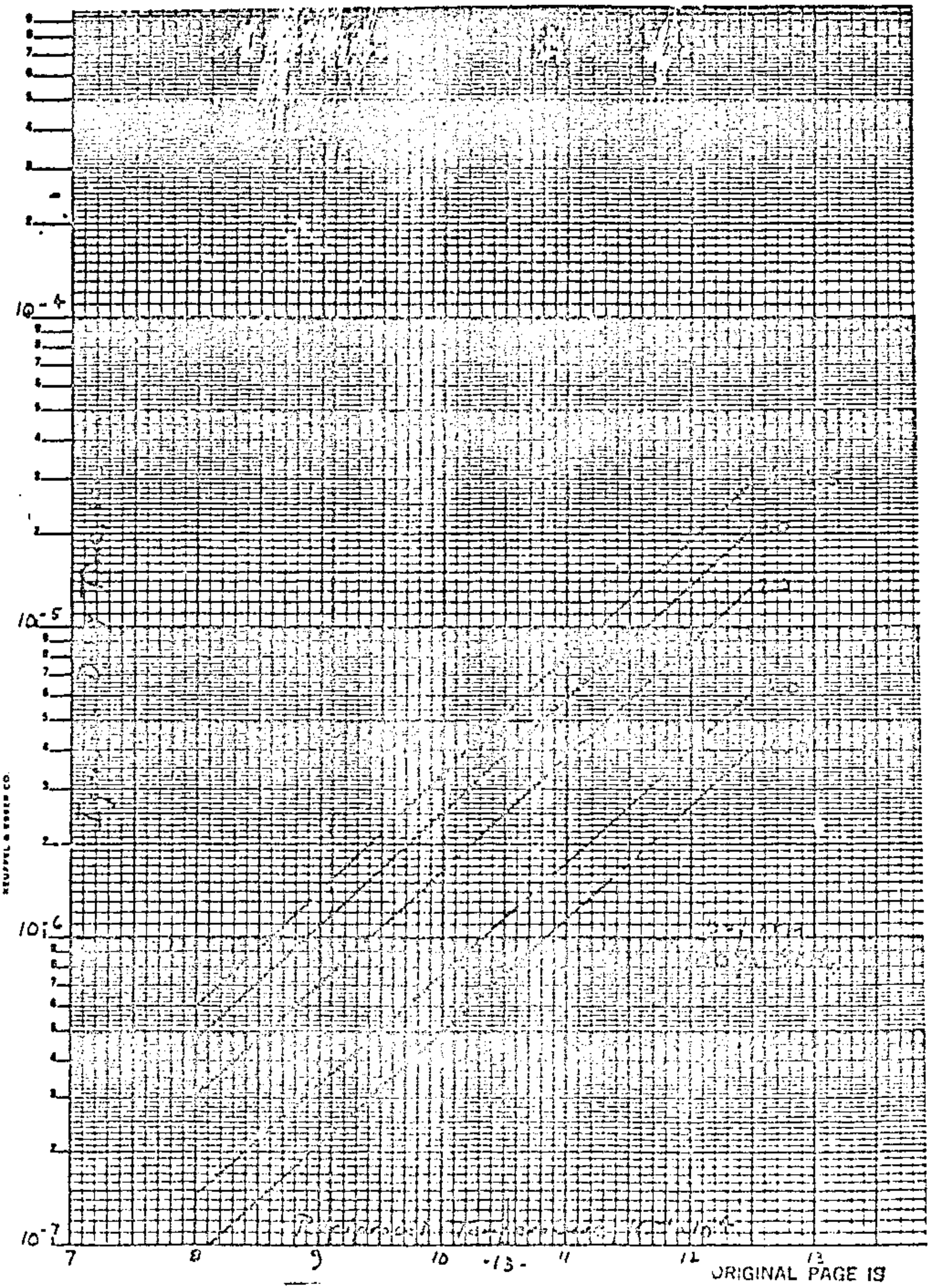

K&E SEMI-LOGARITHMIC 46 6013
4 CYCLES X 70 DIVISIONS
KEUFFEL & ESSER CO.

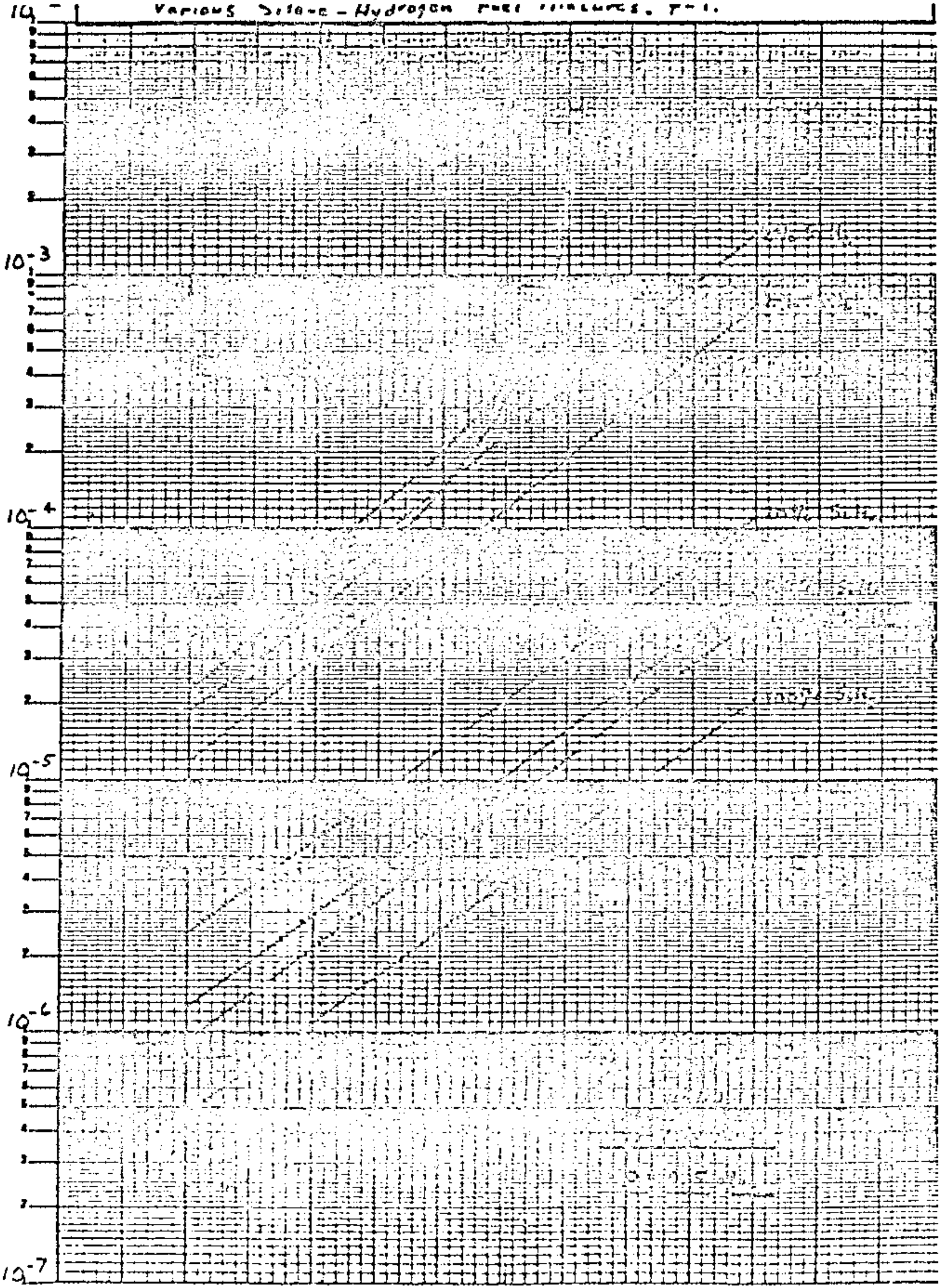

K+E SEMI-LOGARITHMIC 359-91
KEUFFEL & ESSER CO.

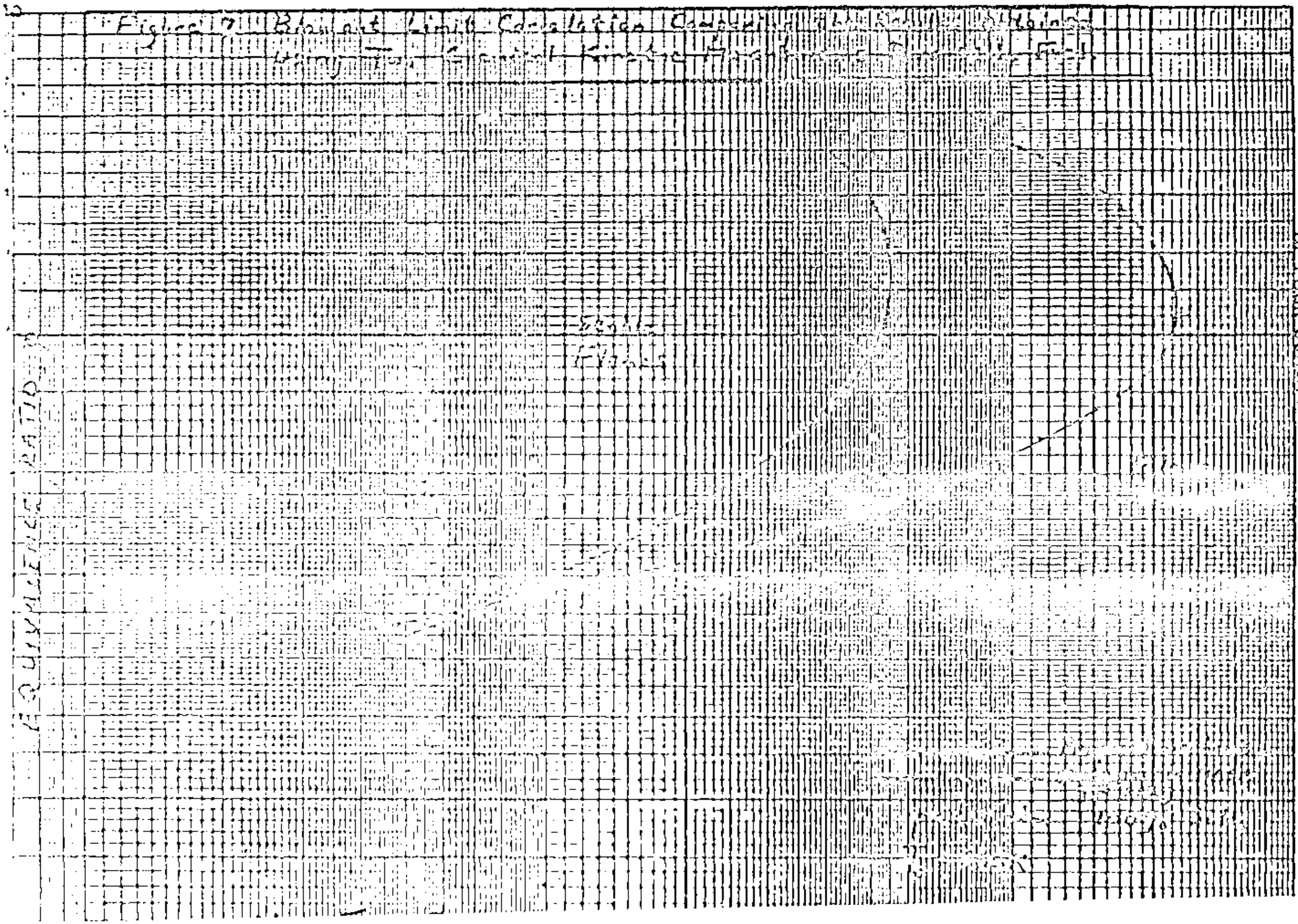

Figure 7 Blowout Limit Correlation Compared [illegible]

ORIGINAL PAGE IS
OF POOR QUALITY

Figure 8. Blowout Limit Correlations for Various Silane-Hydrogen Fuels. 300K, 1 atm.

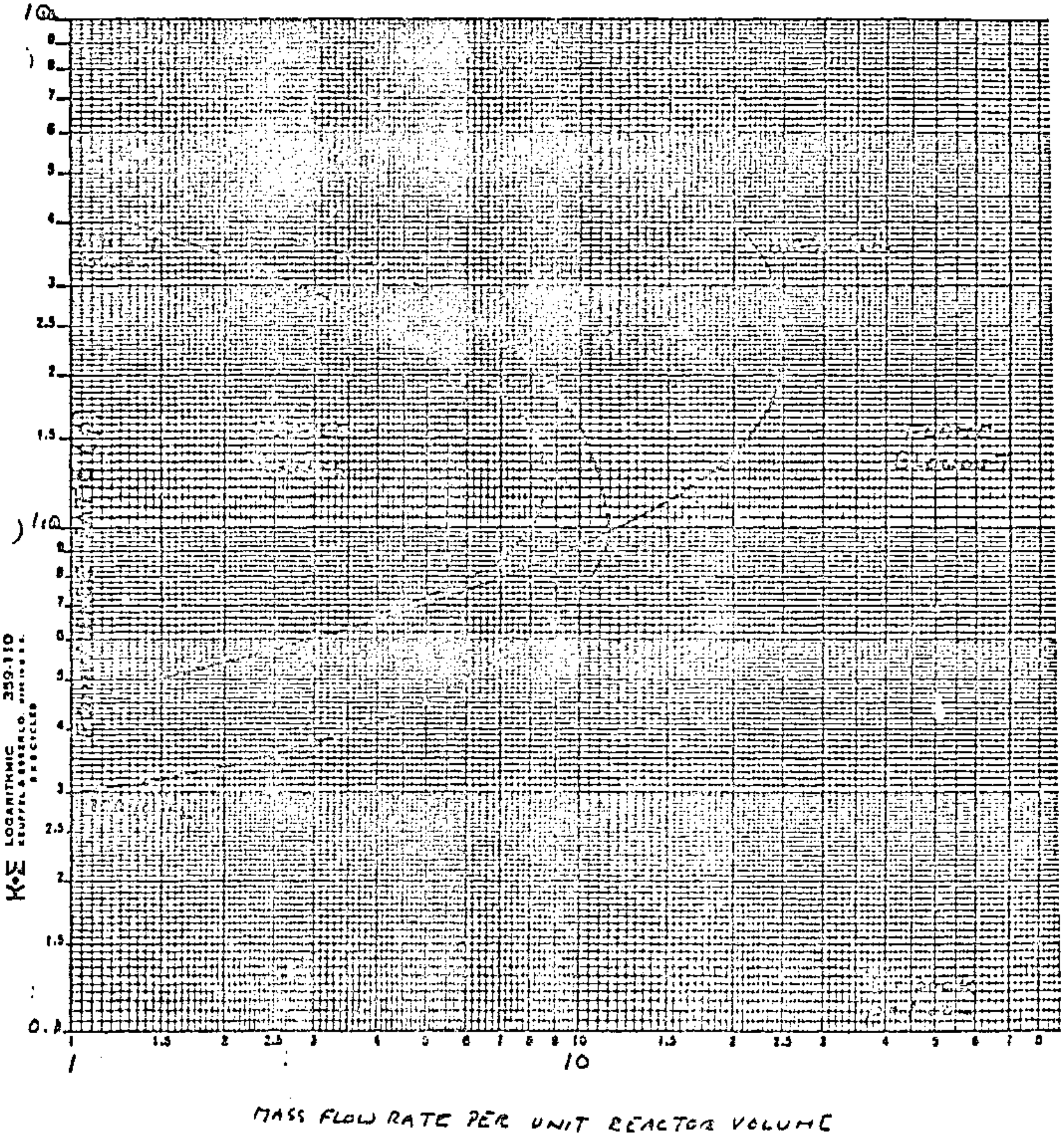

Figure 9. Blowout Limit Correlations for Various Silane-Hydrogen Fuels, 600K, 1 atm.

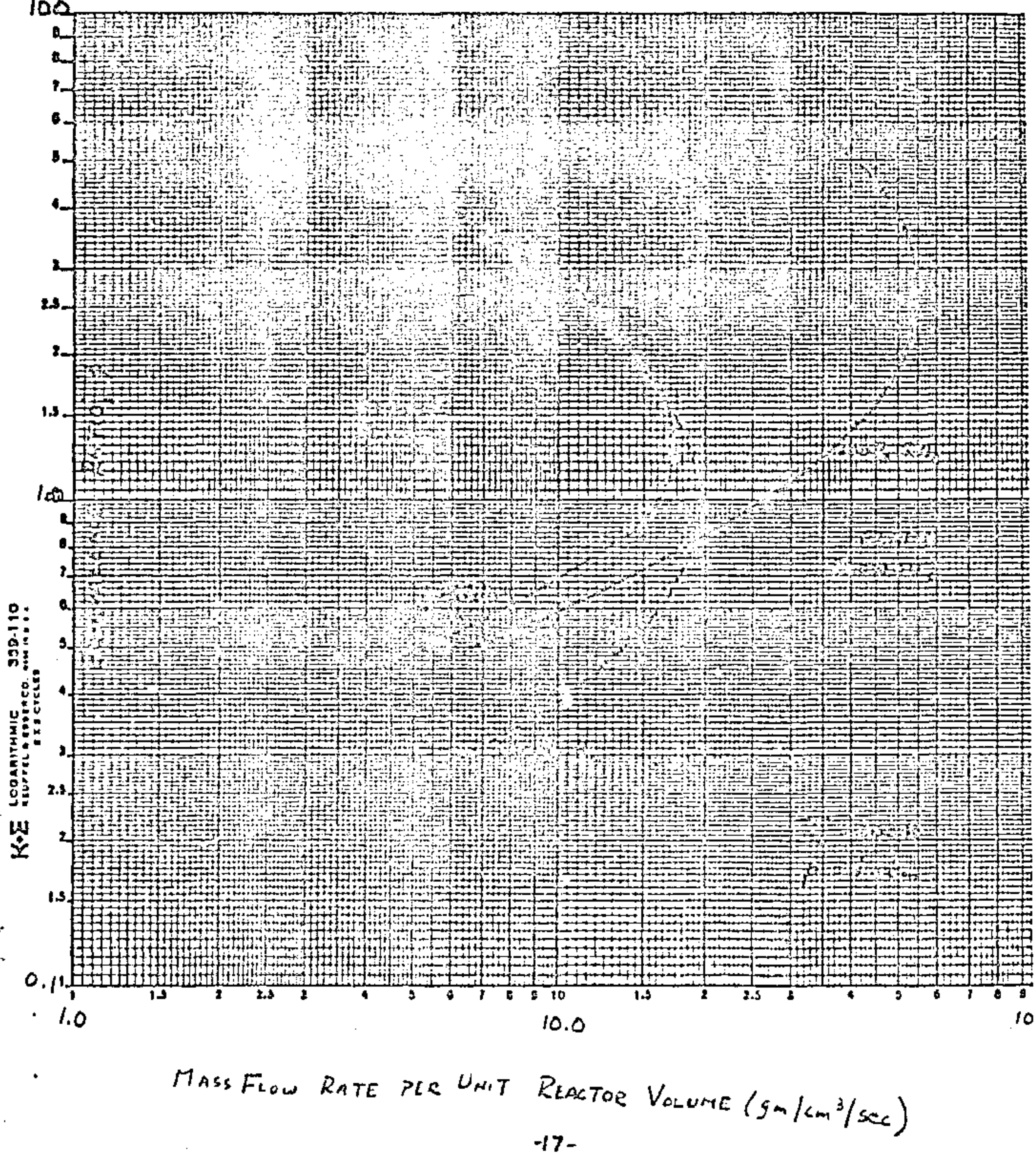

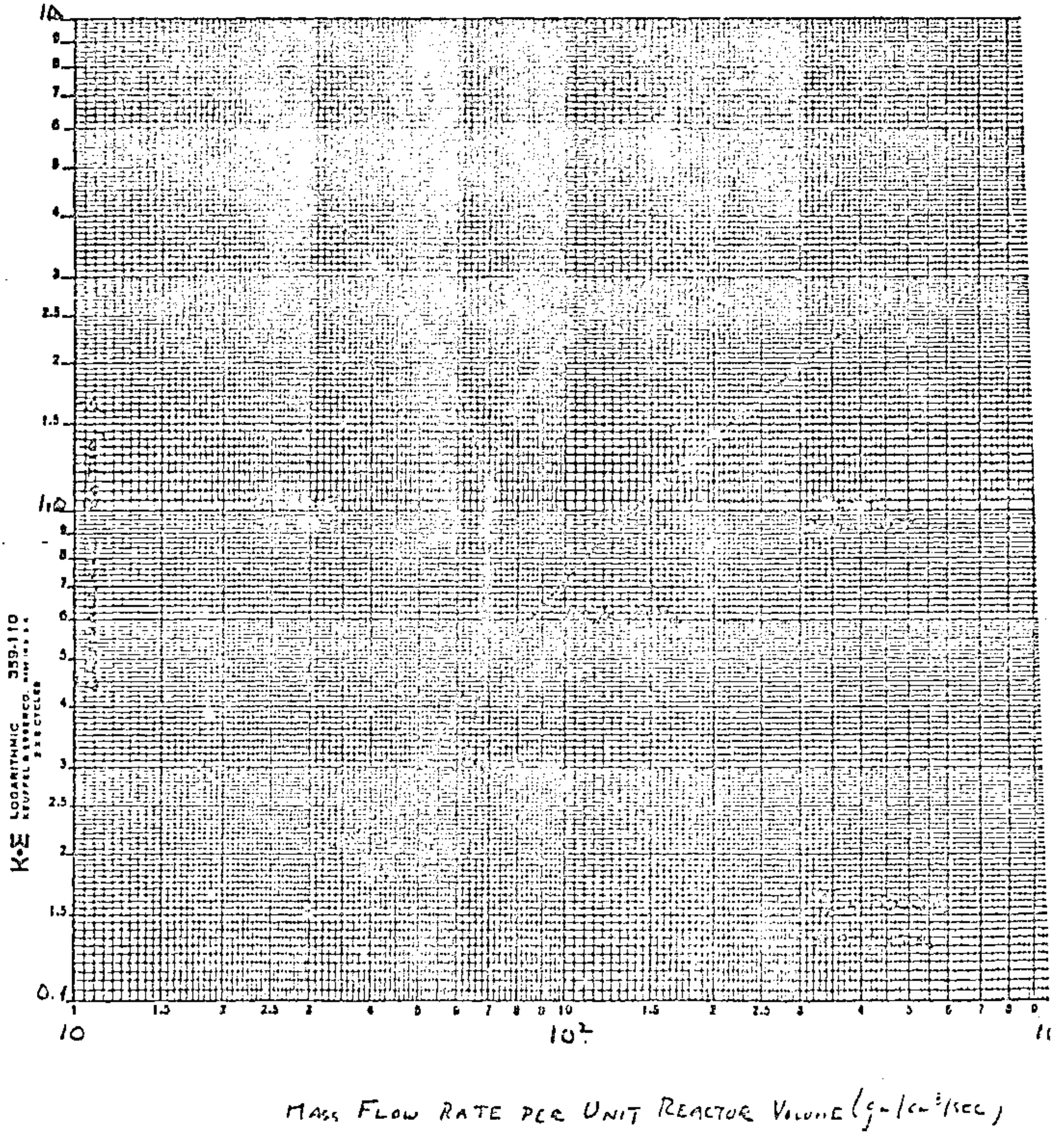

Figure 10. Blowout Limit Correlations for Various Silane-Hydrogen Fuels. 1200K, 1 atm.

ORIGINAL PAGE IS
OF POOR QUALITY

K+E SEMI-LOGARITHMIC 359-71
KEUFFEL & ESSER CO. MADE IN U.S.A.
3 CYCLES X 70 DIVISIONS

Figure 11. Residence Time Correlations for Various Silane-Hydrogen Fuels, 300 K, 1 atm

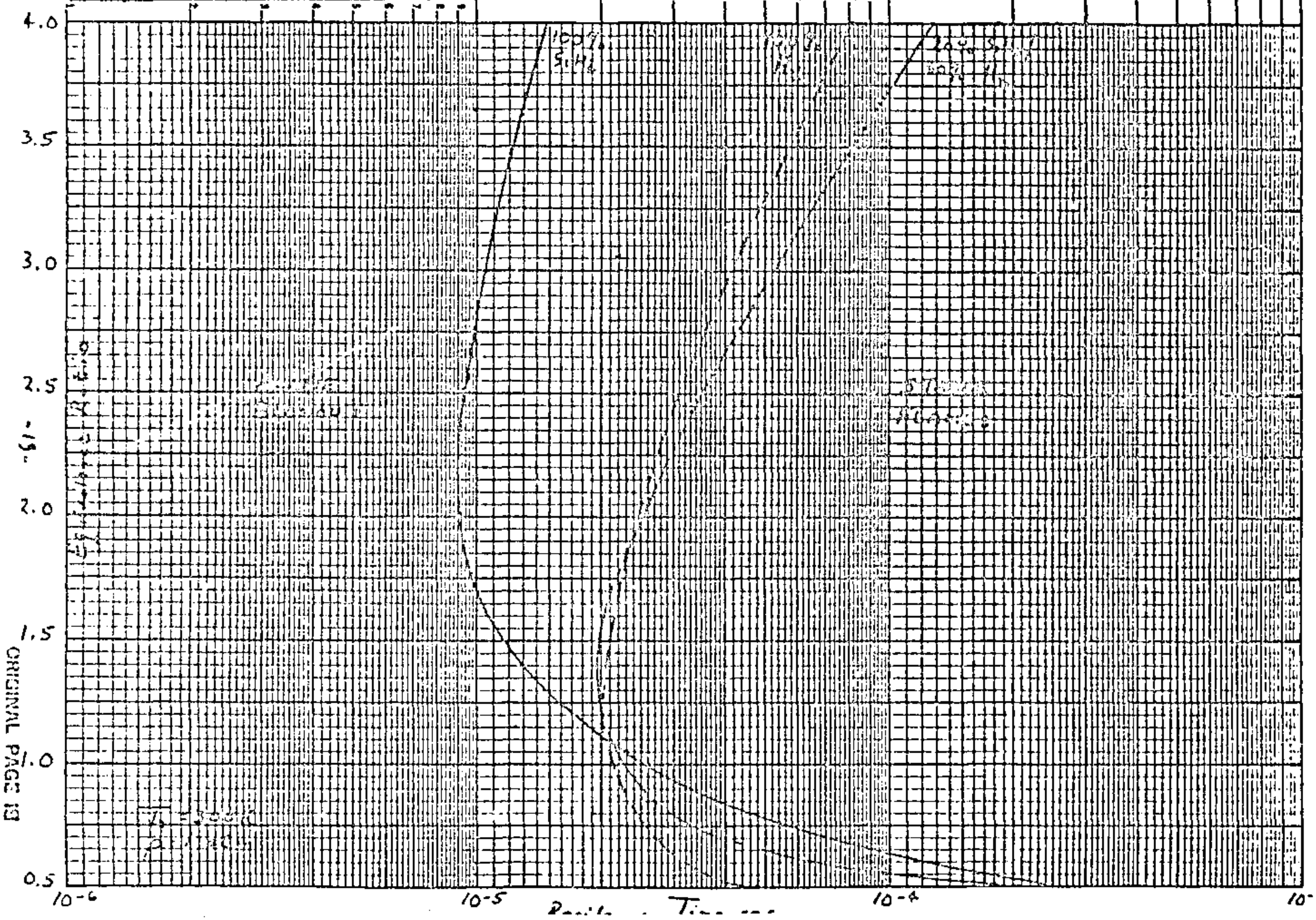

Figure 12. Residence Time Correlations for Various Silane-Hydrogen Fuels. 600K, 1 atm.

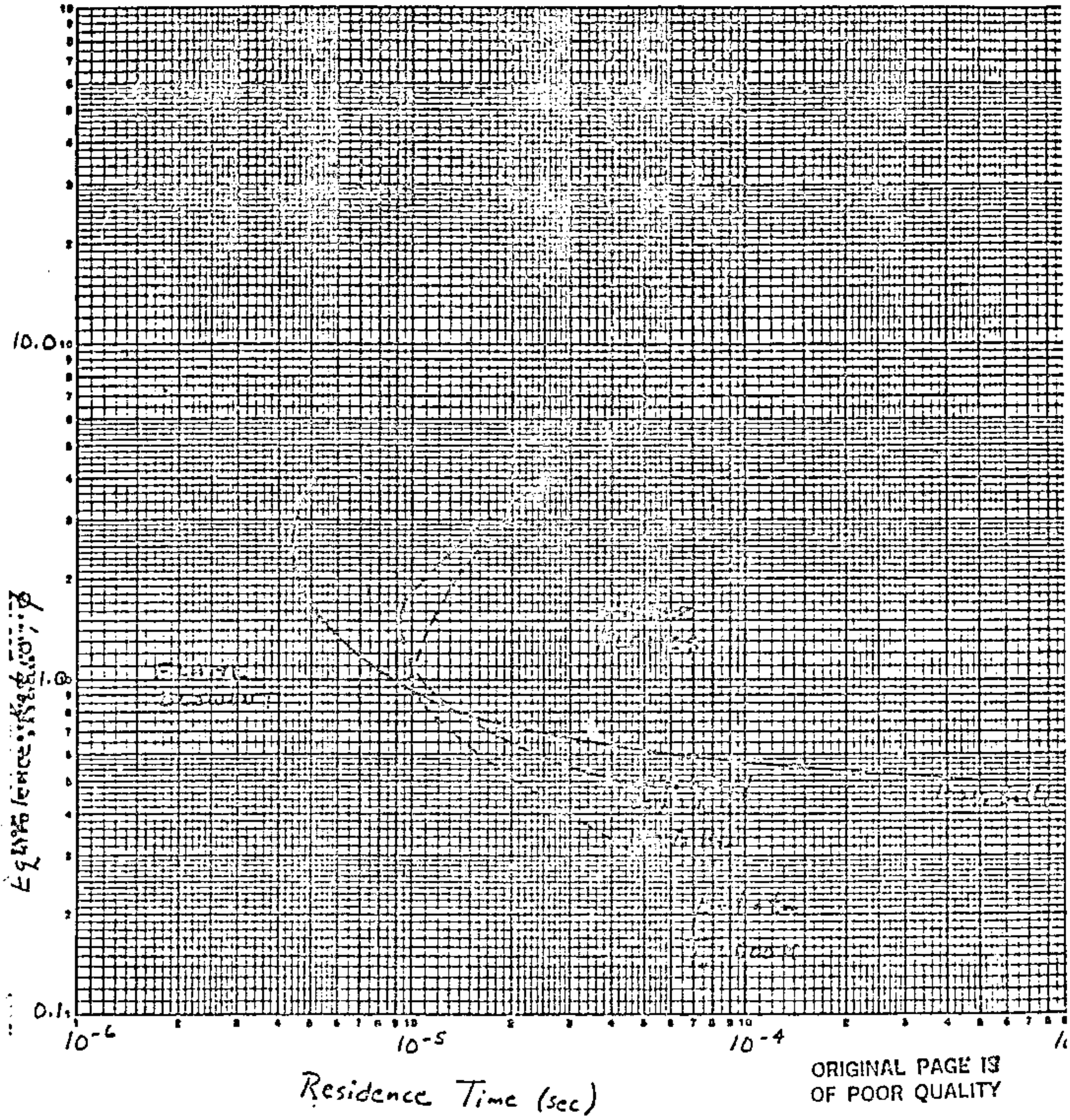

K•E LOGARITHMIC 359-111G
KEUFFEL & ESSER CO.
2 X 3 CYCLES

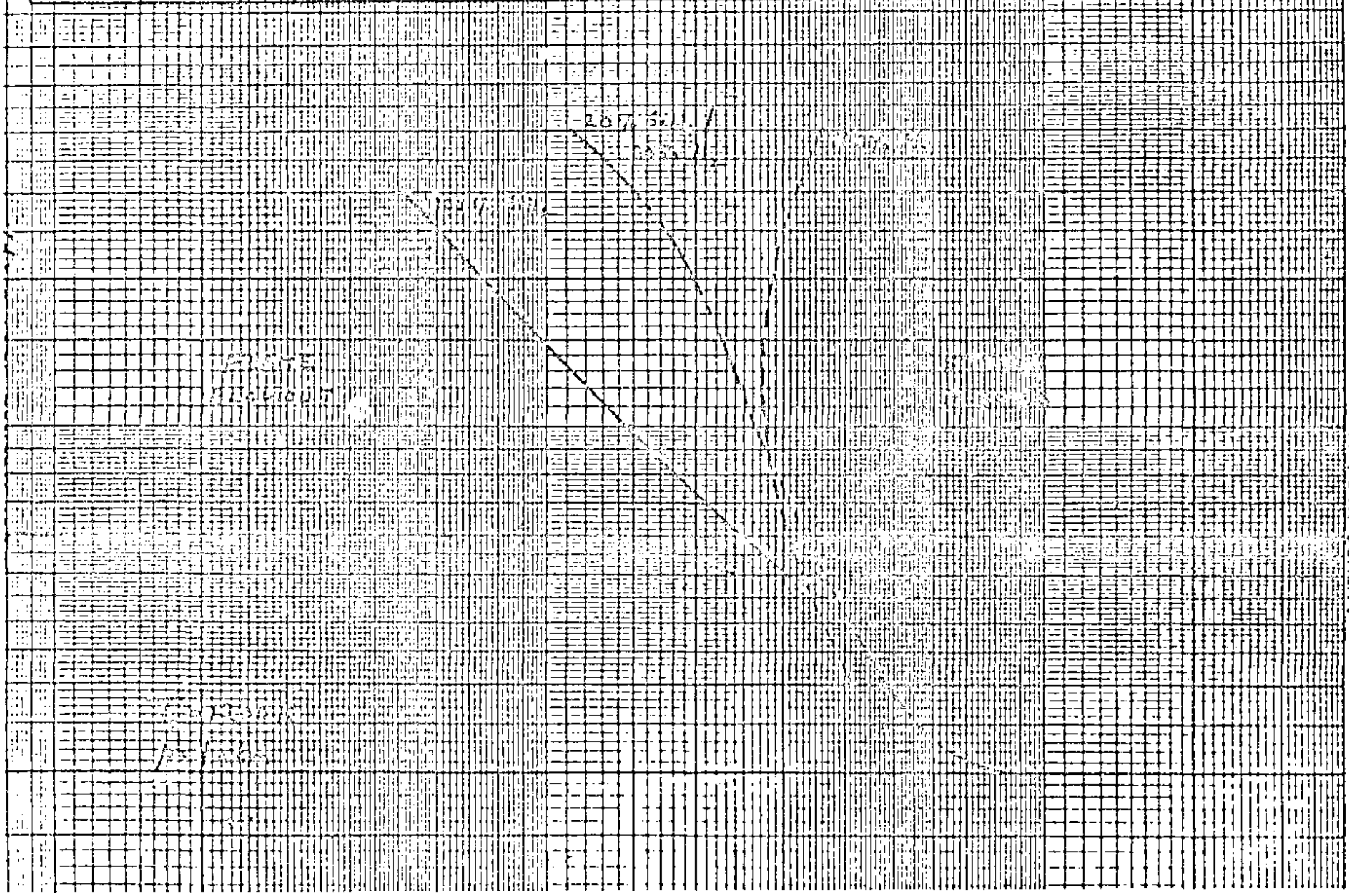

Figure 13 Residence Time Correlations [illegible]
1200 K, 1.2 m

ORIGINAL PAGE IS OF POOR QUALITY

Figure 14. The Effect of Pressure on the Blowout Limit Correlation for 20% SiH_4/80% H_2 Fuel. T_0 = 600K.

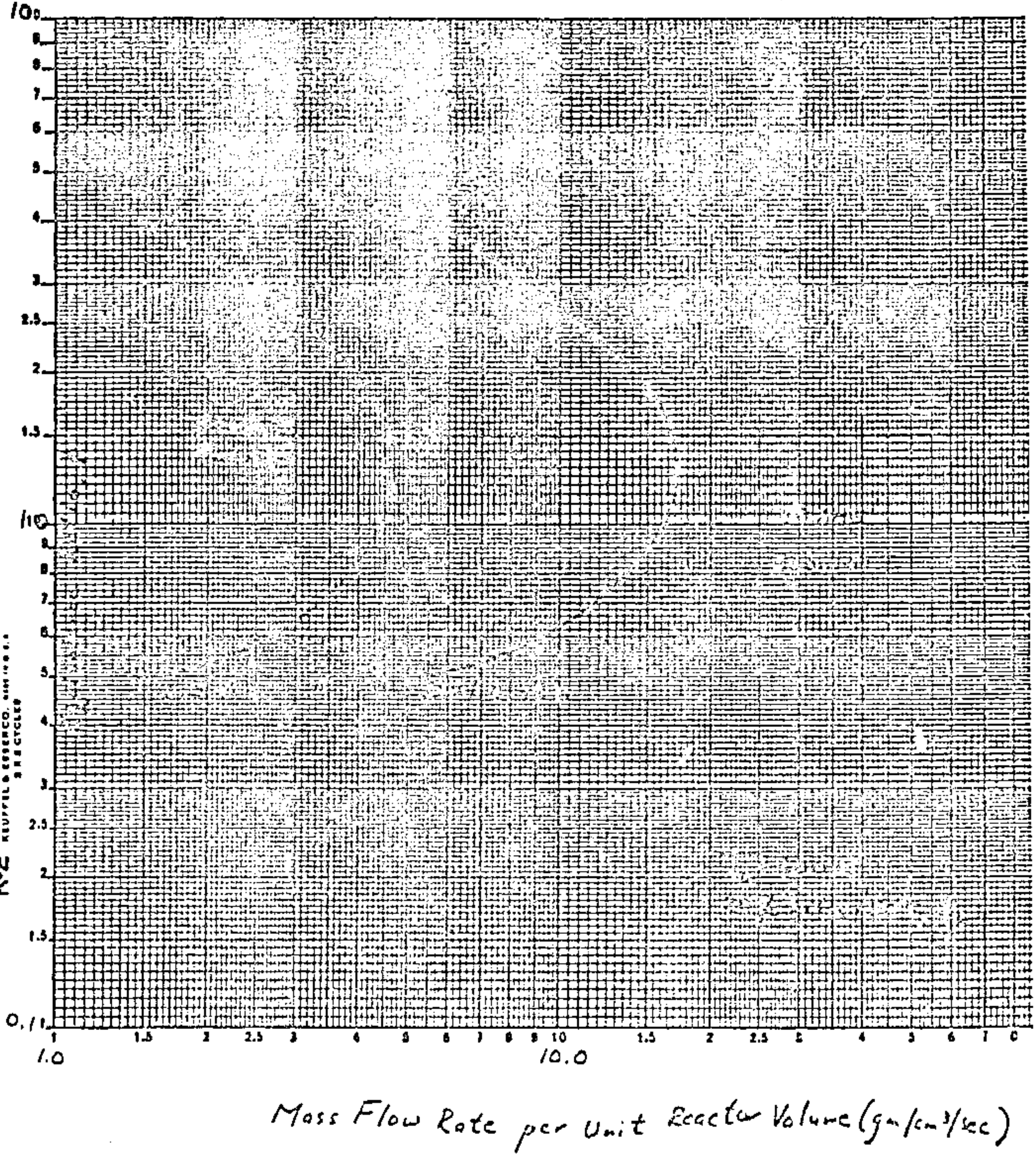

ORIGINAL PAGE IS OF POOR QUALITY

Figure 15 : The Effect of Pressure on the Residence Time Correlation for 20% SiH_4/100% H_2 Fuel. T_0 = 600 K.

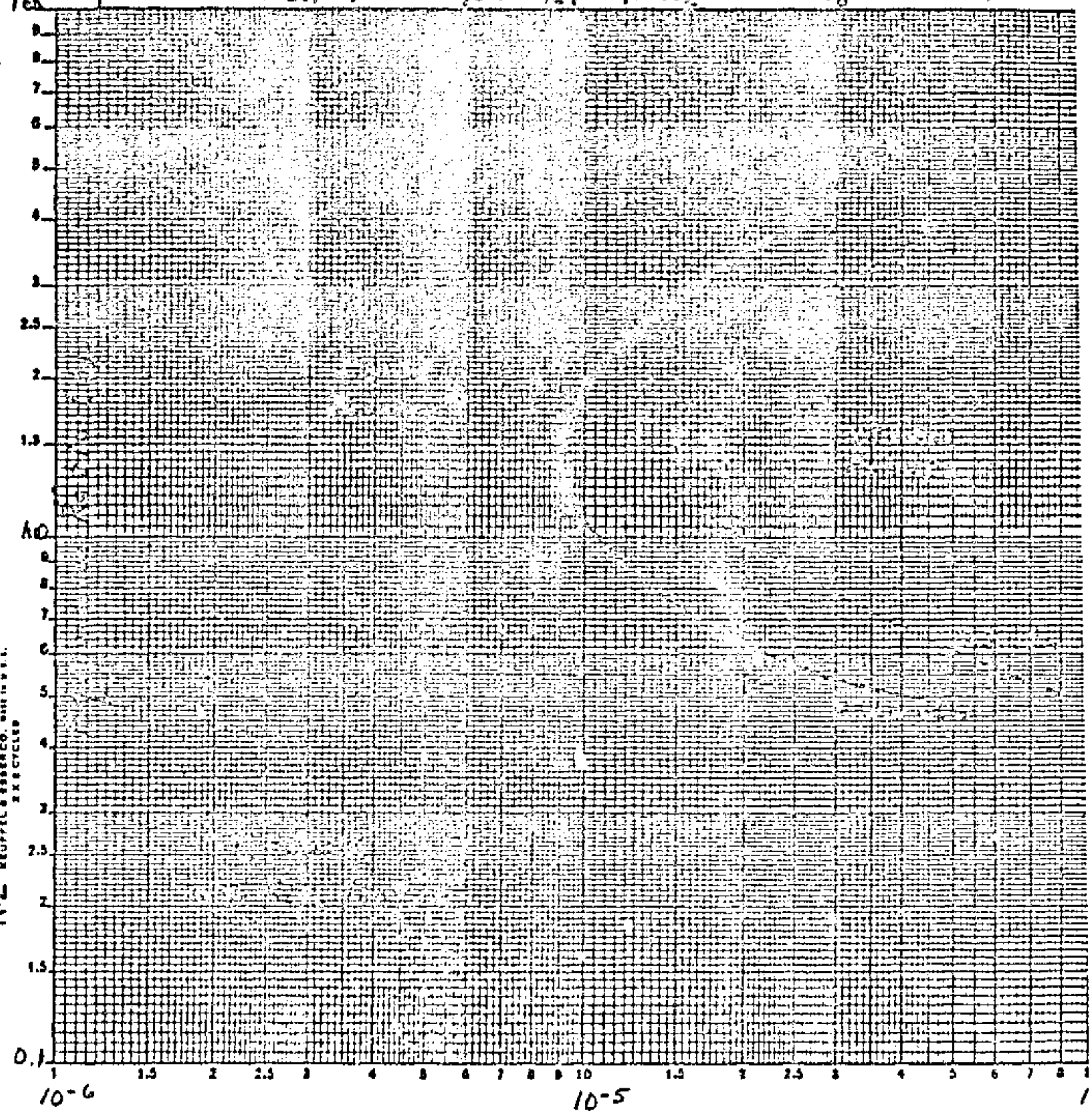

K+E SEMI-LOGARITHMIC 46 6013
4 CYCLES X 70 DIVISIONS MADE IN U.S.A.
KEUFFEL & ESSER CO.

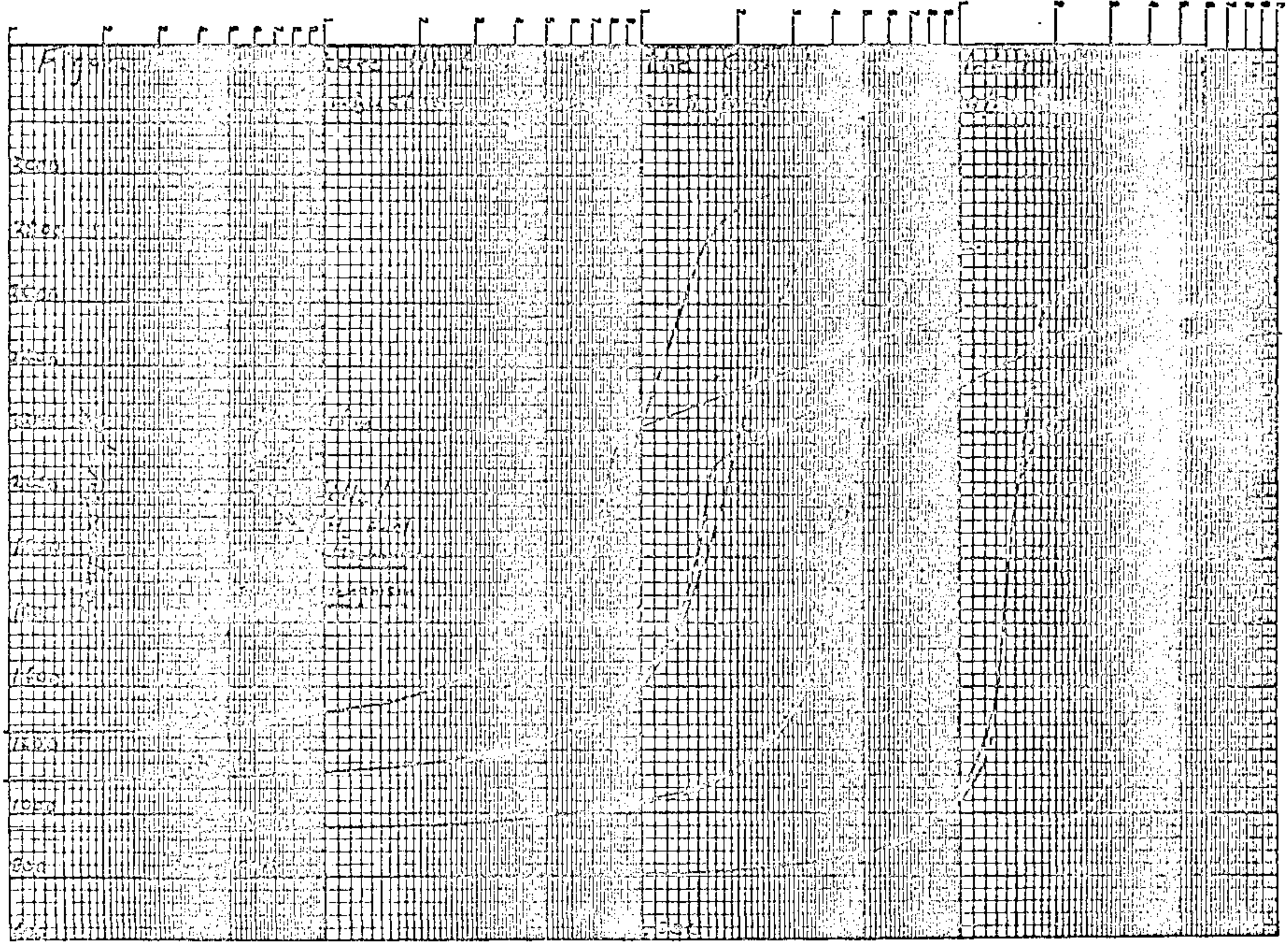

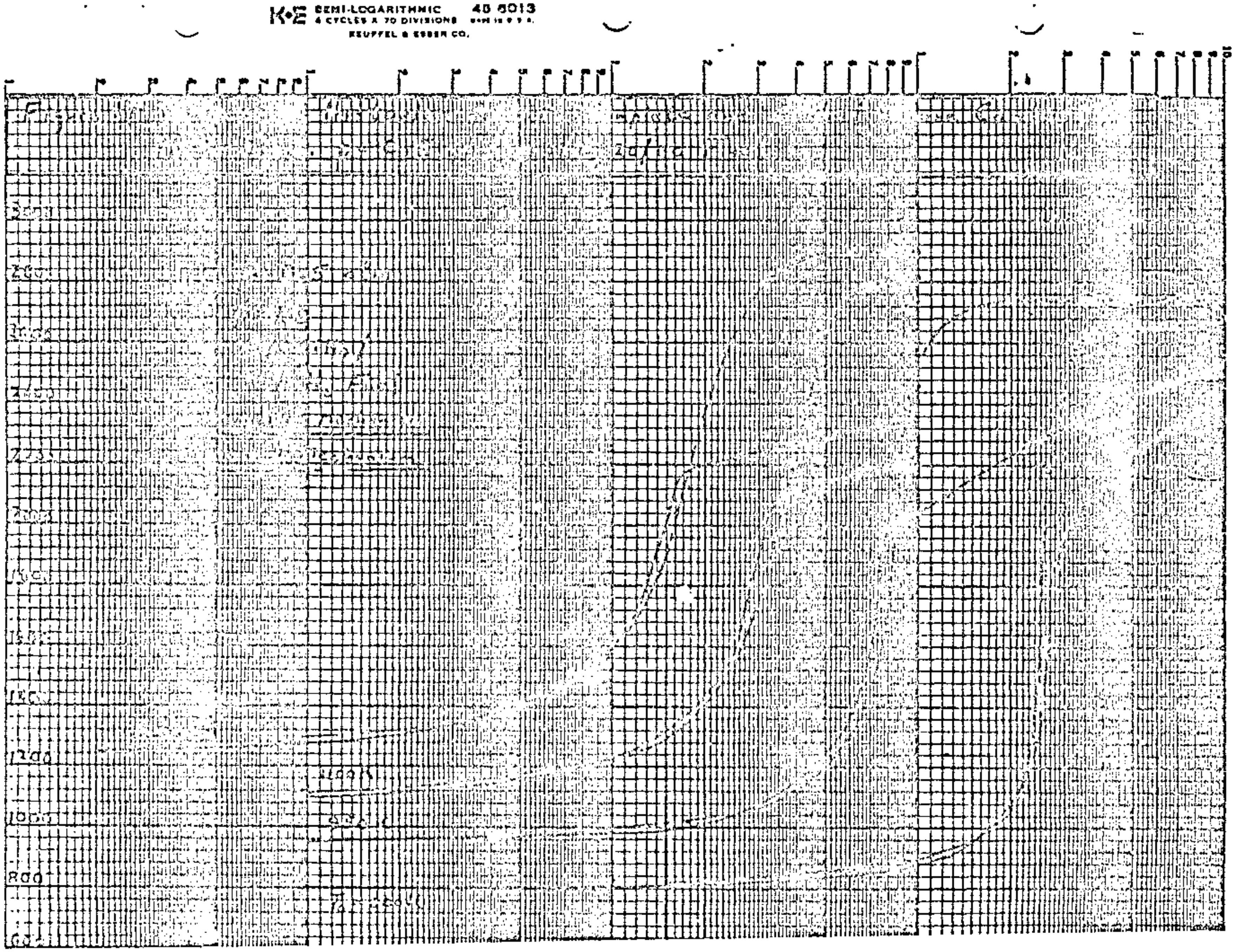
K+E SEMI-LOGARITHMIC 46 6013
4 CYCLES X 70 DIVISIONS MADE IN U.S.A.
KEUFFEL & ESSER CO.
3000
2800
2600
2400
2200
2000
1800
1600
1400
1200
1000
800
600

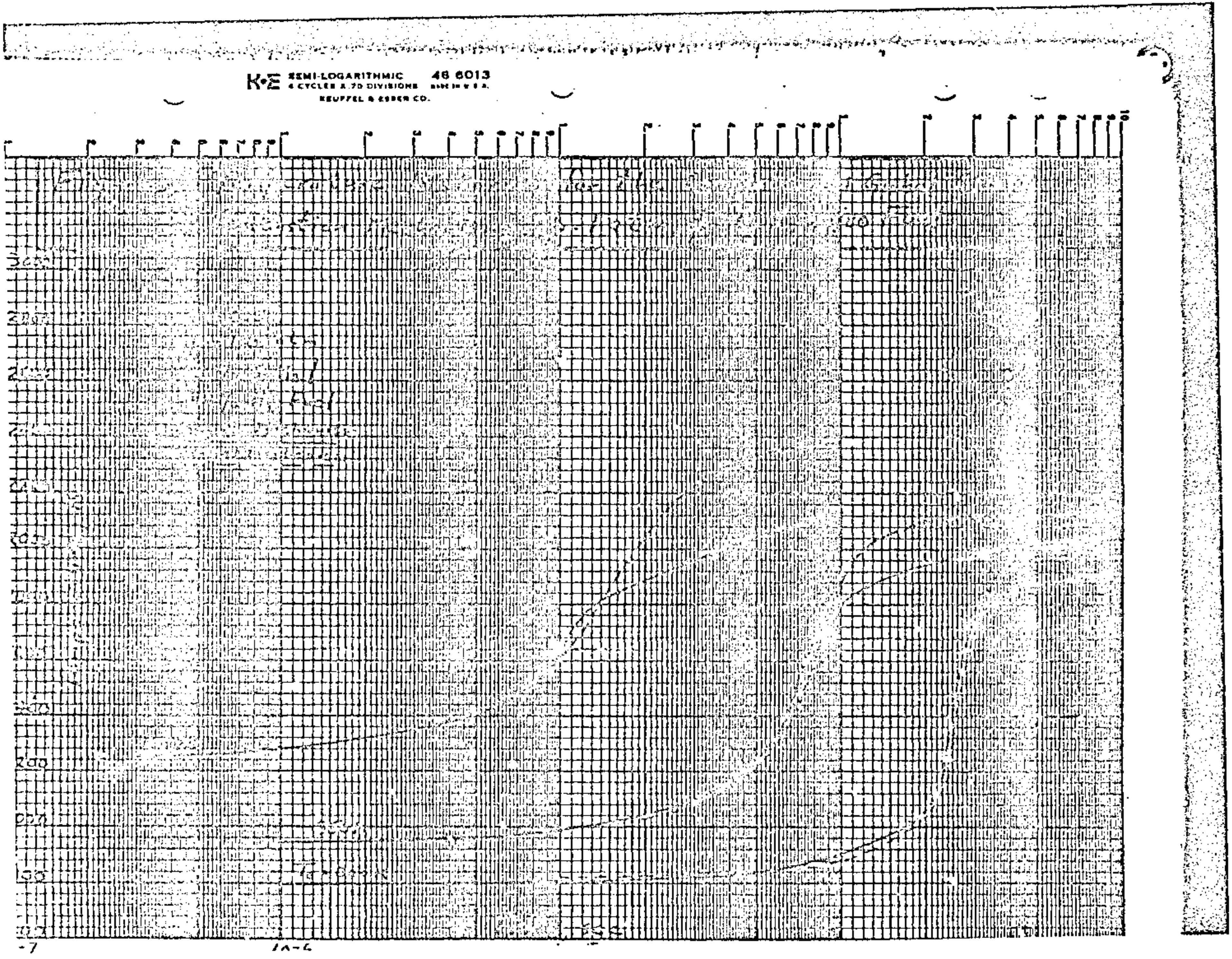
K·E SEMI-LOGARITHMIC 46 6013
4 CYCLES X 70 DIVISIONS MADE IN U.S.A.
KEUFFEL & ESSER CO.
200
100
-7
10-6

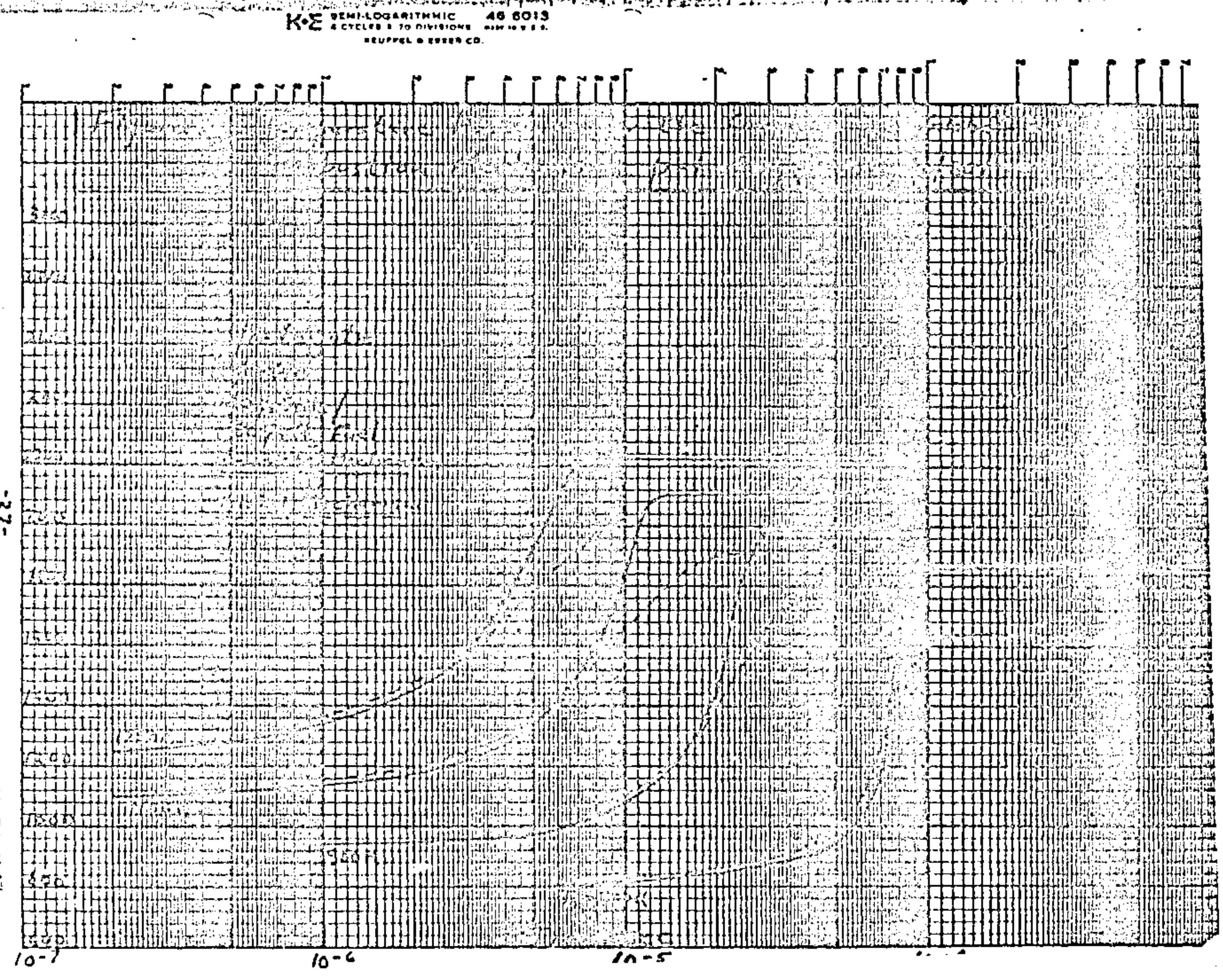

ORIGINAL PAGE IS
OF POOR QUALITY

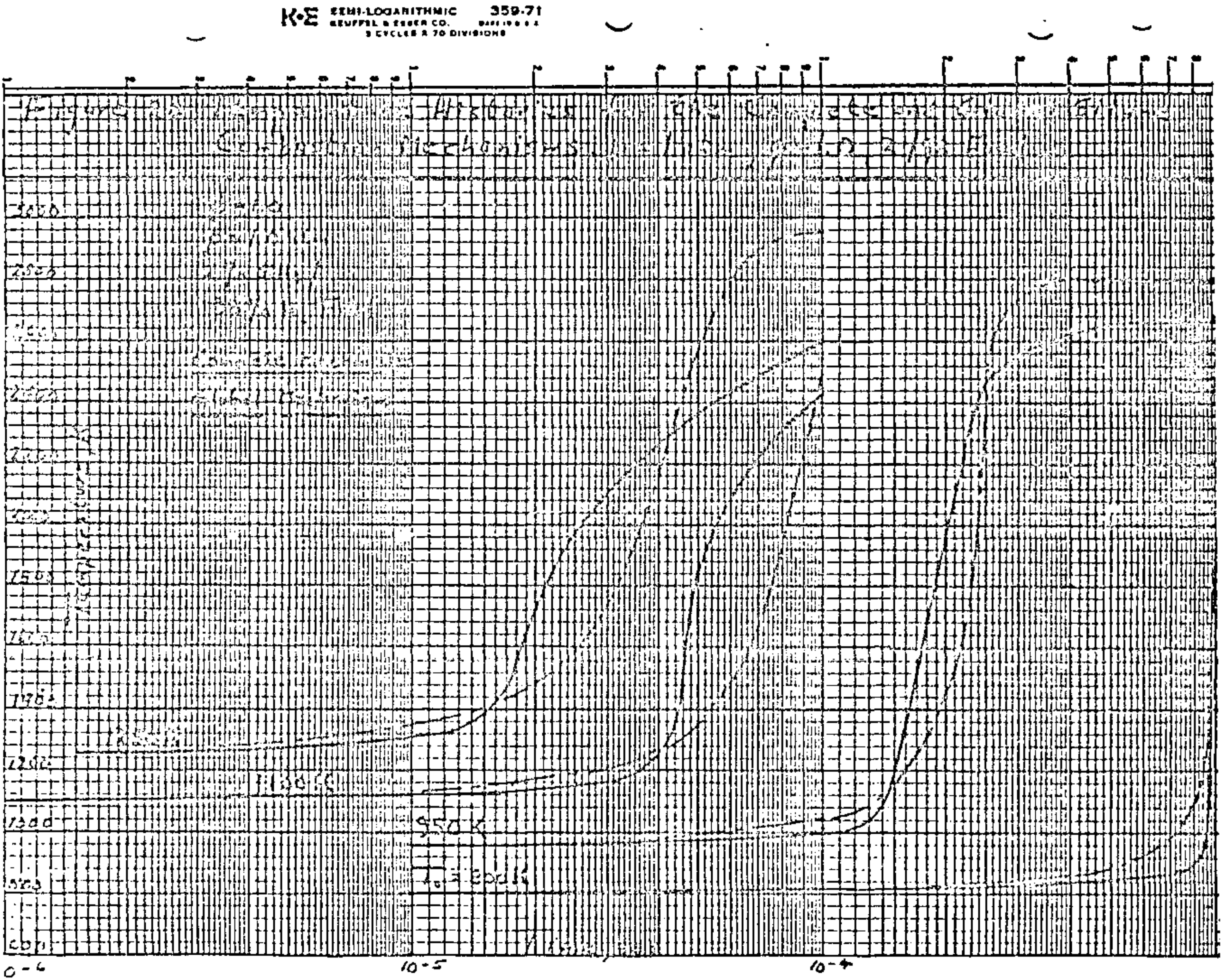
K·E SEMI-LOGARITHMIC 359-71
KEUFFEL & ESSER CO.
3 CYCLES X 70 DIVISIONS
3000
2500
2000
1500
1000
950 K
T = 800 K
10⁻⁶
10⁻⁵
10⁻⁴

3. EFFECTS OF HYDROGEN ADDITION ON HYDROCARBON IGNITION AND FLAME STABILIZATION

Current interest in the use of hydrocarbon fuels in SCRAMJET engines requires that methods be sought for reducing the well-documented lengthy ignition delays and reaction times of hydrocarbon fuels. Two possible approaches to reducing these times are: (1) injecting (relatively) small quantities of hydrogen along with the hydrocarbon fuel with the hope that ignition delay times will be more like those for H_2 than for the CxHy; and (2) regeneratively heating the hydrocarbon prior to its injection into the combustion chamber so as to pyrolyze (thermally crack) it, with the expectation that substantial quantities of hydrogen will be among the pyrolysis products. Studies are underway to investigate both possibilities. Some preliminary results are presented here, with additional results to be reported upon in a future status report.

Ignition delay times are shown in fig. 1. Calculations have been carried out selecting propane (C_3H_8) as the representative hydrocarbon fuel using the chemical kinetic mechanism for propane in ref. 1. To date, runs have been made using H_2/C_3H_8 fuel mixtures up to 33% (by volume) H_2. As can be seen in fig. 1, at 1.0 atm, $\phi = 1.0$, the reduction in ignition delay time compared with that for pure C_3H_8 is slight. For example, at $T_o = 1000K$, $t_{ID} \simeq 0.05$ sec for C_3H_8 and about 0.025 sec for the 33% H_2/67% C_3H_8 mixture. On the other hand, $t_{ID} \approx 10^{-4}$ sec for pure H_2 at $T_o = 1000K$ (ref. 2). It is recognized, however, that 33% H_2 in the fuel mixture represents very little hydrogen by mass. As an example, the mass equivalent of the 20% SiH_4/80% mixture as applied here would result in a fuel mixture of 98.88% H_2/1.12% C_3H_8 by volume. Clearly, then, calculations must be carried out for fuel mixtures substantially in excess of 33% H_2 (by volume). A similarly wide range of H_2/CxHy ratios was utilized in the experiments of Cookson (ref. 3), shown schematically in fig. 2. His tests, the results of which are in fig. 3, would span the range from about 3% H_2 to nearly 96% H_2 (by volume) had his "main" fuel been C_3H_8 rather than kerosene. It is interesting to note that using mode A (see fig. 2), ignition could be achieved at reasonable kerosene injection pressure ratios using relatively small quantities of H_2 (about 3% to 33% by volume), whereas mode B required much more substantial quantities of H_2 (33% - 96% by volume).

Blowout limit correlations obtained using the PSR code are shown in figs. 4 - 7. Fig. 4 duplicates the conditions of Longwell and Weiss (ref. 4) and, as can be seen, the calculated curve compares well with the experimental one, thereby increasing confidence in the chemical kinetic mechanism in ref. 1. In figs. 5 and 6, for C_3H_8/H_2 mixtures, little improvement is noted in the flame stabilizing properties of these mixtures over pure C_3H_8 up to 20% H_2. A similar conclusion holds for CH_4/H_2 mixtures, as seen in fig. 7. Additional results will be obtained for CxHy/H_2 mixtures having higher concentrations of hydrogen.

An investigation has been made of the likely equilibrium products resulting from propane pyrolysis. The pyrolysis reaction was assumed to be (in accordance with ref. 5)

$$C_3H_8 \rightarrow a\ C_3H_8 + b\ C_2H_4 + d\ CH_4 + e\ H_2$$

In this case, the equilibrium concentration of H_2 in the ranges $800K \leq T \leq 1200K$, $0.5 \leq p \leq 1.0$ atm is calculated to be about 40% by volume (see fig. 8). It is also of interest to note that in these ranges, the remaining 60% by volume is almost entirely C_2H_4 (see fig. 9). Streamtube and PSR calculations with these concentrations as input to assess ignition and reaction times and flame stabilization behavior are planned.

REFERENCES FOR SECTION 3

1. Jachimowski, C. J., "Chemical Kinetic Reaction Mechanism for the Combustion of Propane", to be published in Combustion and Flame.
2. Rogers, R. C. and Schexnayder, C. J., Jr., NASA TO-1856 (1981).
3. Cookson, R. A., "Mixing and Ignition of Enclosed Supersonic Diffusion Flames", Aerospace Rsch. Labs., Wright-Patterson AFB, ARL 73-0070, April 1973.
4. Longwell, J. P. and Weiss, M.A., I. and E. Chem., vol. 47, no. 8, Aug. 1955, pp. 1634-1643.
5. Chinitz, W., "On the Pyrolysis of Hydrocarbon Fuels", GASL TM-153, Sept. 1966.

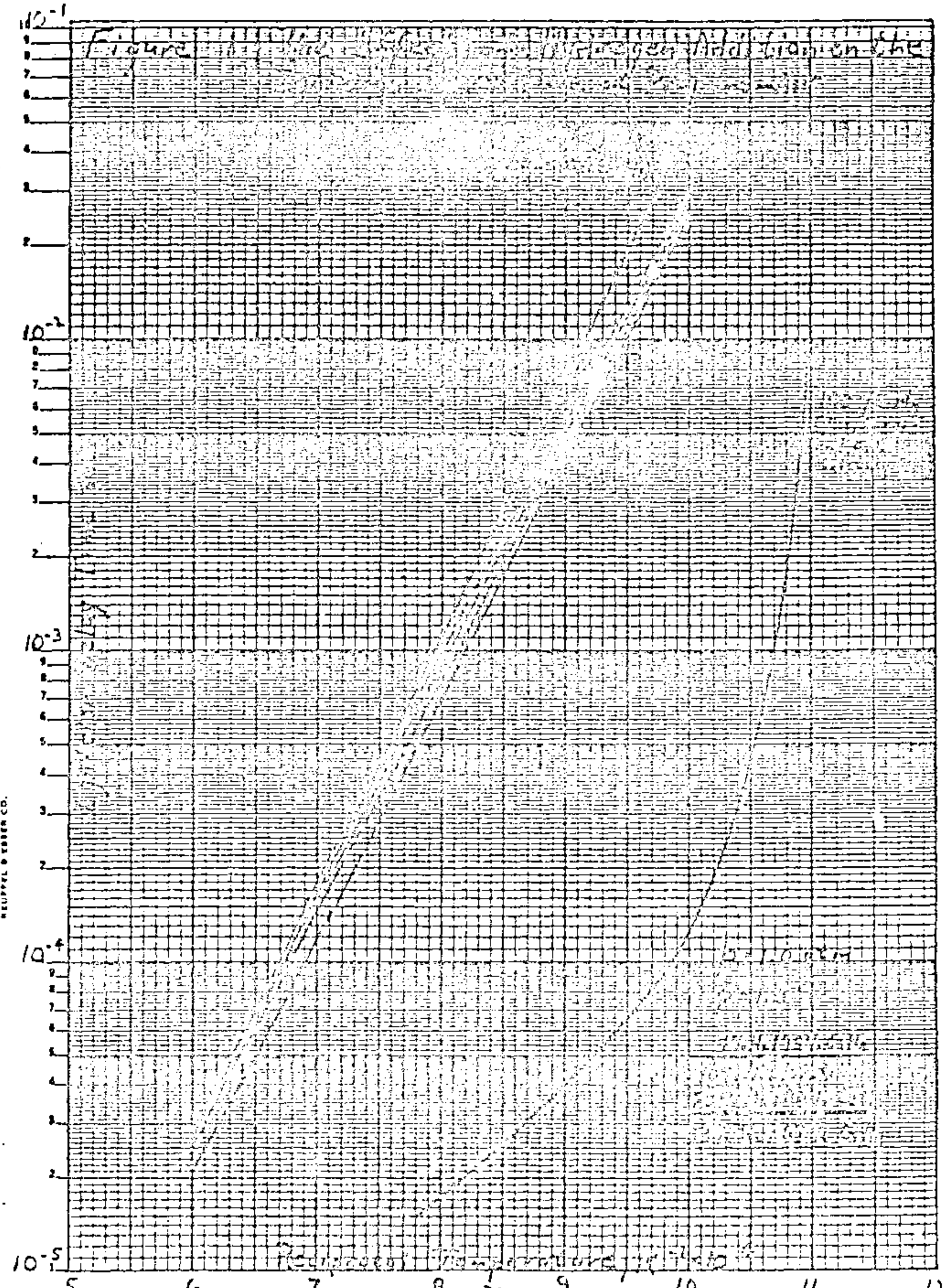Figure
10^{-1}
10^{-2}
10^{-3}
10^{-4}
10^{-5}
5
6
7
8
9
10
11
12
K&E SEMI-LOGARITHMIC 46 6013
5 CYCLES X 70 DIVISIONS
KEUFFEL & ESSER CO.

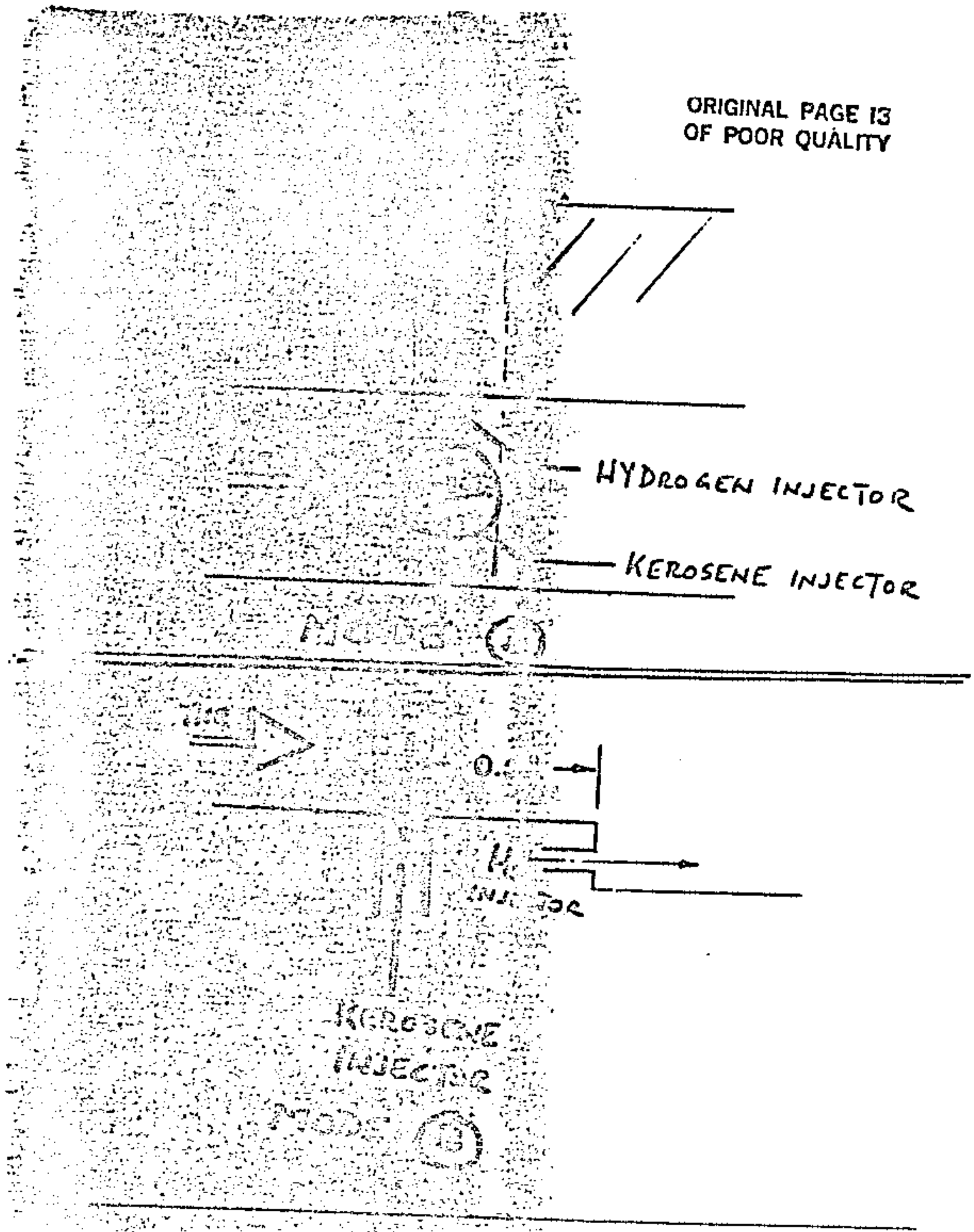
HYDROGEN INJECTOR
KEROSENE INJECTOR
MODE (A)
0.
H
INJECTOR
KEROSENE
INJECTOR
MODE (B)

[illegible] CLARKSON EXPERIMENTS

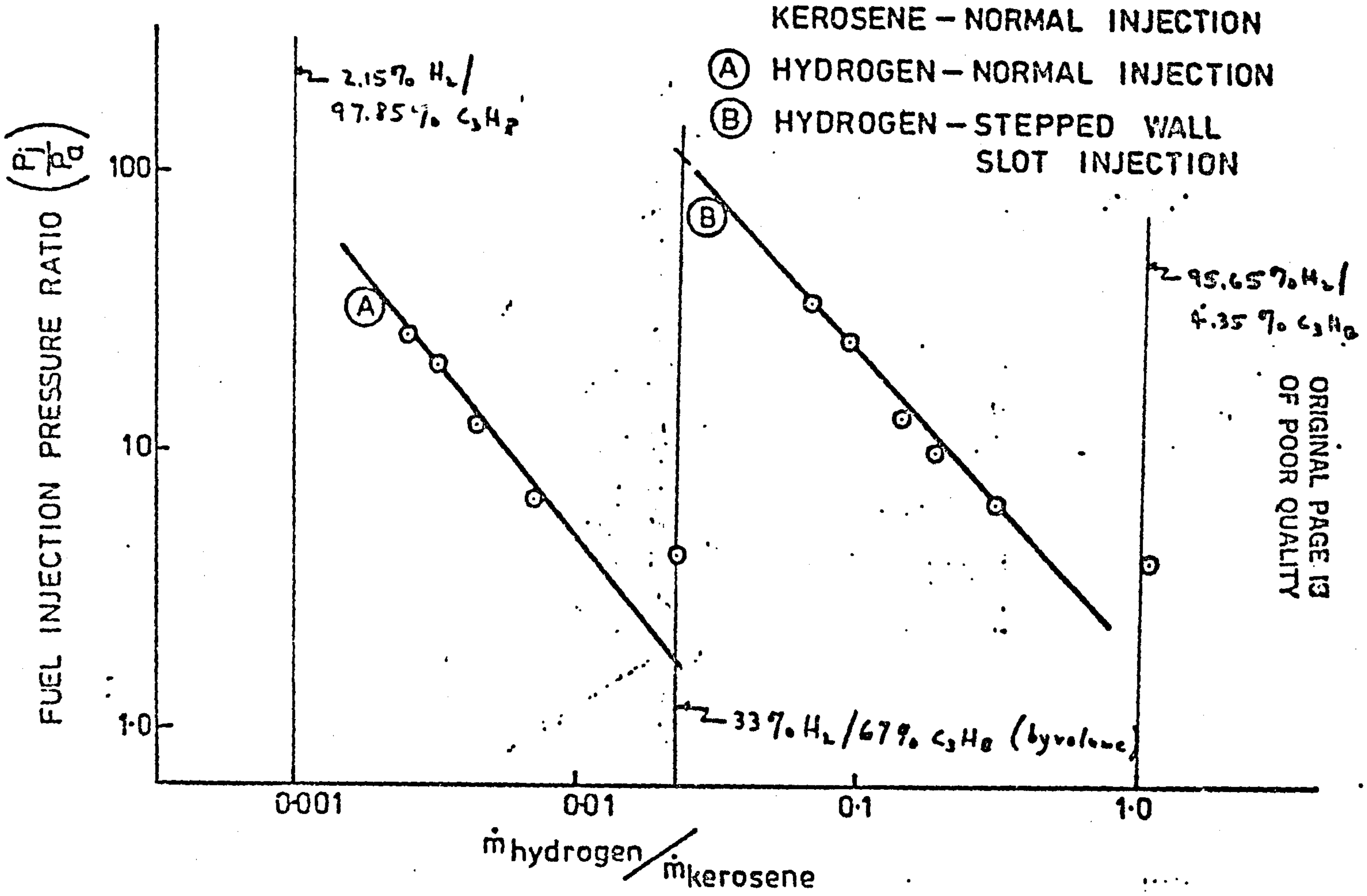

FIGURE 3. MINIMUM HYDROGEN FOR SUSTAINED COMBUSTION OF KEROSENE. (COOKSON)

ORIGINAL PAGE IS OF POOR QUALITY

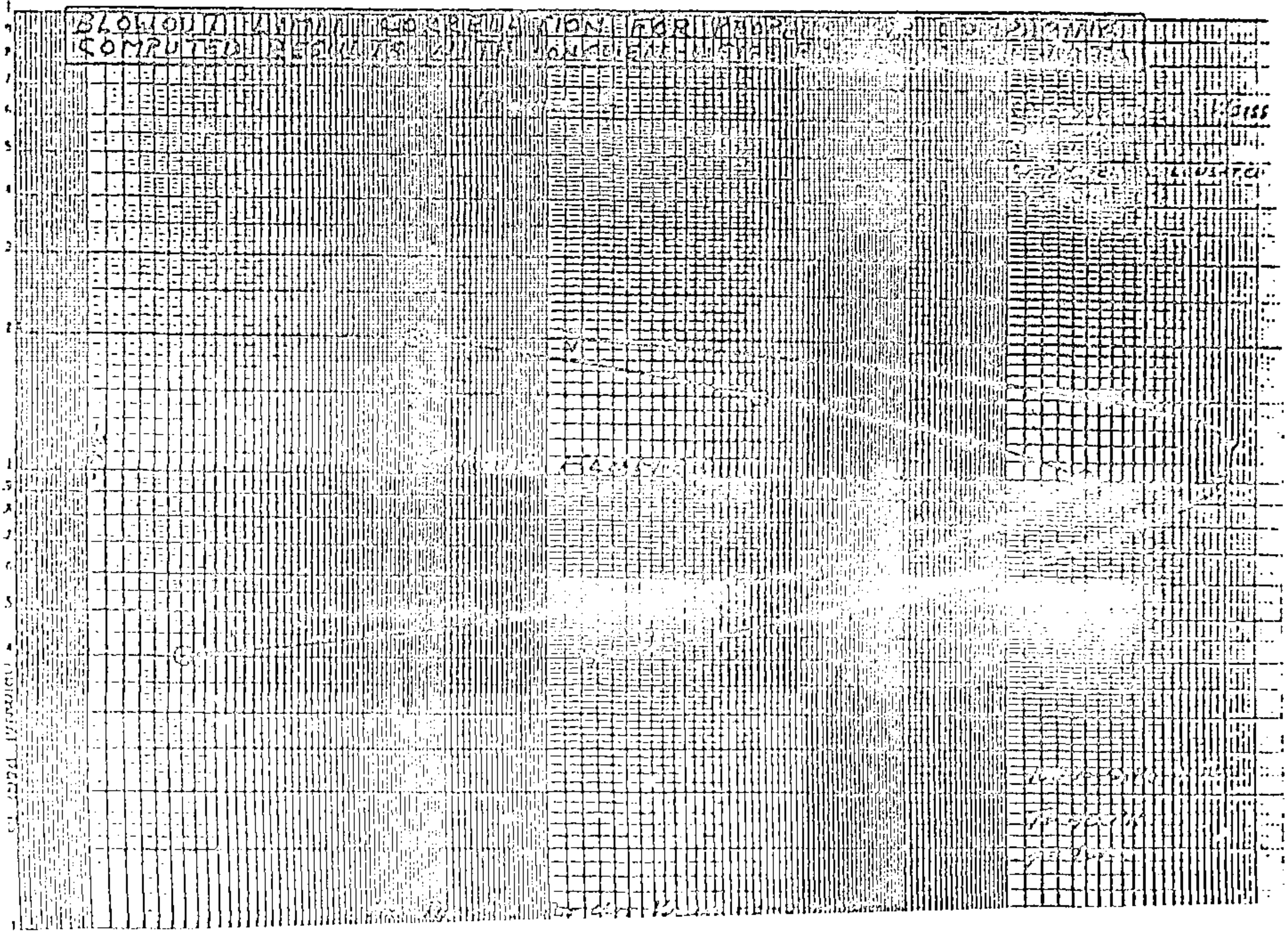
BLOWOUT
EVALUATION FOR
COMPUTED

C_3H_8

600°K
1 ATM

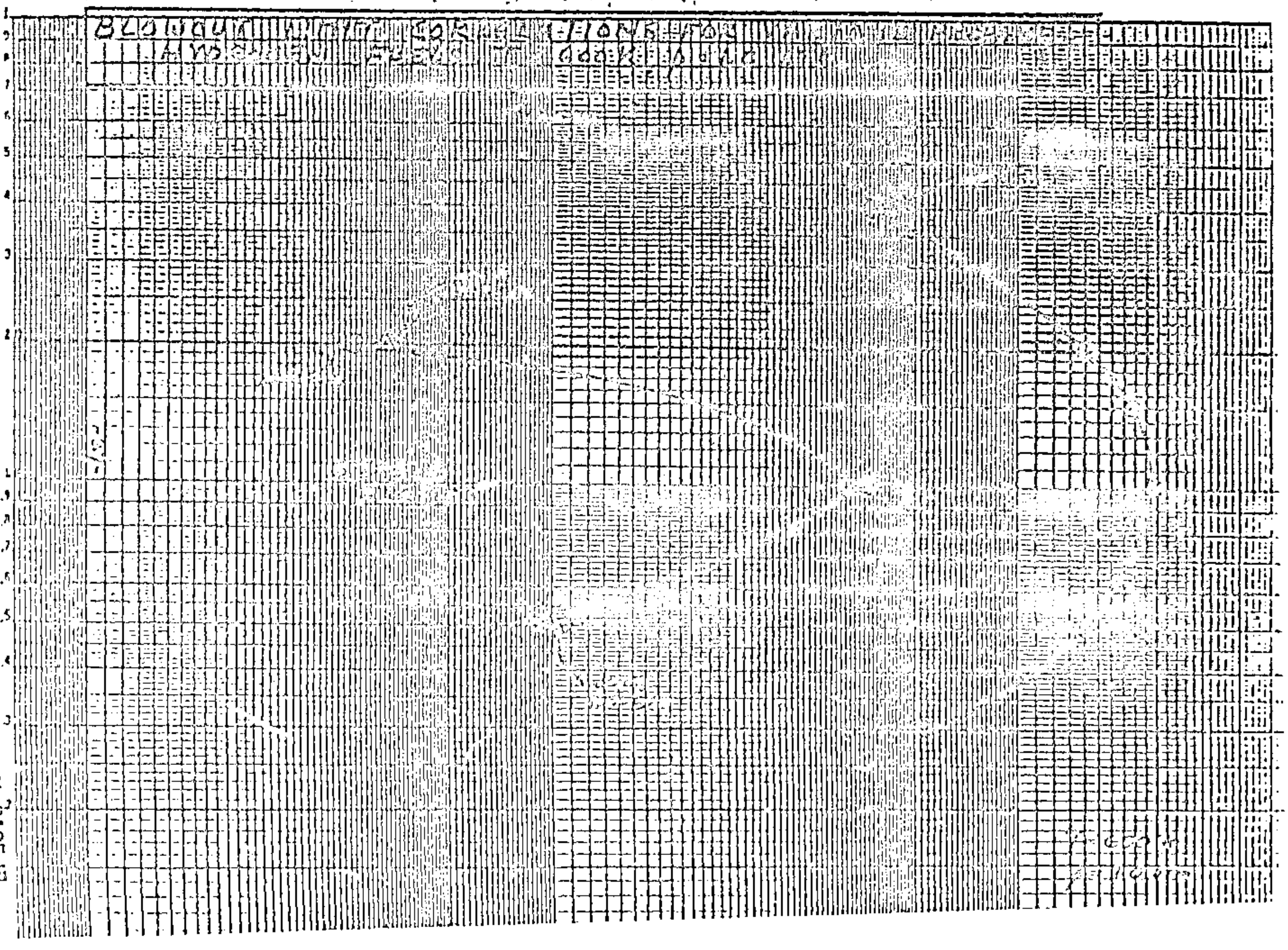

C_3H_8 1800°K
10 ATM

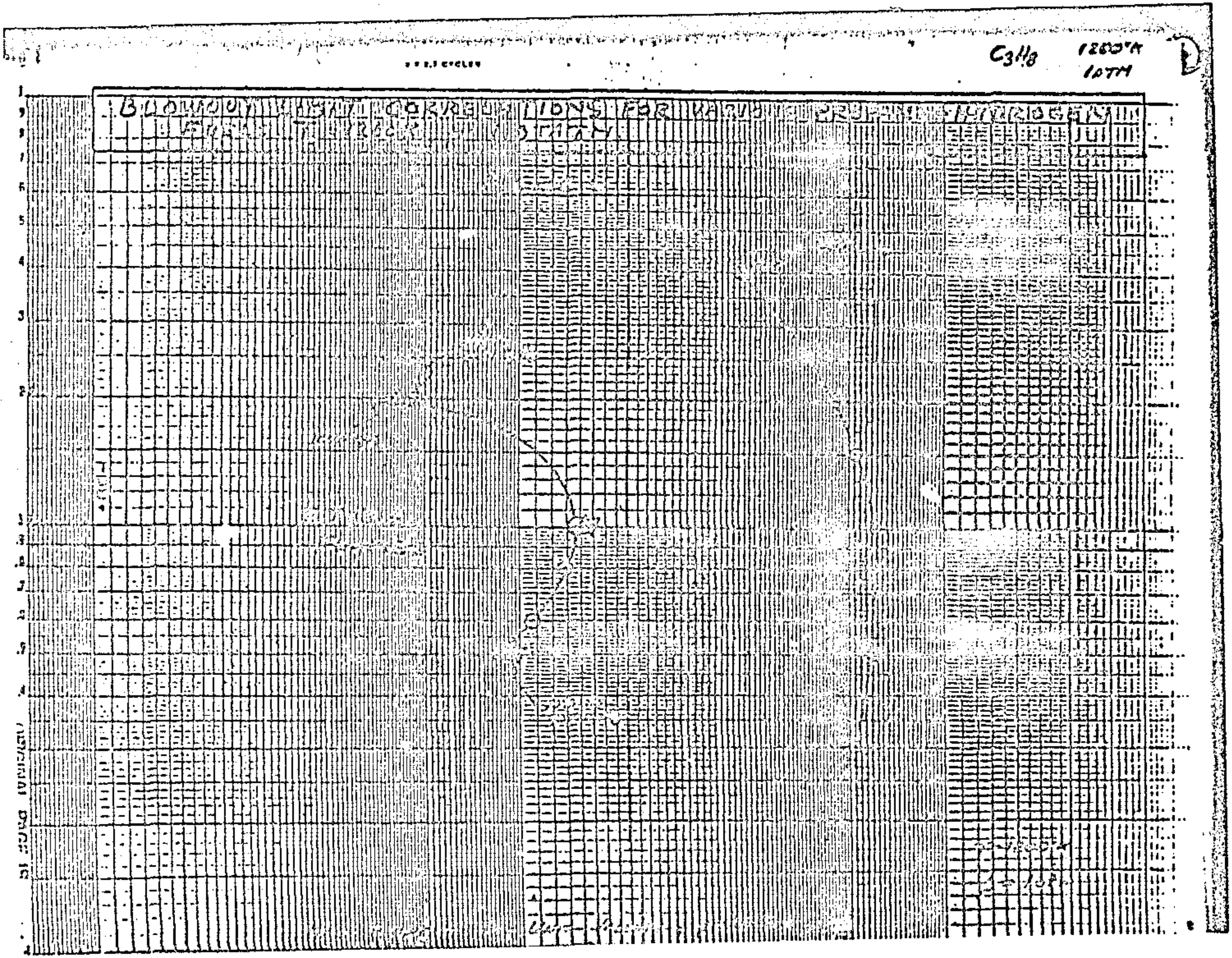

CH4 605°F 1 ATM

④

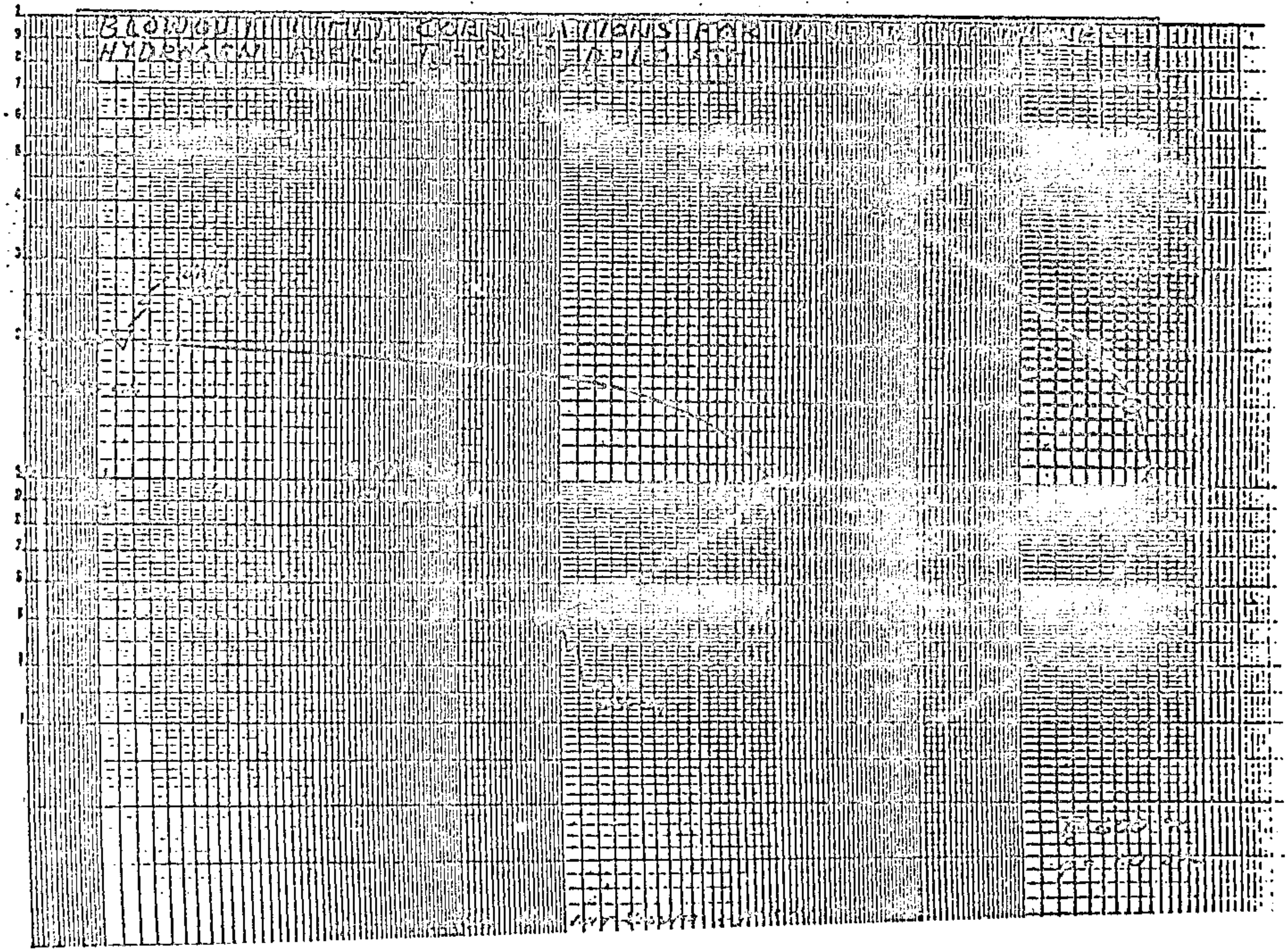

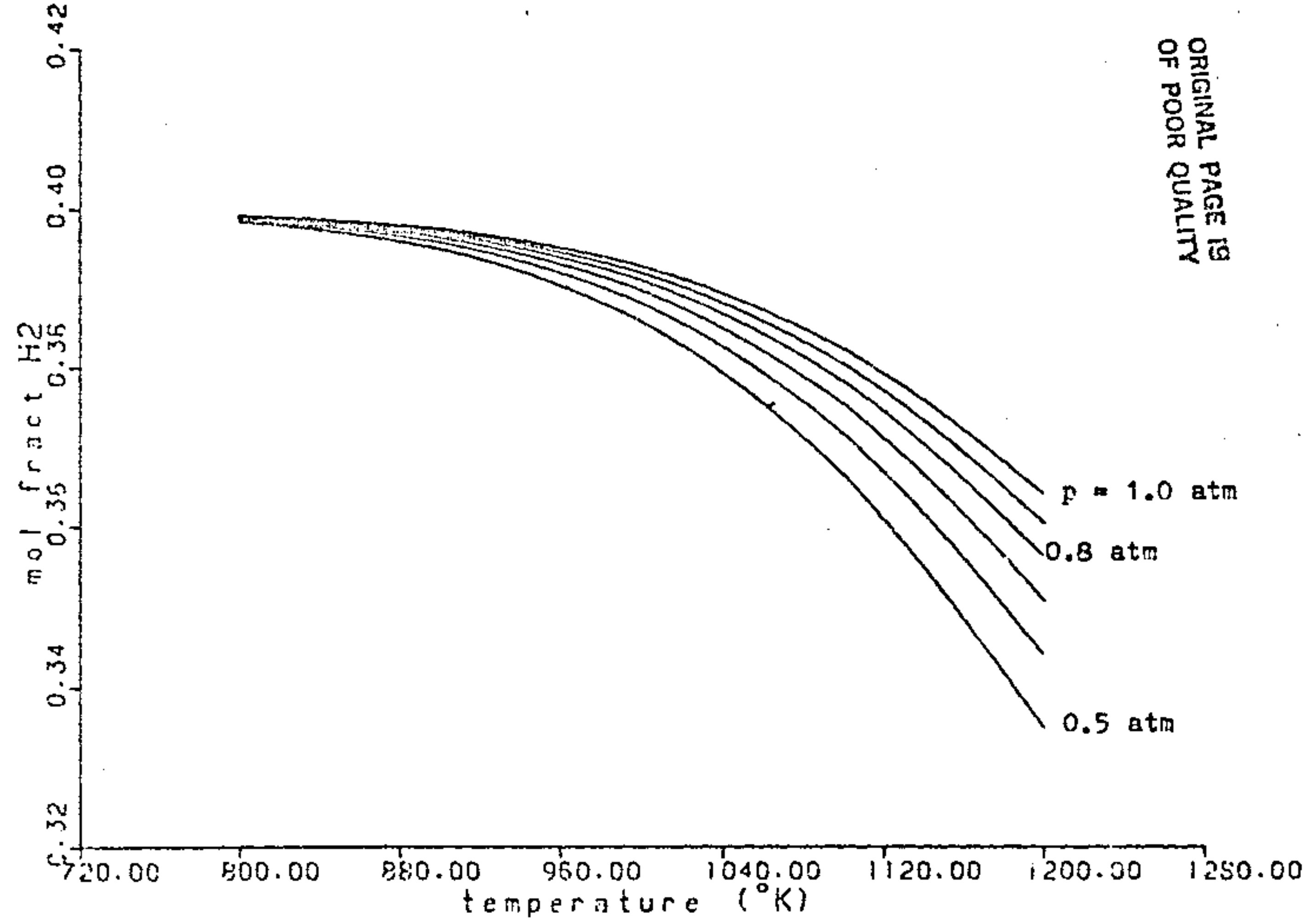

Figure 8. Hydrogen mole fraction versus temperature.

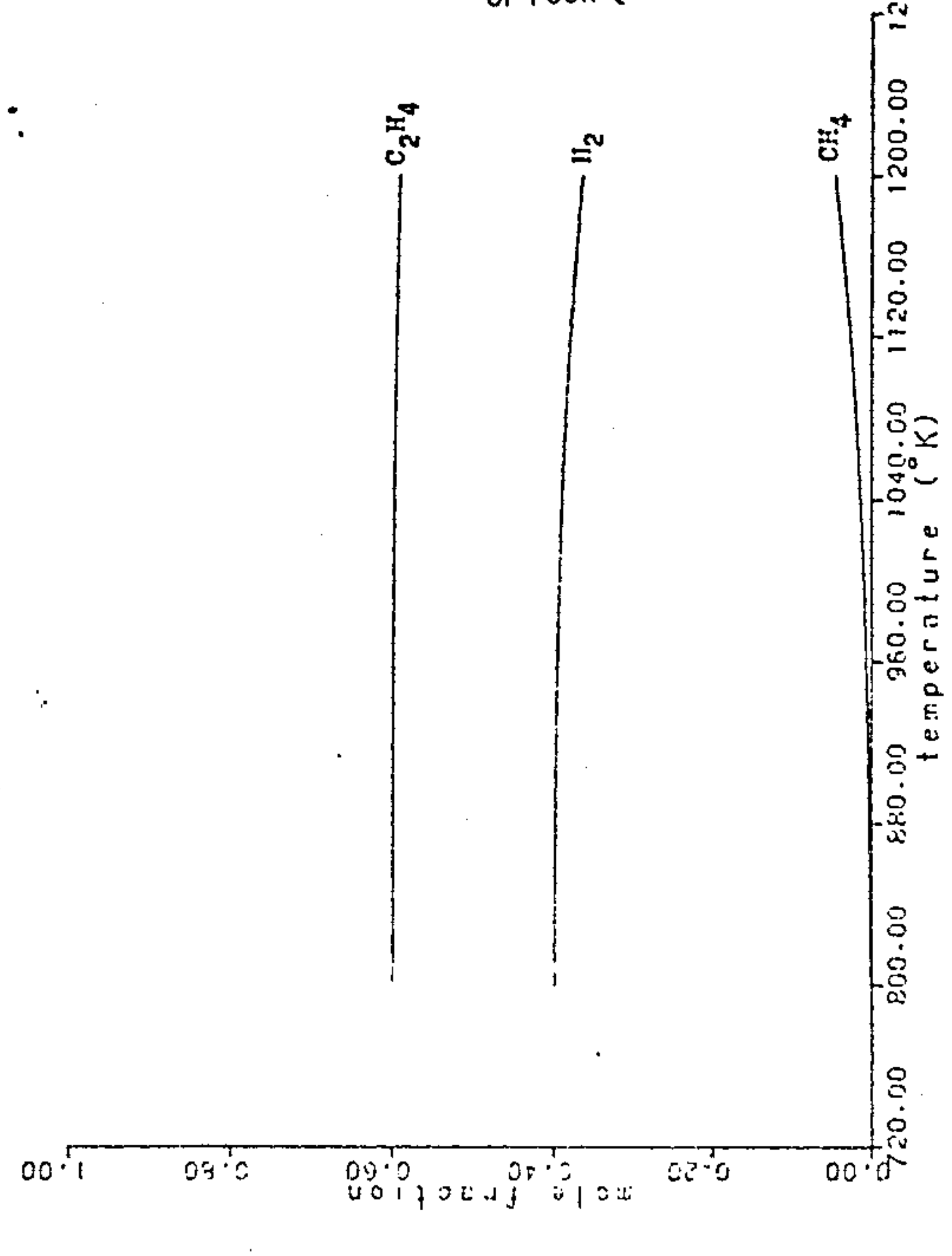

Figure 9. Equilibrium mole fractions versus temperature.

4. INVESTIGATION OF THE RANGES OF APPLICABILITY OF CHEMICAL KINETIC MODELS OF HYDROGEN-AIR COMBUSTION

This section is an upgraded and refined version of Section 4 in our previous Semi-Annual Status Report and represents a final report on this subject.

4.1. Introduction

4.1.1 Motivation for the Present Study

The study of hydrogen-fueled supersonic combustion ramjets (scramjets) has been a major part of the research programs of the Hypersonic Propulsion Branch at the Langley Research Center. Scramjets take advantage of high flight Mach numbers (greater than 5) to achieve propulsion efficiencies greater than that of ramjet engines.[1] Propulsion efficiency is a measure of the thrust energy out divided by the combustion energy in. Due to the great flight speeds of scramjets (Mach numbers range from 4 to 7), there are time constraints for combustion within a combustor of reasonable size.

As a result of these time constraints, minimal ignition delay times are desirable. Figure 1 shows a plot of the log of the ignition time versus initial temperature for various fuels. Hydrogen fuel has a very low ignition delay time relative to hydrocarbon fuels. It is this low ignition delay time which makes hydrogen a valuable fuel for scramjets. It becomes a necessity, therefore, to study in detail hydrogen-air combustion.

Most studies, thus far, have been experimental investigations. This dependence on empirical results is due to the complexity of the flow around fuel injectors with three-dimensional geometries, which are not easily treated analytically. Numerical solutions have generally been restricted to two- or three-dimensional parabolic flow with oversimplified chemistry models of the H_2-air system. These numerical solution schemes are applicable only in the parabolic flow region well downstream of the disturbance caused by the transverse fuel injection used by scramjet combustors in order to achieve rapid mixing and reaction. A priori knowledge of the extent of fuel mixing, ignition, and reaction is required to initiate calculations.

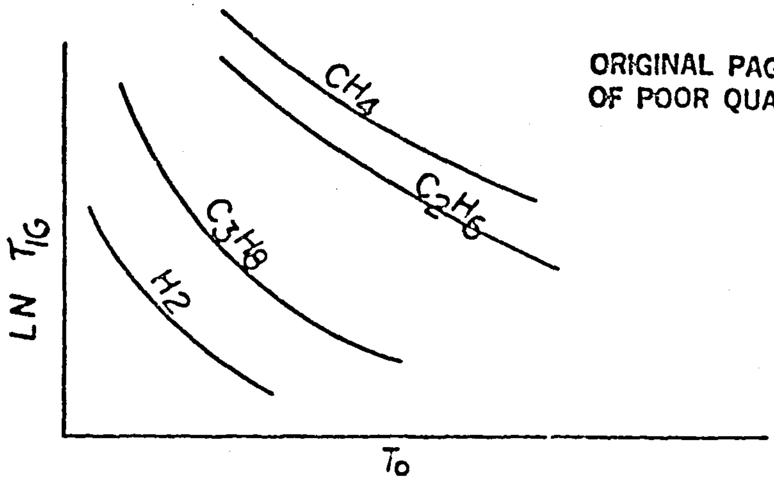

FIGURE 1 IGNITION DELAY TIME VS. INITIAL TEMPERATURE

In spite of the difficulty in obtaining quantitative information, a sufficient data base has been established to define a scramjet engine concept and to permit fabrication of subscale engine models with integrated inlet, combustor, and nozzle components. The current scramjet is designed to operate at stagnation temperatures between 900°K and 2200°K[2] which correspond to a flight Mach number range from 4 to 7. In ground tests of subscale engine models[3], however, problems were encountered in obtaining ignition and sustaining reaction at test conditions where ignition and sustained reaction were expected.

The need to better understand the chemical mechanism of the ignition and reaction of H_2-air mixtures at conditions typical of a scramjet combustor has led to many analytical studies. Most of the analytical studies at the Langley Research Center, as well as this present study, use a computer program (references 4 and 5) to solve flowing, chemical-kinetic, isobaric, stream-tube problems involving many chemical species. It is known that the computational time requirements for any computer program employing detailed chemical kinetics is proportional to the number of species and reactions being treated. It is the purpose of this effort to develop a method which reduces these numbers in the study of H_2-air combustion and at the same time preserve the correct physical-chemical behavior. The result of this work will be to reduce computer time and computer storage requirements. Methods for reducing computational times are presented in section two of this work.

4.2. Methods to Reduce Computational Times

The method proposed in this work to reduce computer run times is an extension and refinement of the method proposed by Chinitz in reference 9. This method involves the tracking of a "trigger" species which is used to determine whether the flow is in an "ignition" mode or in a "combustion" mode. Ignition and combustion are defined in the classical sense. Ignition delay time is taken to be the time required for the temperature increase to reach five percent of the overall temperature increase:

$$T_{ig} = T_o + 0.05(T_{eq} - T_o) \qquad (1)$$

When the temperature is less than the ignition temperature, the flow is in the "ignition" mode. Otherwise, the flow is in the "combustion" mode. (See Figure 2).

It will be shown that while an extensive chemical package is needed to describe the "ignition" mode, a smaller package is sufficient to deal with the "combustion" mode. Evans and Schexnayder[10] concluded that a 25-reaction scheme involving 12 species (designated 25(12) herein), was required to describe "ignition" processes, while an 8(7) sufficed to deal with the "combustion" mode. The work discussed herein describes efforts to minimize the computational time requirements once the "combustion" process is initiated (i.e. a smaller package or one that takes less computational time than the 8(7) system might suffice to deal with the "combustion" mode).

A 37(13) system is used as the "test" chemical-kinetic package (Table 1). Any smaller system is "tested" against the 37(13) system to see if the correct physical chemical behavior is preserved. This is accomplished in the following way.

First, the full 37(13) system is run from the initial state to equilibrium. Next, the test system is run from the point where the "combustion" in the 37(13) system initiates. The test system's initial values (pressure, temperature, equivalence ratio and chemical composition) are that of the 37(13) system's values at the point of "combustion". Temperature-time profiles and chemical behavior are compared (see Figure 3). If the difference between the 37(13) system and the test system is within an acceptable range, the test system will be sufficient to deal with the "combustion" process.

Graphs of the mass fraction of the trigger species versus time and ignition temperature versus mass fraction of the trigger species at ignition are made in accordance with reference 9. The cases from the 37(13) system serve as the data base.

An 8(7) system (Table 2) is tested to confirm the results of Evans and Schexnayder.[10]. The 8(7) system is run from the initial state to equilibrium to determine if there are any initial conditions where the 8(7) system describes the entire process (i.e. both ignition and combustion).

In order to further reduce computational times, a 2(5) global model (Table 3) developed by Rogers and Chinitz in reference 11 is tested. The method proposed in that paper must be altered to include the effects of pressure. The Arrhenius equation will have the form:

$$k_{fi} = A_i(\phi, \rho)T^{N_i}\exp(-E_i/RT) \quad (2)$$

The values of the paramaters may be different from those in reference 11 because they are fixed arbitrarily so that the 2(5) system describes the 37(13) system.

Lastly, the so-called "partial equilibrium" assumption of reference 12 is examined in connection with an 8(7) system in an effort to minimize computational times. The 8(7) mechanism consists of the following reactions:

$$
\begin{array}{lclr}
H_2O + O & = & OH + OH & \text{(i)} \\
H_2O + H & = & OH + H_2 & \text{(ii)} \\
O_2 + H & = & OH + O & \text{(iii)} \\
H_2 + O & = & OH + H & \text{(iv)} \\
\hdashline
H_2O + M & = & H + OH & \text{(v)} \\
H_2 + M & = & H + H + M & \text{(vi)} \\
O_2 + M & = & O + O + M & \text{(vii)} \\
OH + M & = & O + H + M & \text{(viii)}
\end{array}
$$

During the ignition delay period, all eight reactions play a role; however, in the "combustion" mode, the bimolecular shuffle reactions occur so rapidly in both directions that under some conditions they may be basically in equilibrium. The "partial equilibrium" assumption takes ractions (i)-(iv) to be in equilibrium (infinitely fast reaction rates), while reactions (v)-(viii) continue to occur at a finite rate.

Infinitely fast reaction rates can be approximated by assigning very large values to the preexponential factor in the forward reaction rate constant (e.g. 10^{50}). The backward reaction rate constant is then very large to satisfy $K = k_f/k_b$ The values of the preexponential factors of reaction (i) to (iv) are determined so that the system describes the "combustion" process.

To obtain these results, 45 one-dimensional, constant pressure, H_2-air computations were performed in the ranges:

$$0.5 \leq \phi \leq 1.5$$

$$850 \leq T \leq 1200$$

$$0.5 \leq p \leq 1.0$$

where ϕ is the equivalence ratio, T is the temperature in °K, and p is the pressure in atmospheres. A listing of these individual cases is given in Table 4. Comparison of the computational times are then made and recommendations are discussed.

4.3. Results and Discussion

4.3.1 Summary

All 45 cases in Table 4, as well as the nine cases marked with an exclamation point, were performed on the 37(13) and 8(7) systems, respectively, in both the ignition and combustion modes. In addition, the 15 cases marked with an asterisk were tested on the 8(7) system, the global model, and the "partial equilibrium" model starting at the ignition point. These 15 cases were selected to encompass the entire range of interest.

What follows are the results of these test cases. First, the results from the 37(13) system including the "trigger" concept are presented. Next, the 8(7) system in its entirety and in the combustion mode alone is discussed. Global and partial equilibrium results in the combustion mode follow. Lastly, temperature-time profiles and computational times are compared for all four systems.

4.3.2 The 37(13) System

4.3.2.1 Temperature-Time Profiles

45 cases were run to serve as a basis of comparison for the test systems described

previously. Sufficient data points were obtained for all cases and each case yielded a characteristic S-shaped curve for the temperature versus time profile. For each case, it was necessary to obtain a data point at the ignition temperature, defined in the classical sense as 5% of the temperature rise from the initial state to the final equilibrium state, in order to set initial conditions for the test cases. Problems arose, however, when trying to pinpoint the ignition temperature. As a result, satisfactory ignition conditions could not be calculated for nine cases due to time constraints. These cases were omitted from data base and the remaining 36 cases are given in Table 5 with corresponding ignition temperature, time, and mass fraction of OH.

Tables 4 and 5 show that the ignition delay time is a function of initial temperature, pressure, and equivalence ratio. This function is complicated since it is inversely proportional to initial temperature, nearly independent of equivalence ratio except at low temperatures (850°K and 900°K), proportional to pressure at temperatures of 850°K and 900°K, and is inversely proportional to pressure at temperatures greater than or equal to 1000°K in the ranges studied. These results are similar to the results reported by Rogers and Schexnayder (reference 2) in their extensive study which included 60 reactions and 20 species. Since the results are similar to those of Rogers and Schexnayder, the 37(13) system serves as a good basis for the remaining systems to be compared with.

4.3.2.2 The "Trigger" Concept

In order to test systems in the "combustion" mode it is necessary to determine when the transition to the "combustion" mode takes place. It was to this end that the concept of a "trigger" species was first proposed by Chinitz in reference 9. The concept involes the tracking of the mass fraction of one of the species. When its value becomes greater than a preset value, the system is said to be in the "combustion" mode.

There are several requirements for a species to serve as an effective trigger from ignition to combustion. The concentration of an effective trigger species must be single-valued (the value of the mass fraction at the ignition point is not again obtained) and undergo a sufficiently large change during the ignition process that its crossover into the combustion mode is unmistakeable. It was believed that the hydroxyl radical, OH, would serve that purpose.

Results here confirm the work of reference 9. Table 6 and Figure 4 show how the mass fraction of OH varies with time for a representative case (case number 23). It is easily seen that OH has all the requirements to serve as the trigger species. The ignition point is well-defined and is single-valued.

It is of interest to estimate the trigger point for all values of equivalence ratio, pressure, and temperature studied. A plot of the ignition temperature vs the mass fraction for OH at the ignition point is shown in Figure 5. A least-squares linear fit of $\ln T_{ig}$ is $Y_{OH_{ig}}$ was determined to be

$$\ln T_{ig} = 0.085 \ln Y_{OH_{ig}} + 7.65 \quad (3)$$

This linear relationship predicts values within a factor of 2.5 (generally well within) for all pressures and equivalence ratios examined. This provides a large advantage over the non-linear relationship developed in reference 9 which was limited to an equivalence ratio of 1. With the selection of a trigger species whose value can be estimated, the test systems can now be examined.

4.3.3 The 8(7) System

4.3.3.1 Ignition and Combustion

The 8(7) sytstem was run from time zero to equilibrium for the nine cases marked with an exclamation point in Table 4. Five of these cases (3, 6, 9, 12, 15) represent a set of constant pressure, constant equivalence ratio conditions with varying initial temperature. These were selected to determine how the initial temperature affects the ignition delay time when compared to the 37(13) system. The remaining four cases (13, 22, 25, 29) were arbitrarily picked in an attempt to see the effects of pressure and equivalence ratio.

Figures 6-10 show a comparison of temperature-time histories for the 37(13) and 8(7) systems for cases 3, 6, 9, 12, 15, respectively, in both the ignition and combustion modes. Figures 6 and 7 show the delay time to be more than an order of magnitude lower for the 8(7) system at low temperature. Figures 8-10, however, show that the delay time for the 8(7) system is greater than the 37(13) system at higher temperatures. It is therefore concluded that a transition takes place between an initial temperature of 900°K and 1000°K. (It should be noted that a ten percent mixture of hydrogen in air has an ignition temperature of between 893°K and 1020°K[13]).

Figure 11 shows a plot of ignition delay time vs. $1000T_o^{-1}$ for the 8(7) and 37(13) systems at a pressure of one atmosphere and an equivalence ratio of 0.5. The two curves cross at a temperature of 970°K where their ignition delay times are equal.

These results imply that for any constant pressure and constant ϕ there is a T_o for which the two systems have the same ignition delay time. At these conditions, the 8(7) system can describe the 37(13) system in both the ignition and combustion modes. It also might be expected that at temperatures away from this particular initial temperature, the 8(7) system might lag behind or proceed ahead of the 37(13) system when tested at ignition conditions in the "combustion" mode.

The remaining four cases all had initial temperatures at or above 1000°K. The results of these cases were again that the delay time was higher for the 8(7) system than that of the 37(13) system. No significant effects of pressure or equivalence ratio were found in these limited case. The 8(7) system was now tested in the "combustion" mode with a focus on the effect of initial temperature.

4.3.3.2 The "Combustion" Mode

The 15 cases marked with an asterisk in Table 4 were run for the 8(7) system in the "combustion mode." For all pressures, temperatures, and equivalence ratios studied, the 8(7) system had a higher equilibrium temperature than that of the 37(13) system. This result was expected in that the 8(7) system neglects nitrogen dissociation. It was also found that for all conditions, the 8(7) system lagged behind the 37(13) system after the ignition point then equaled and surpassed the 37(13) curve (see Figure 12). This result was contrary to the expectations of section 4.3.2.1. It was thought that for some initial temperatures the 8(7) system would reach equilibrium more equickly than the 37(13) system. This, however, was not the case.

The amount of lag, however, was found to be a function of the relationship between the actual ignition temperature and the ignition temperature calculated from equation 1 (designated herein as "classical" ignition temperature). If the ignition temperature used (and also all other initial conditions) was between the initial temperature and the classical ignition temperature, then the 8(7) system described the 37(13) system very well. If the temperature used was greater than the classical ignition temperature, there was an appreciable lag (see Figure 12). Therefore, as the difference between the initial temperature and ignition temperature used increased, the lag became greater. No cases were found where the 8(7) system reached equilibrium more quickly than the 37(13) system. It is concluded, therefore, that ignition temperatures lower than the classical ignition temperature should be used. It was not determined what percent below five percent should be used.

4.3.4 The Global Model

The global model in Table 3 was first proposed in reference 11. The reaction rate constant for each reaction is adjusted so that the global model describes the 37(13) system in the combustion mode.

Before determining these adjusted rate constants, it was useful to observe how varying each rate constant affected the temperature-time profile. It was observed that increasing k_{f4} (the subscript 4 refers to the first reaction; subscript 5 refers to the second reaction using the notation in reference 11) slows down the reaction. This was referred to as a "lagging" system in the previous section. Increasing k_{f5} speeds up the reaction. The system is very sensitive to an increase or decrease in k_{f5} while being rather insensitive to a variation in k_{f4}. It was decided to fix Ni and Ei at the same values as in reference 10; namely,

E_4 = 4865 cal/mol
N_4 = -10
E_5 = 42,500 cal/mol
N_5 = -13

Due to the insensitivity of the system to k_{f4}, it was also decided that A_4 could be retained as in reference 11:

$$A_4(\phi) = (8.917\phi + 31.433)\phi - 28.950) \times 10^{47},\ \text{cm}^3/\text{mol}\cdot\text{s}. \quad (4)$$

It should be noted that A_4 is a function of ϕ only.

The effect of pressure, which was neglected in reference 11, was included in the determination of A_5. As a result, A_5 is a function of pressure and equivalence ratio and has the form $A_5(\phi, p)$. The sensitivity of the system to k_{f5} permitted substantial changes to be made to the temperature profiles produced by the global system.

Table 8 shows the values of A_4 and A_5 determined in order to describe the temperature-time profile required. Figure 13 shows a plot of A_4 (which is independent of pressure) vs. ϕ. Figure 14 shows plots of A_5 vs. pressure for various ϕ's.

As other authors have reported, large discrepancies exist between results for equivalence ratios less than or greater than one. The relationship between A_5 and pressure and equivalence ratio must be broken up into two equations for the ranges studied:

For $\phi \geq 1$

$$A_5 = \left(8.80 + 5.85/\phi - 3.67\phi - 4.80p - 3.20p/\phi + 2.00p\cdot\phi\right) \times 10^{64} \qquad (5$$

For $\phi < 1$

$$A_5 = 0.67\phi^{-1\ 5}p^{-0.7}\ (8.80 + 5.85/\phi - 4.80p - 3.20p/\phi + 2.00p\phi) \times 10^{64} \qquad (6$$

These equations predict values of A_5 to within 10% for the ϕ's studied..

In all cases, the global mode lags behind the 37(13) system for a short period following ignition. Then the global model equals and exceeds the 37(13) system and reaches equilibrium (see Figure 15). The equilibrium temperature of the global model should be higher than that of the 37(13) system due to dissociation.

This again, however, is controlled by the ignition temperature used by the global model. If the ignition temperature used is greater than the classical ignition temperature, then the equilibrium temperature is less than the classical ignition temperature. If the ignition temperature is less than the classical, then the equilibrium temperature reached is greater than the 37(13) system as expected.

Initial temperature also has an effect on the accuracy of the global model. As the initial temperature increases, the difference between the global model and the 37(13) system increases. No effect on pressure or equivalence ratio was found.

The global model predicts very well the temperature-time profile of the 37(13) system. These results, however, show the importance of the ignition temperature used. It is suggested that ignition temperature be a variable to be tested in future work. Nonetheless, the global model shows promise in accurately reproducing temperature-time profiles with a minimum of computational time and computer storage requirements.

4.3.5 The "Partial Equilibrium" Assumption

The "partial equilibrium" assumption is already in use in combustion analysis; however its applicability to this present study in the ranges of interest has not been determined. This assumption states that the bimolecular shuffling reactions occur so rapidly that the are basically in equilibrium. If this is the case, the kinetics equations can be replaced by the algebraic laws of mass action as discussed in reference 12. Therefore, a number of partial differential equations are replaced by algebraic equations and the remaining partial differential equations are simplified. If appropriate criteria are specified as to when this assumption is applicable, computer running times will be greatly reduced.

It was to this end that an approximation to the "partial equilibrium" assumption was tried. Instead of incorporating algebraic equations into the computer program, infinitely fast reaction rates would be approximated by using extremely large numbers (on the order of 10^{50}) for the preexponential factor. It was anticipated that this would sufficiently approximate the "partial equilibrium" assumption.

Substantial numerical difficulties arose in trying the approximation. First, the largest preexponential factors that could be used were of the order of 10^{24}. Still, this was at least 5 orders of magnitude greater than any other preexponential factors, Next, the precision of the program needed to be upgraded two orders of magnitude by adjusting the

EMAX parameter. Finally, this approach produced erroneous results such as temperatures exceeding the equilibrium temperature when the Gear integration procedure was used. The slower Adams method was then used which gave results which were physically plausible. Due to these problems, running times were very long. This was not the main concern, however. Rather, the primary goal was to test the partial equilibrium assumption against the 37(13) system in the ranges studied.

Figures 16-30 show how the approximation to the "partial equilibrium" assumption compared to the 37(13) system. For low temperatures (850°K, 900°K) and for all cases with an equivalence ratio of 0.5, the partial equilibrium assumption reproduced the 37(13) curve well. In the remaining cases, however, the assumption did not approximate the profile accurately. The shape of the curve was not even preserved.

It appears that the approach to approximating the "partial equilibrium" assumption has a narrow region of validity; namely, low initial temperatures and low equivalence ratios. As stated before, no conclusion can be drawn about the assumption itself. It is suggested that future work include the incorporation of algebraic laws of mass action into the computer program to more precisely determine the validity of the assumption.

4.3.6 Comparison of the Four Systems

4.3.6.1 Temperature-Time Profiles

Figures 16-30 show a comparison of the 37(13) systems for the 15 cases marked with an asterisk in Table 4. The ignition mode of all 15 cases is that of the 37(13) system which continues in the combustion mode. The test systems start at the ignition point and reach an equilibrium temperature different from the 37(13) system.

The lag of the 8(7) system is shown in these figures. The lag is more a function of the relationship between the ignition temperature used and the classical ignition temperature than the initial temperature, pressure, or equivalence ratio. The 8(7) system reproduces the temperature-time curve very well, as expected.

The inital lag and eventual higher equilibrium temperature of the global model is shown in all 15 cases. Initial temperature has a substantial effect on the accuracy of the global mode. As the initial temperature increases, the temperature differences between the global model and the 37(13) curves become large. These perhaps could be corrected by starting the global model at a different ignition temperature.

Partial equilibrium curves accurately reproduced the temperature-time curves for cases 2, 4, 9, 11, 15, 18, 20 and 31. This suggests that the partial equilibrium assumption might suffice at lower initial temperatures and equivalence ratios. The numerical difficulty in obtaining these results sheds uncertainty on this conclusion.

Figures 31 and 32 represent the results of using an ignition temperature higher than the classical one to cases 11 and 15, respectively. The 8(7) system is observed to lag behind the 37(13) system to a greater extent than usual. The global model, in fact, has an equilibrium temperature which is 200 degrees below normal. These figures reinforce the importance in the selection of initial conditions for any test system.

4.3.6.2 Computational Time

Results of the average computational times for the various systems are shown in Table 9. The global model has the lowest computational time as expected, with an average time of approximatley 1/8 that of the 37(13) system. Excessive computational time of the partial equilibrium system was related to the relatively high reaction rate constants employed, the use of the Adams method rather than the Gear method, and the precision which was required to perform "partial equilibrium" calculations.

4.4. Conclusions and Recommendations

4.4.1 Summary

A data base, in the ranges of initial temperature between 850°K and 1200°K, pressure between 0.5 and 1.00 atmospheres and equivalence ratio between 0.5 and 1.5, was established with the 37(13) system serving as the basis. Due to the large amount of data produced, it is necessary to clarify these results. First, these results are summarized. Next, conclusions are enumerated. Finally, recommendations for future work are given.

The first part of the work was selecting a good trigger species. It was concluded that the hydroxyl radical, OH, serves as an effective trigger. The value of the mass fraction of OH at ignition can be estimated in the ranges studied within a factor of 2.5 (generally well within) according to equation 32.

Next the 8(7) system was studied in the "ignition" and "combustion" modes together and then in the "combustion" mode alone. It was concluded that a transition takes place between an initial temperature of 900°K and 1000°K (at a pressure of one atmosphere and an equivalence ratio of 0.5) where the ignition delay time of the 8(7) system switches from less than to greater than the 37(13) system. It was further concluded that at an equivalence ratio of 0.5, pressure of 1.0 atmosphere and initial temperature of 970±30°K the 8(7) system can approximate the temperature-time profiles of the 37(13) system in both the ignition and combustion modes. It is recommended that future work include the investigation of conditions where the 8(7) system can describe the 37(13) system in both modes.

In the combustion mode alone, the 8(7) system reproduces the temperature-time profiles very well for all cases studied. The variables which were major factors in the accuracy of these profiles were the temperatures and species' concentrations used at ignition. If the temperature used was less than, but close to, the classical ignition temperature, then the profiles were very accurate. If, however, the temperature used was greater than the classical ignition temperatures, then the 8(7) system lagged behind the 37(13) system somewhat. Future work, should include the investigation of this phenomenon.

Next, the global model was studied in the combustion mode. Preexponential factors were determined with a rather large discrepancy between results for an equivalence ratio less than or greater than one. For all cases, the global model lags behind the 37(13) system initially then exceeds it at equilibrium. Two variables had an effect on the accuracy of this model. First, the conditions used at ignition had a substantial effect on accuracy again. A lag was produced by using a temperature greater than the classical ignition temperature. Secondly, as the initial temperature increases the accuracy of the global model decreases.

Finally, an approximation to the "partial equilibrium" assumption was tried. Numerical difficulties arose in the execution of this approximation. Nonetheless, it was concluded that at low temperatures and low equivalence ratios the approach to approximating the partial equilibrium assumption is valid. No conclusions could be drawn about the "partial equilibrium" assumption itself.

Results for the various systems show the global model to have the lowest average computational time followed by the 8(7) system, the 37(13) system, and the "partial equilibrium" model. The two-step global model has a computational time of approximatley 1/8 that of the 37(13) system.

4.4.2 Conclusions

The following conclusions can be drawn based on the results of this study:

(1) The hydroxyl radical, OH, serves as an effective trigger species.

(2) A transition takes place between 900°K and 1000°K (at a pressure of 1 atmosphere and an equivalence ratio of 0.5) where the ignition delay time of the 8(7) system switches from less than to greater than the 37(13) system.

(3) At a pressure of one atmosphere, an equivalence ratio of 0.5 and an initial temperature of 970±30°K the 8(7) system can accurately approximate the temperature-time profile of the 37(13) system in both the ignition and combustion modes.

(4) For all cases, the 8(7) system describes the 37(13) system very well in the combustion mode.

(5) A lag is produced in the 8(7) and global models when using ignition temperatures greater than the classical ignition temperature.

(6) The global model satisfactorily reproduces the temperature-time profiles of the 37(13) system with a minimum of computational time and computer storage requirements.

(7) As the initial temperature increases, the accuracy of the global model decreases.

(8) No conclusions can be drawn concerning the "partial equilibrium" assumption.

(9) The approach to approximating the "partial equilibrium" assumption has a narrow region of validity; namely, low initial temperatures and low equivalence ratios.

(10) The global model can approximate the 37(13) system with an average of 1/8 the computational time.

4.3 Recommendations

Based on the results of this study, the following recommendations are made for future work:

(1) Investigate conditions where the 8(7) system can accurately describe both the ignition and combustion processes.

(2) Study the effects of varying ignition conditions; namely, above and below the classicial ignition temperature. This will show the relationship between ignition conditions and the lag of the system.

(3) Continue to investigate the two-step global model as it seems to have the most promise in reproducing temperature-time profiles with a minimum of computational time.

(4) Incorporate the algebraic laws of mass action into the computer program to more precisely determine the validity of the "partial equilibrium" assumption.

Table 1 - 37(13) System

REACTION NUMBER							
1	M	+	1*O2	=	1*O	+	1*O
2	M	+	1*H2	=	1*H	+	1*H
3	M	+	1*H2O	=	1*H	+	1*OH
4	1*H	+	1*O2	=	1*HO2	+	M
5	M	+	1*NO2	=	1*NO	+	1*O
6	M	+	1*NO	=	1*N	+	1*O
7	M	+	1*H2O2	=	1*OH	+	1*OH
8	M	+	1*O3	=	1*O2	+	1*O
9	1*O	+	1*H	=	1*OH	+	M
10	1*H2O	+	1*O	=	1*OH	+	1*OH
11	1*H2	+	1*OH	=	1*H2O	+	1*H
12	1*O2	+	1*H	=	1*OH	+	1*O
13	1*H2	+	1*O	=	1*OH	+	1*H
14	1*H2	+	1*O2	=	1*OH	+	1*OH
15	1*H	+	1*HO2	=	1*H2	+	1*O2
16	1*H2	+	1*O2	=	1*H2O	+	1*O
17	1*H	+	1*HO2	=	1*OH	+	1*OH
18	1*H2O	+	1*O	=	1*H	+	1*HO2
19	1*O	+	1*HO2	=	1*OH	+	1*O2
20	1*OH	+	1*HO2	=	1*O2	+	1*H2O
21	1*H2	+	1*HO2	=	1*H2O	+	1*OH
22	1*HO2	+	1*H2	=	1*H	+	1*H2O2
23	1*H2O2	+	1*H	=	1*OH	+	1*H2O
24	1*HO2	+	1*OH	=	1*O	+	1*H2O2
25	1*HO2	+	1*H2O	=	1*OH	+	1*H2O2
26	1*HO2	+	1*HO2	=	1*H2O2	+	1*O2
27	1*O	+	1*O3	=	1*O2	+	1*O2
28	1*O3	+	1*NO	=	1*NO2	+	1*O2
29	1*O3	+	1*H	=	1*OH	+	1*O2
30	1*O3	+	1*OH	=	1*O2	+	1*HO2
31	1*O	+	1*N2	=	1*NO	+	1*N
32	1*H	+	1*NO	=	1*OH	+	1*N
33	1*O	+	1*NO	=	1*O2	+	1*N
34	1*NO2	+	1*H	=	1*NO	+	1*OH
35	1*NO2	+	1*O	=	1*NO	+	1*O2
36	1*HO2	+	1*NO	=	1*2O	+	1*OH
37	1*O3	+	1*HO2	=	2*O2	+	1*OH

N_2 is an inert species

TABLE 2 - 8(7) SYSTEM

REACTION NUMBER	REACTION						
1	M	+	O2	=	O	+	O+M
2	M	+	H2	=	H	+	H+M
3	M	+	H2O	=	H	+	OH+M
4	M+O	+	H	=	OH	+	M
5	H2O	+	O	=	OH	+	H
6	H2	+	OH	=	H2O	+	H
7	O2	+	H	=	OH	+	O
8	H2	+	O	=	OH	+	H

N_2 is an inert species

TABLE 3 - 2 STEP GLOBAL MODEL

$$H2 + O2 \xrightarrow{k_{f4}} 2*OH \qquad (1)$$

$$2*OH + H2 \xrightarrow{k_{f5}} 2*H2O \qquad (2)$$

N_2 is an inert species

TABLE 4 - 45 CASES

CASES	ϕ	p, atm	T, K
1	0.5	0.5	850
* 2	0.5	0.75	850
! 3	0.5	1.0	850
* 4	0.5	0.5	900
5	0.5	0.75	900
! 6	0.5	1.0	900
7	0.5	0.5	1000
8	0.5	0.75	1000
!* 9	0.5	1.0	1000
10	0.5	0.5	1100
*11	0.5	0.75	1100
!12	0.5	1.0	1100
!13	0.5	0.5	1200
14	0.5	0.75	1200
*!15	0.5	1.0	1200
16	1.0	0.5	850
17	1.0	0.75	850
*18	1.0	1.0	850
19	1.0	0.5	900
*20	1.0	0.75	900
21	1.0	1.0	900
!22	1.0	0.5	1000
*23	1.0	0.75	1000
24	1.0	1.0	1000
*!25	1.0	0.5	1100
26	1.0	0.75	1100
27	1.0	1.0	1100
*28	1.0	0.5	1200
!29	1.0	0.75	1200
30	1.0	1.0	1200
*31	1.5	0.5	850
32	1.5	0.75	850
33	1.5	1.0	850
34	1.5	0.5	900
35	1.5	0.75	900
*36	1.5	1.0	900
37	1.5	0.5	1000

TABLE 4 (Cont.)

CASES	ϕ	p, atm	T, K
38	1.5	0.75	1000
*39	1.5	1.0	1000
40	1.5	0.5	1100
*41	1.5	0.75	1100
42	1.5	1.0	1100
*43	1.5	0.5	1200
44	1.5	0.75	1200
45	1.5	1.0	1200

TABLE 5 - 37(13) DATA

CASE	T_{ig}	τ_{ig}	$Y_{OH,ig}$
2	918	0.48E0	0.66E-4
4	961	0.80E-3	0.10E-3
5	960	0.13E-2	0.13E-3
6	974	0.11E-1	0.16E-3
7	1045	0.21E-3	0.51E-3
8	1063	0.15E-3	0.60E-3
9	1024	0.12E-3	0.15E-3
11	1160	0.69E-4	0.90E-3
13	1260	0.60E-4	0.34E-2
15	1260	0.29E-4	0.22E-2
18	935	0.46E0	0.19E-3
19	970	0.76E-3	0.40E-3
20	985	0.12E-2	0.19E-3
21	966	0.48E-2	0.10E-3
22	1027	0.20E-3	0.20E-3
23	1012	0.14E-3	0.11E-3
24	1039	0.12E-3	0.19E-3
25	1170	0.10E-3	0.16E-3
26	1117	0.60E-4	0.27E-3
27	1170	0.45E-4	0.90E-3
28	1275	0.55E-4	0.30E-2
29	1275	0.38E-4	0.30E-2
30	1270	0.36E-4	0.30E-2
31	926	0.11E-1	0.80E-4
32	892	0.27E0	0.17E-4
34	934	0.80E-3	0.57E-4
35	968	0.11E-2	0.11E-3
36	954	0.35E-2	0.61E-4
37	1012	0.20E-3	0.67E-4
38	1024	0.15E-3	0.11E-3
39	1062	0.13E-3	0.26E-3
40	1160	0.10E-3	0.91E-3
41	1163	0.70E-4	0.91E-3
42	1160	0.45E-4	0.90E-3
43	1275	0.59E-4	0.17E-2
45	1303	0.30E-4	0.29E-2

TABLE 6 - TRIGGER SPECIES vs. TIME

TIME	Y_{OH}
0	0
0.1E-5	0.68E-9
0.2E-4	0.38E-8
0.3E-4	0.81E-8
0.4E-4	0.17E-7
0.6E-4	0.75E-7
0.7E-4	0.16E-6
0.8E-4	0.35E-6
0.9E-4	0.82E-6
0.1E-3	0.21E-5
0.12E-3	0.15E-4
*0.14E-3	0.11E-3
0.2E-3	0.15E-1
0.3E-3	0.19E-1
0.4E-3	0.19E-1
0.5E-3	0.18E-1
0.8E-3	0.17E-1

* ignition point

TABLE 7

COMPARISON OF IGNITION TIMES FOR 37(13) AND 8(7) SYSTEMS

T_o	37(13) τ_{ig} (sec)	8(7) τ_{ig} (sec)
850	6.7×10^{-1}	1.1×10^{-3}
900	1.1×10^{-2}	6.6×10^{-4}
1000	1.3×10^{-4}	2.6×10^{-4}
1100	0.5×10^{-4}	1.5×10^{-4}
1200	0.3×10^{-4}	0.7×10^{-4}

TABLE 8

PREEXPONENTIAL FACTORS FOR GLOBAL MODEL

CASE	A_4	A_5
2	3.8E48	4.1E65
4	3.8E48	4.4E65
9	3.8E48	2.3E65
11	3.8E48	2.3E65
15	3.8E48	1.1E65
18	1.2E48	5.5E64
20	1.2E48	9.0E64
23	1.2E48	6.0E64
25	1.2E48	9.0E64
28	1.2E48	8.0E64
31	5.0E47	6.3E64
36	5.0E47	3.7E64
39	5.0E47	4.0E64
41	5.0E47	4.6E64
43	5.0E47	5.1E64

TABLE 9

COMPARISON OF COMPUTATIONAL TIMES

SYSTEM	AVERAGE COMPUTIONAL TIME (seconds)
37(13)	87.5
8.(7)	12.3
Global	11.4
Partial	1258

REFERENCES
FOR SECTION 4

1) Chinitz, W., Personal Communication, Cooper Union, New York, Apr., 1983.

2) Rogers, R.C., and Schexnayder, C.J., Jr., "Chemical Kinetic Analysis of Hydrogen-Air and Reaction Times", NASA TP-1856, July, 1981.

3) Guy, Robert W., and Mackley, Ernest A., "Initial Wind Tunnel Tests at Mach 4 and 7 of a Hydrogen-Burning, Airframe-Integrated Scramjet," NASA paper presented at the 4th International symposium on Air Breathing Engines (Lake Buena Vista, Fla.), Apr. 1-6, 1979.

4) Bittker, David A., and Scullio, Vincent J., "General Chemical Kinetics Computer Program for Static and Flow Reactions, with application to Combustion and Shock-Tube Kinetics," Nasa TN D-6586, 1972.

5) McLain, Allen G., and Rao, C.S.R., "A Hybrid Computer Program for Rapidly Solving Flowing or Static Chemical Kinetic Problems Involving Many Chemical Species," NASA TM X-3403, 1976.

6) Yee, Barbara, "The Chemical Kinetic Modeling of Silane-Hydrogen-Air Reactions", M.E. Thesis, Cooper Union, School of Engineering, April, 1982.

7) Hindmarsh, A.C., "Gear: Ordinary Differential Equation System Solveer," UCID-30001, Rev.1, Computer Documentation, Lawrence Livermore Lab, Univ. California, Aug. 20, 1972.

8) Gear, C. William, "Numerical Value Problems in Ordinary Differential Equations", Prentice-Hall, Inc., C. 1971.

9) Chinitz, W., "Simplifying Chemical Kinetic Analyses of Reacting Flows Using an Ignition-Combustion Model, "Report Submited to the Hypersonic Propulsion branch (HSAD), NASA LaRC, August, 1979.

10) Evans, J.S., and Schexnayder, C.J., Jr., "Influence of Chemical Kinetics and Unmixedness on Burning in Supersonic Hydrogen Flames", AIAA J., 21, 4, April, 1983, pp. 586-592.

11) Rogers, R.C., and Chinitz, W., "Using a Global Hydrogen-Air Combustion Model in Turbulen Reacting Flow Calculations", AIAA J. 21, 4, April, 1983, pp. 586-592.

12) Chinitz, W., "The Application of the Partial Equilibrium Assumption to Non-Equilibrium Analyses of Reacting Flows," Hypersonic Propulsion Branch NASALangley Research Center, July-Aug., 1980.

13) Baumeister et. al., "Mark's Standard Handbook for Mechanical Engineers," McGraw-Hill Eighth Ed., 1978.

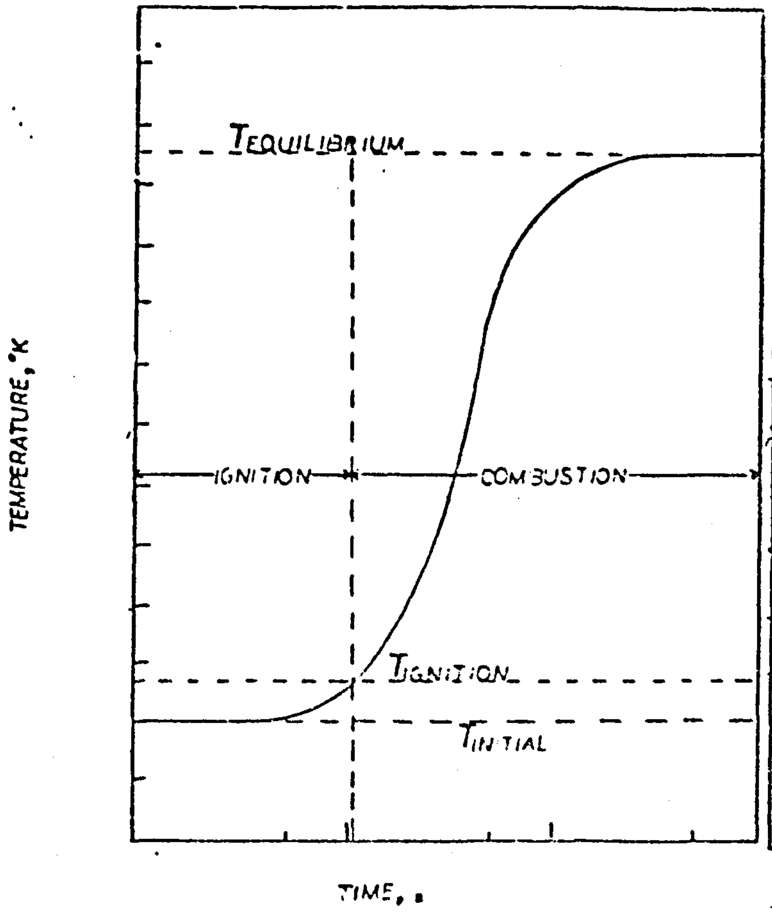

FIGURE 2 DEFINING IGNITION AND COMBUSTION

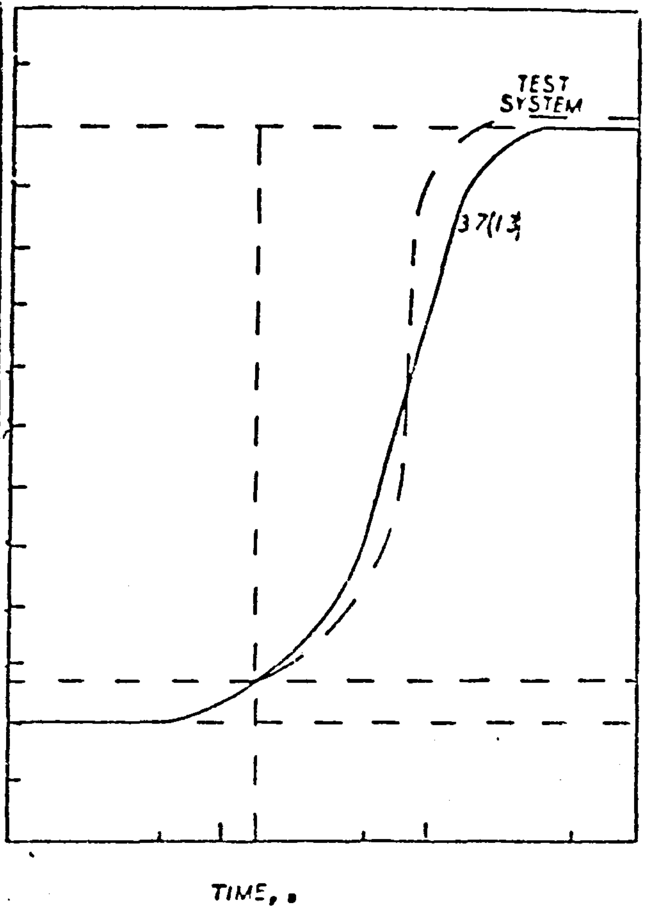

FIGURE 3 COMPARISON OF TEMPERATURE - TIME PROFILES FOR 37 (13) AND TEST SYSTEMS

ORIGINAL PAGE IS
OF POOR QUALITY

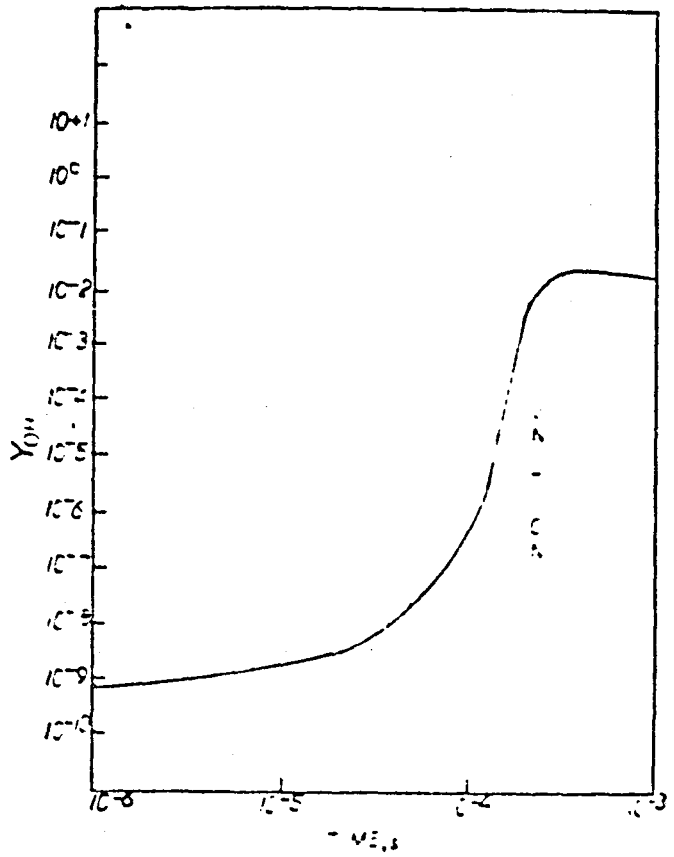

FIGURE 4 MASS FRACTION OH VS TIME

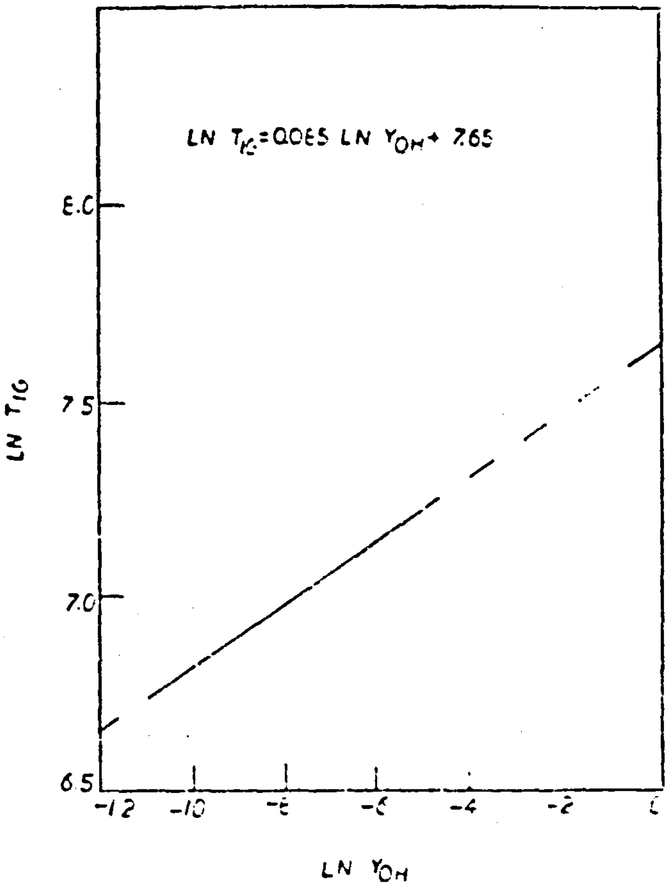

FIGURE 5 IGNITION TEMPERATURE VS. MASS FRACTION OH

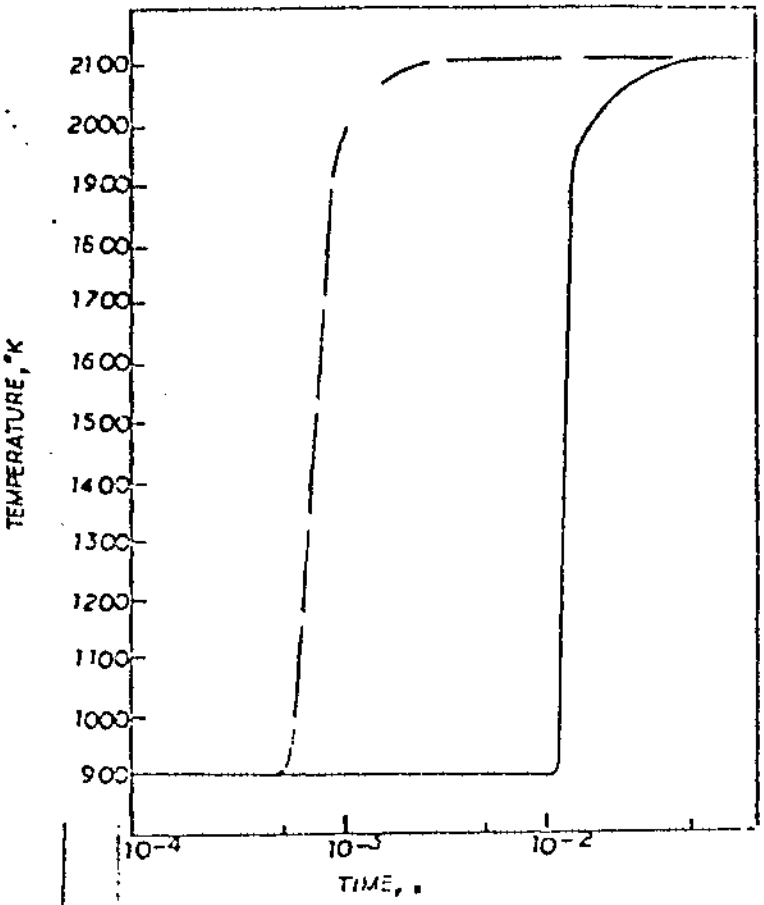

FIGURE 7 $\phi = 0.5$, $P = 1.0$, $T_o = 900$

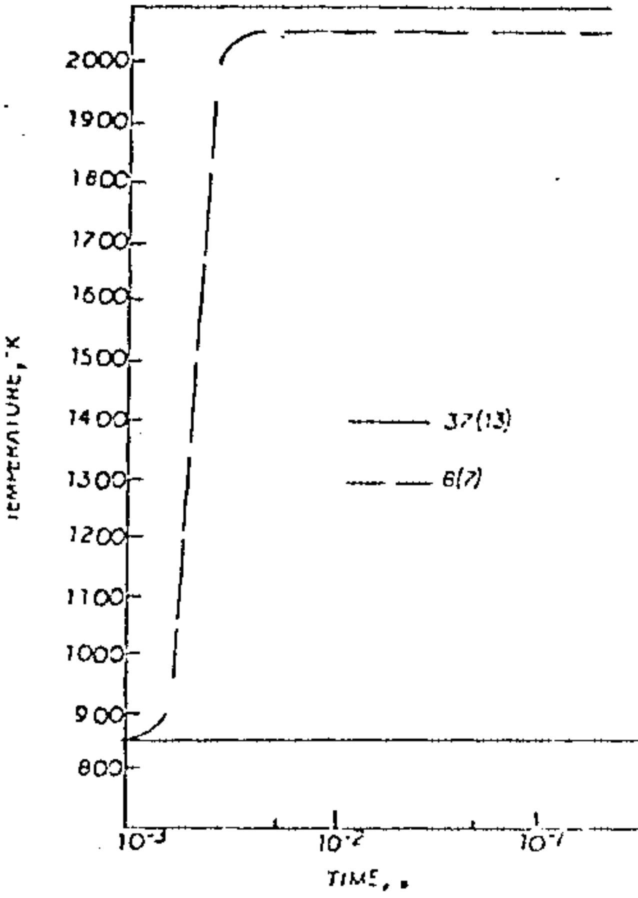

FIGURE 6 $\phi = 0.5$, $P = 1.0$, $T_o = 850$

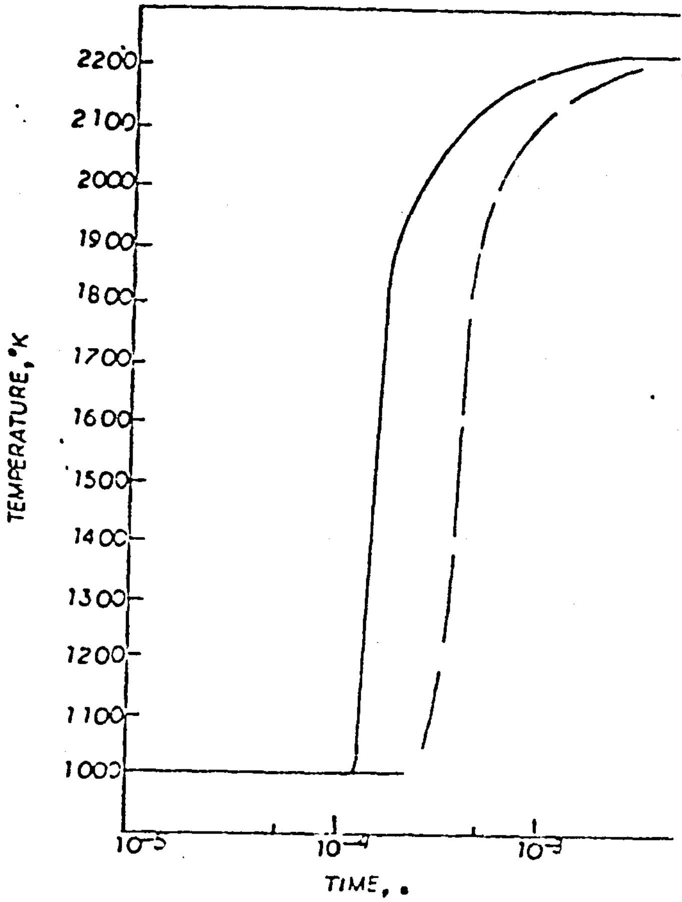

FIGURE 8 $\phi=0.5, P=1.0, T_c=1000$

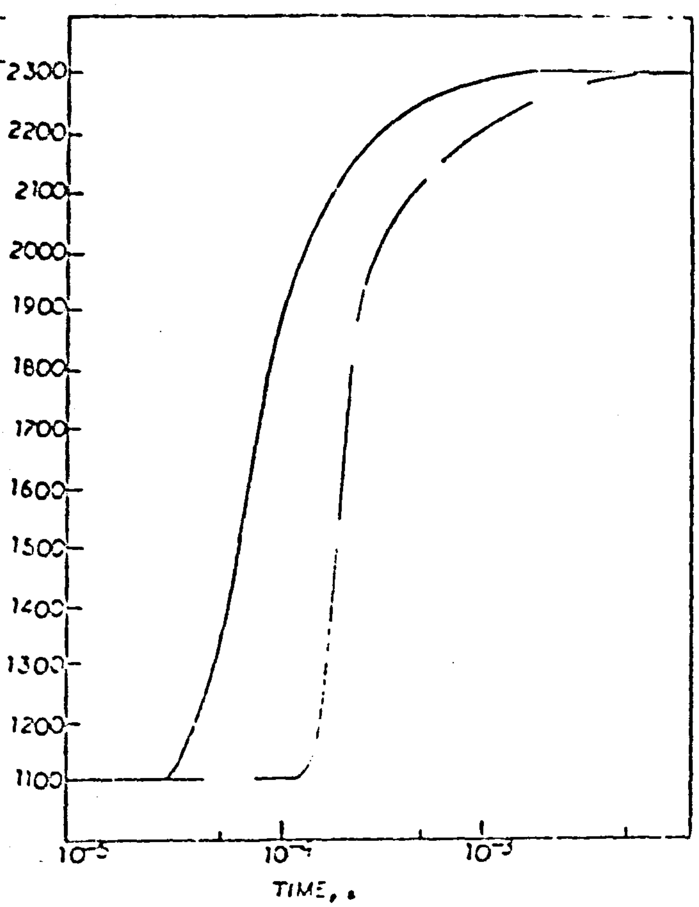

FIGURE 9 $\phi=0.5, P=1.0, T_c=1100$

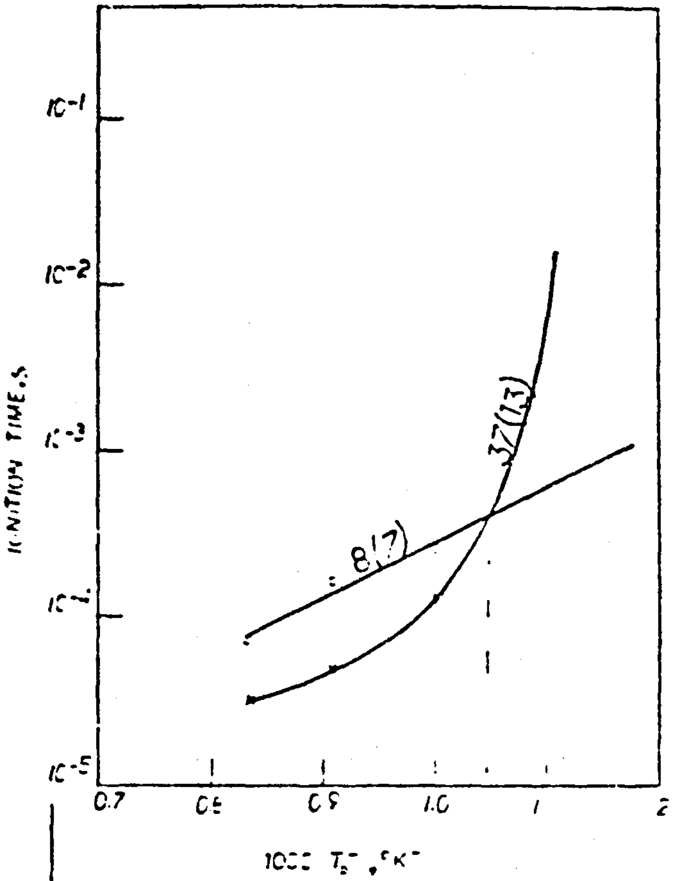

FIGURE 11 IGNITION TIME VS 1000 T_0^{-1}

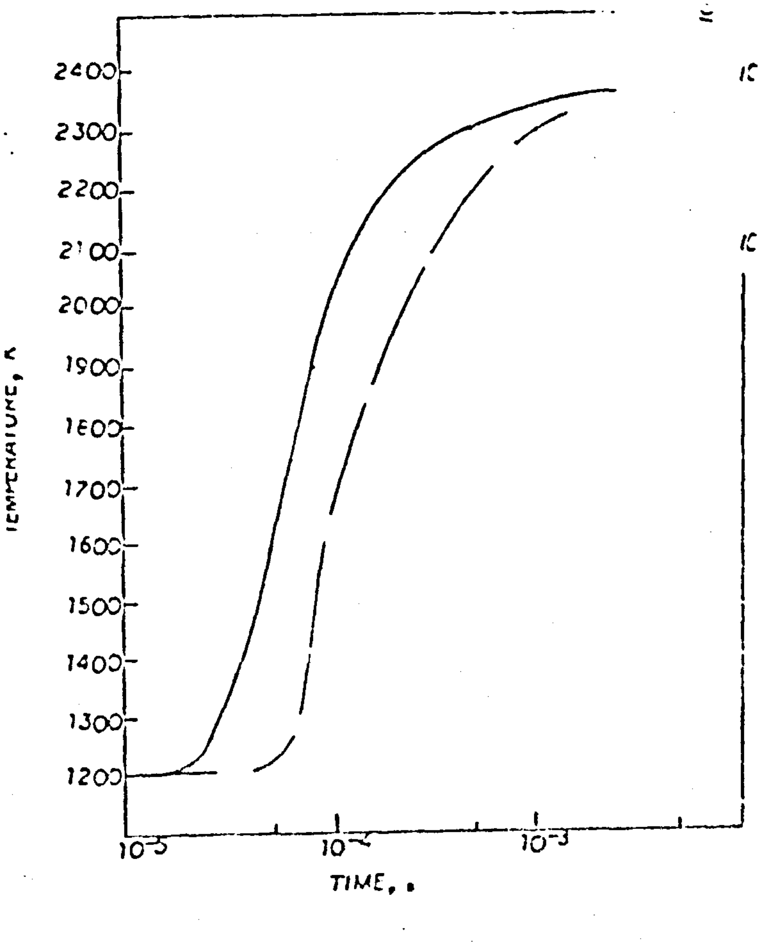

FIGURE 10 $\phi=0.5$, $P=1.0$, $T_0=1200$

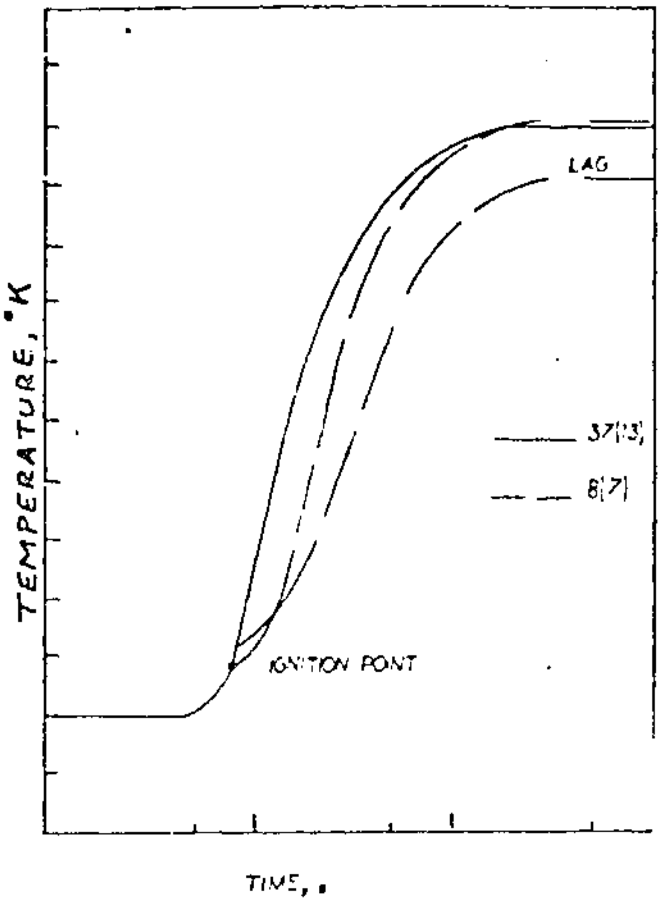

FIGURE 12 COMPARISON OF 37(13) AND 8(7) SYSTEMS IN COMBUSTION MODE

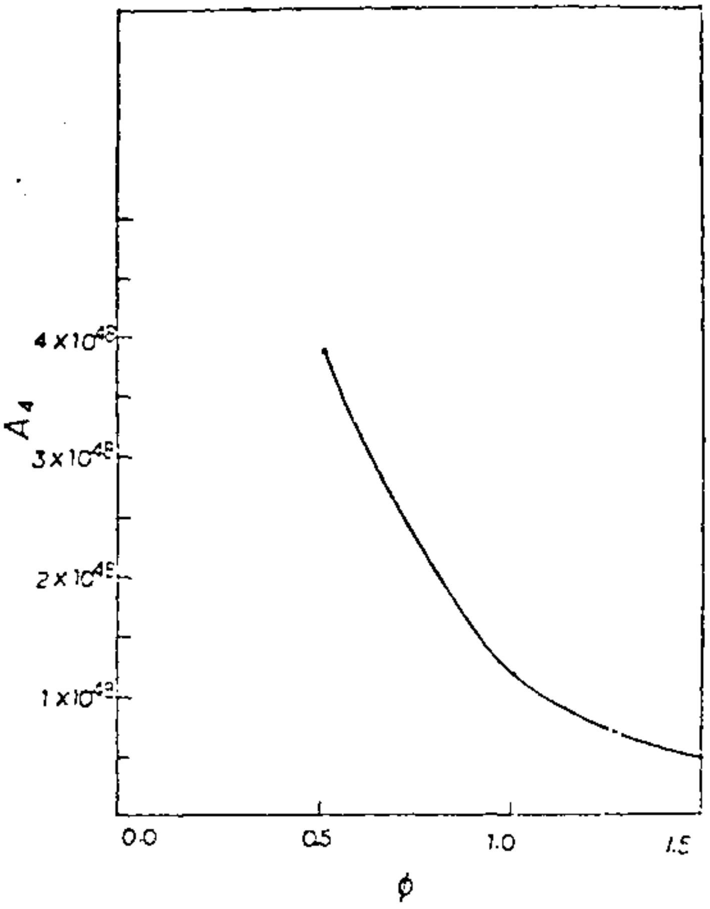

FIGURE 13 A_4 VERSUS ϕ

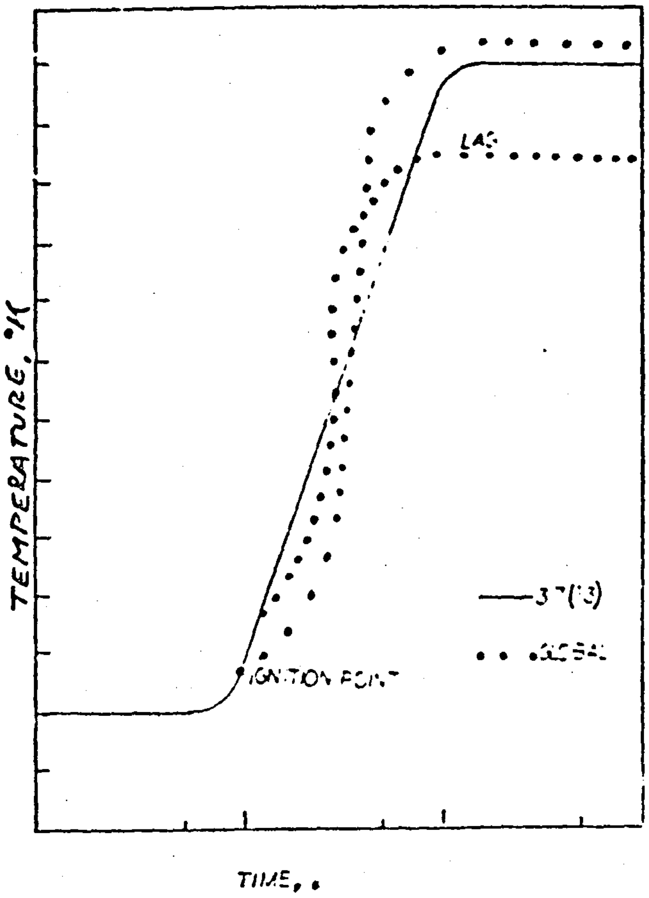

FIGURE 15 COMPARISON OF 37 (13 AND GLOBAL SYSTEMS IN COMBUSTION MODE

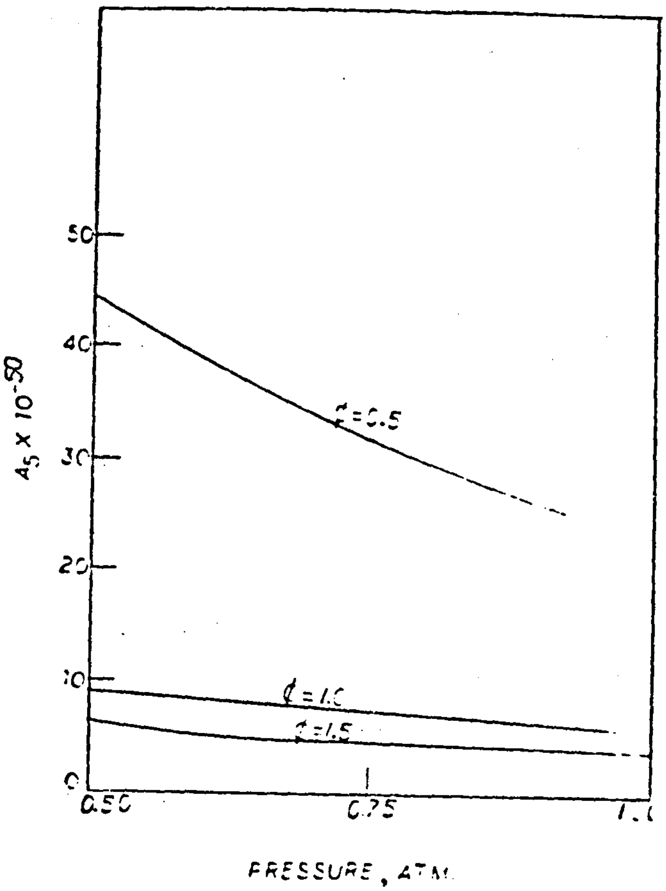

FIGURE 14 A_5 VS. P FOR VARIOUS φ'S

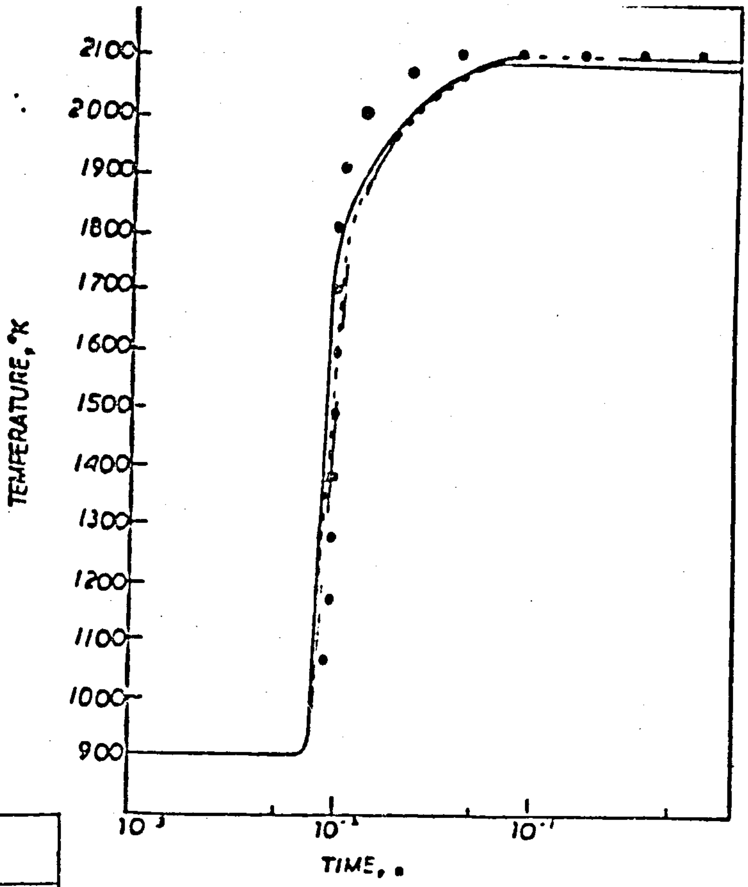

FIGURE 17 $\phi=0.5, P=0.50, T_0=900$

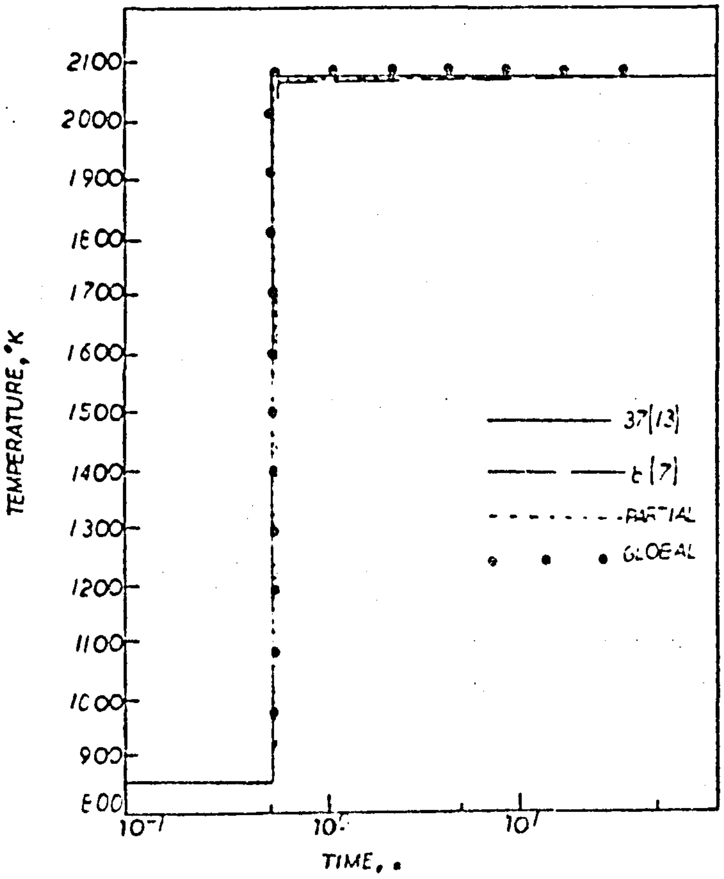

FIGURE 16 $\phi=0.5, P=0.75, T_0=850$

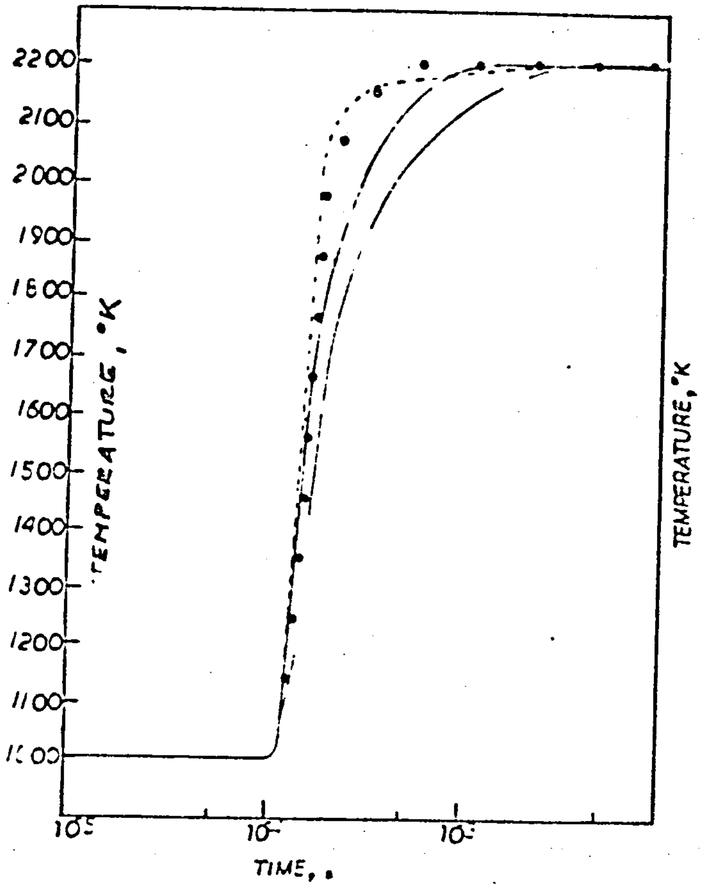

FIGURE 18 $\phi = 0.5$, $P = 1.00$, $T_c = 1000$

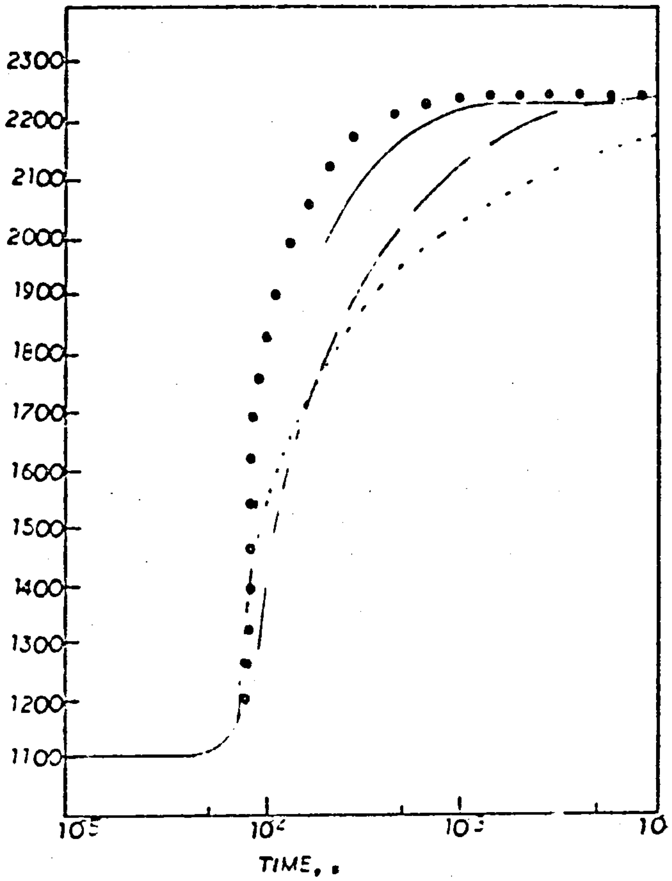

FIGURE 19 $\phi = 0.5$, $P = 0.75$, $T_c = 1100$

ORIGINAL PAGE IS
OF POOR QUALITY

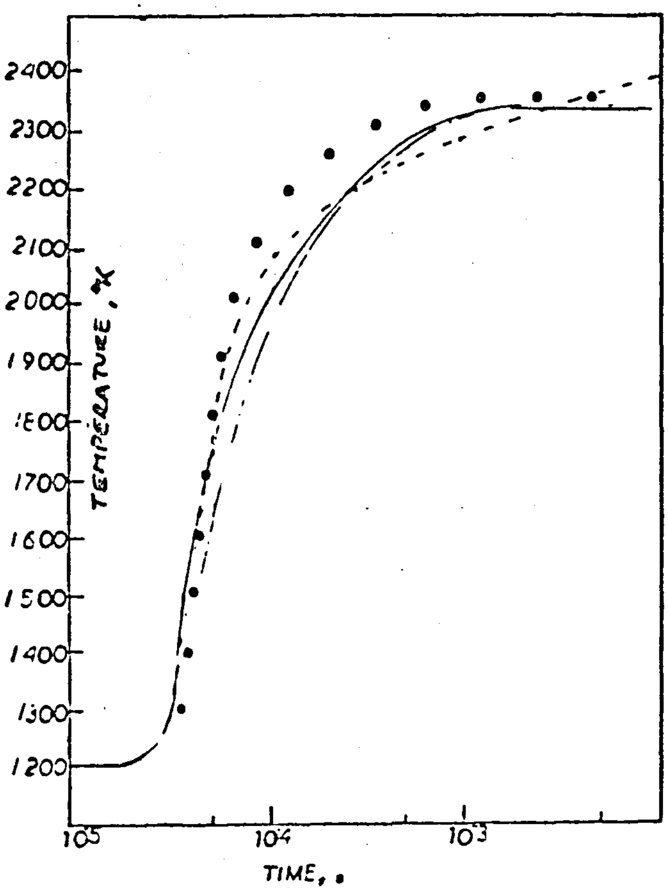

FIGURE 20 ϕ=0.5, P=1.00, T_c=1200

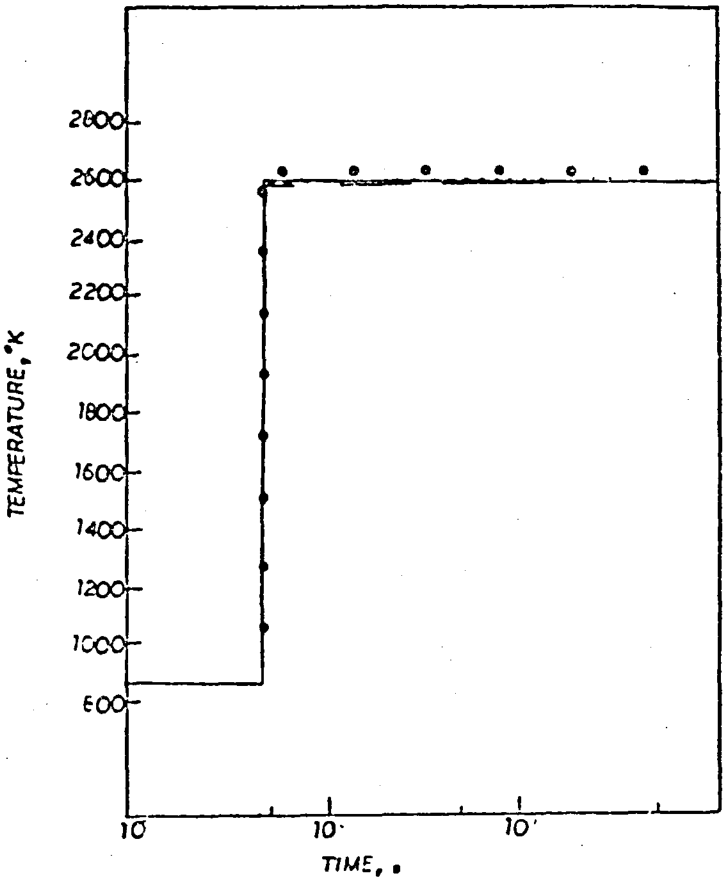

FIGURE 21 ϕ=1.0, P=1.00, T_c=850

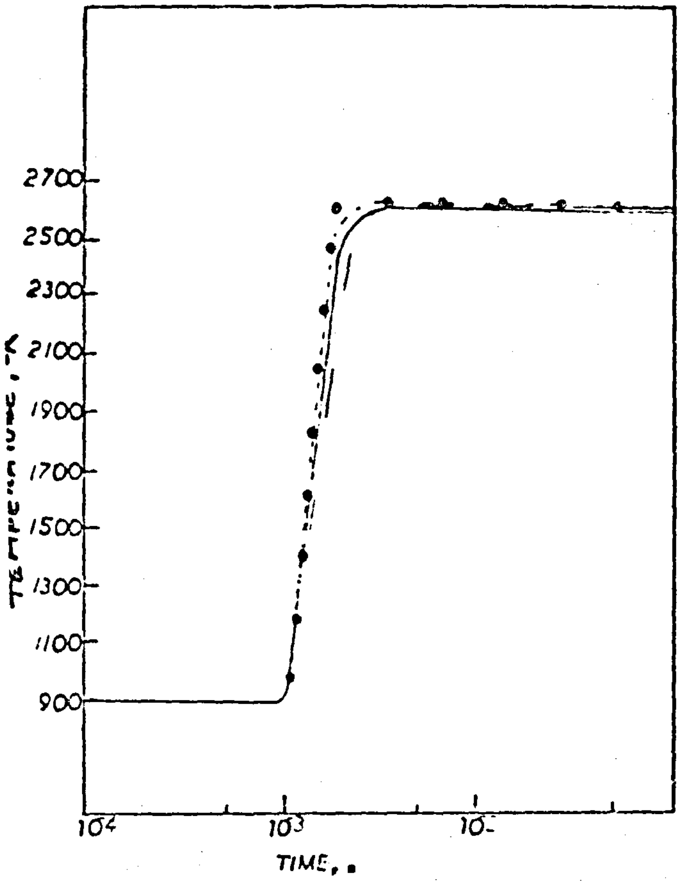

FIGURE 22 $\phi = 1.0, P = 0.75, T_0 = 900$

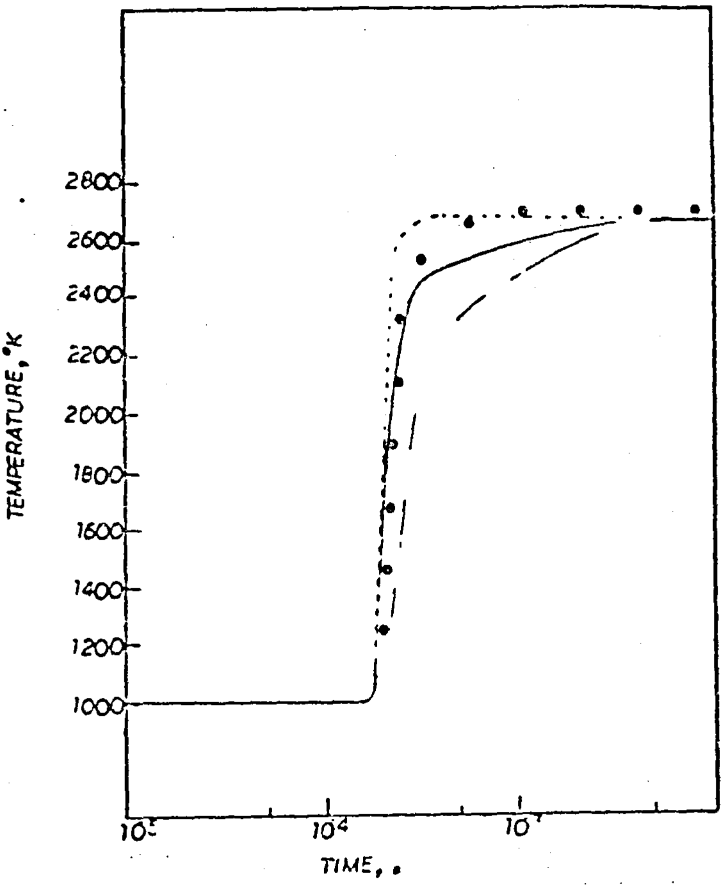

FIGURE 23 $\phi = 1.0, P = 0.75, T_0 = 1000$

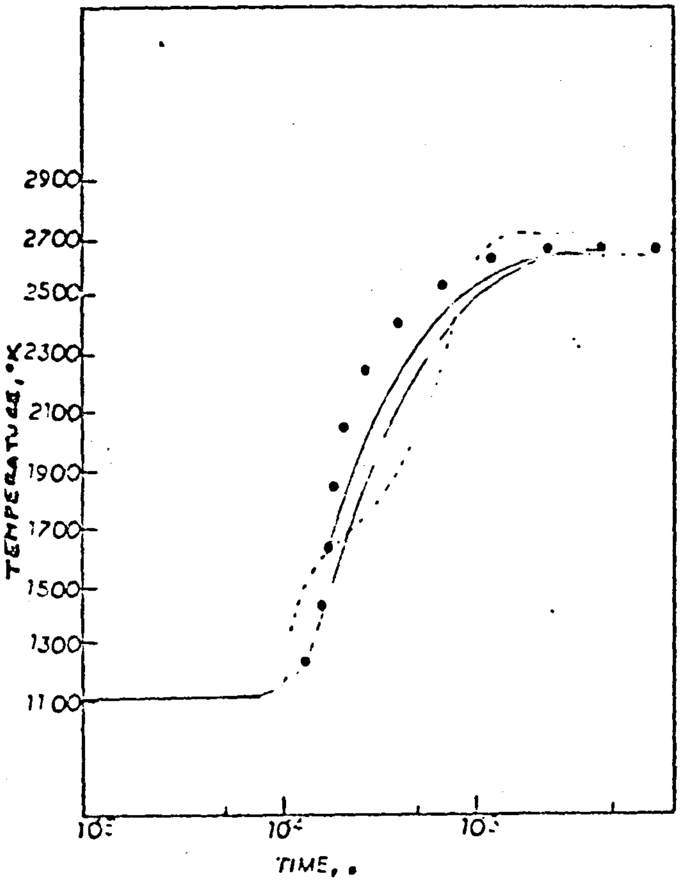

FIGURE 24 ϕ=1.0, P=0.50, T_c=1100

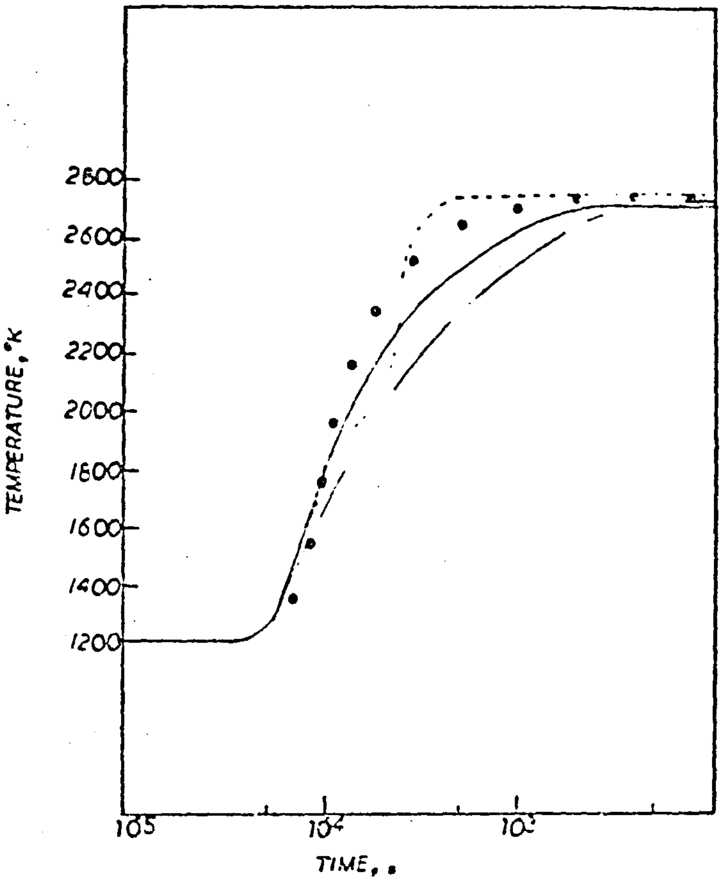

FIGURE 25 ϕ=1.0, P=0.50, T_c=1200

ORIGINAL PAGE IS
OF POOR QUALITY

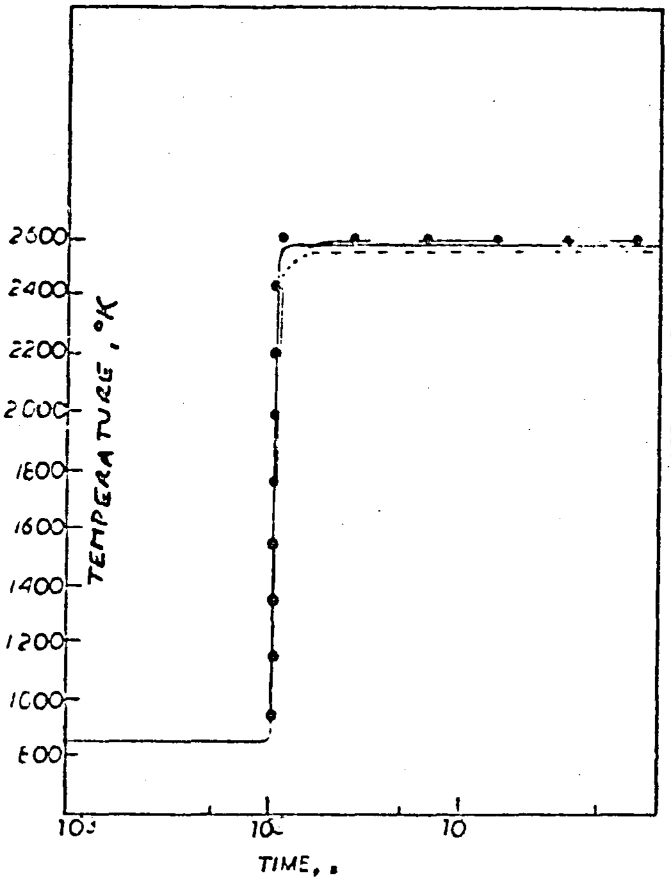

FIGURE 26 $\phi=1.5$, P=0.50, T_c=850

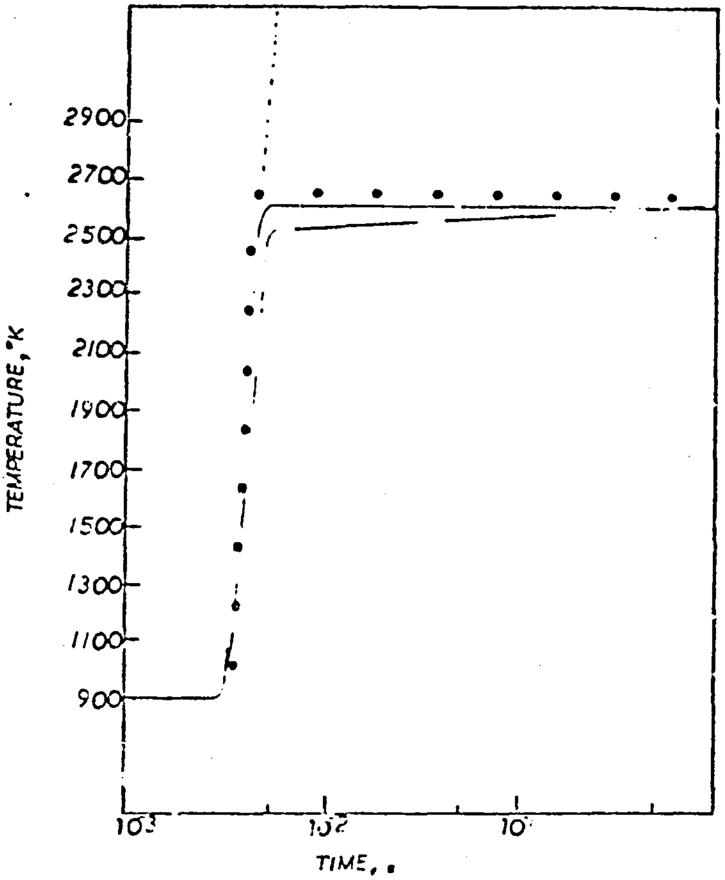

FIGURE 27 $\phi=1.5$, P=1.00, T_c=900

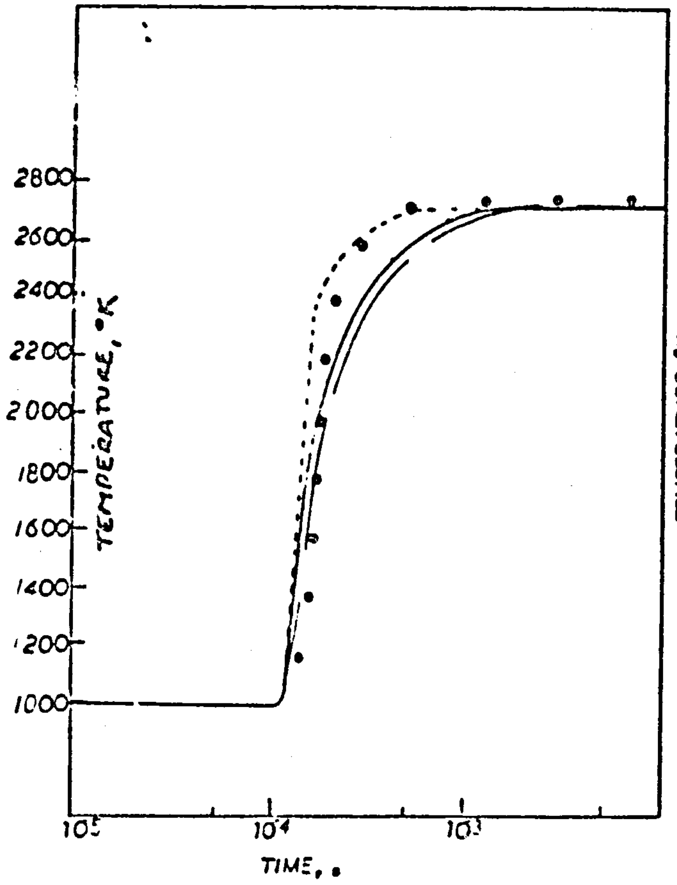

FIGURE 28 $\phi = 1.5, P = 1.0, T_0 = 1000$

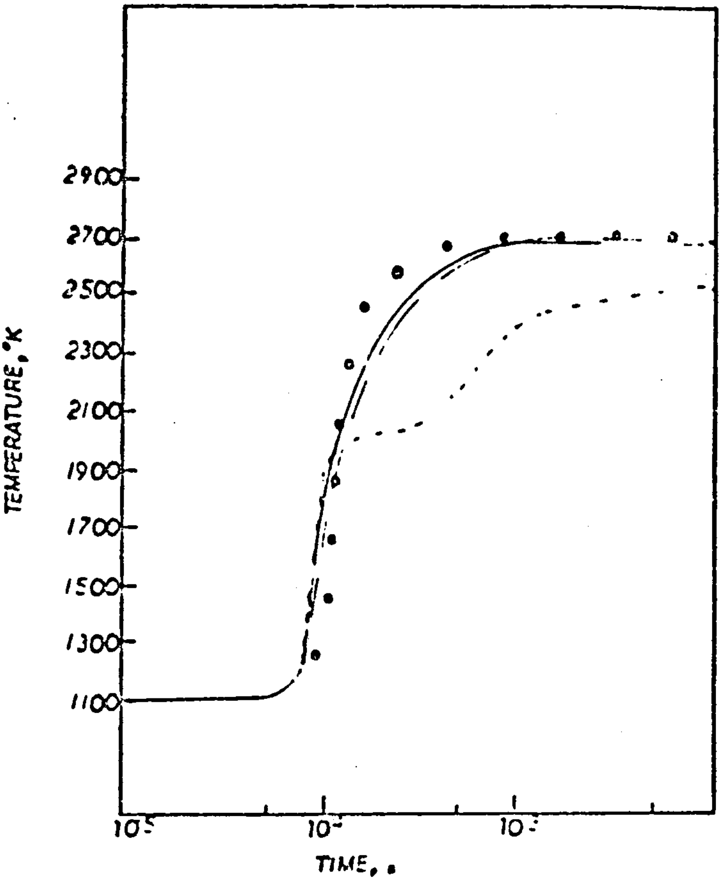

FIGURE 29 $\phi = 1.5, P = 0.75, T_0 = 1100$

C-2

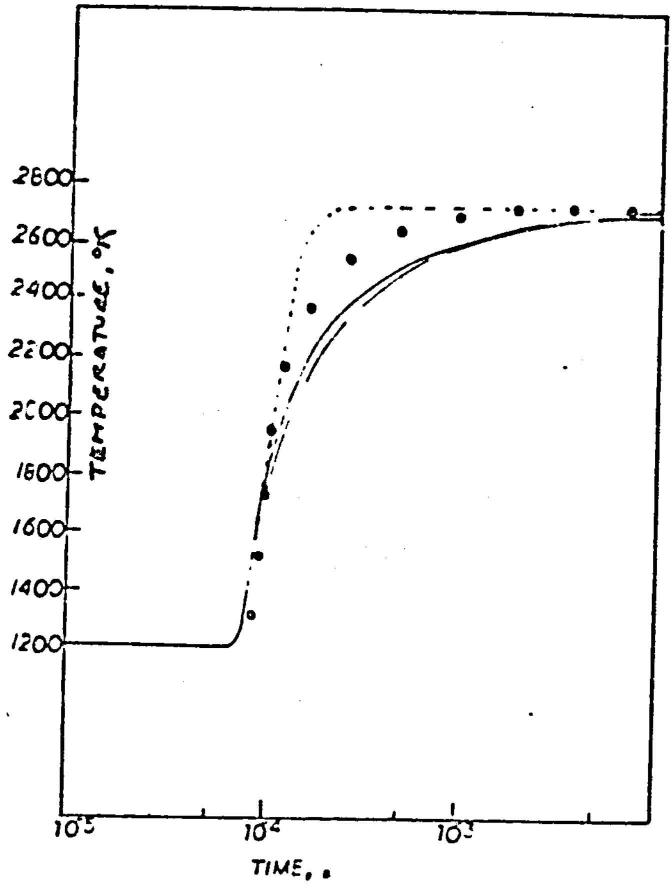

FIGURE 30 $\phi=1.5, P=0.50, T_c=1200$

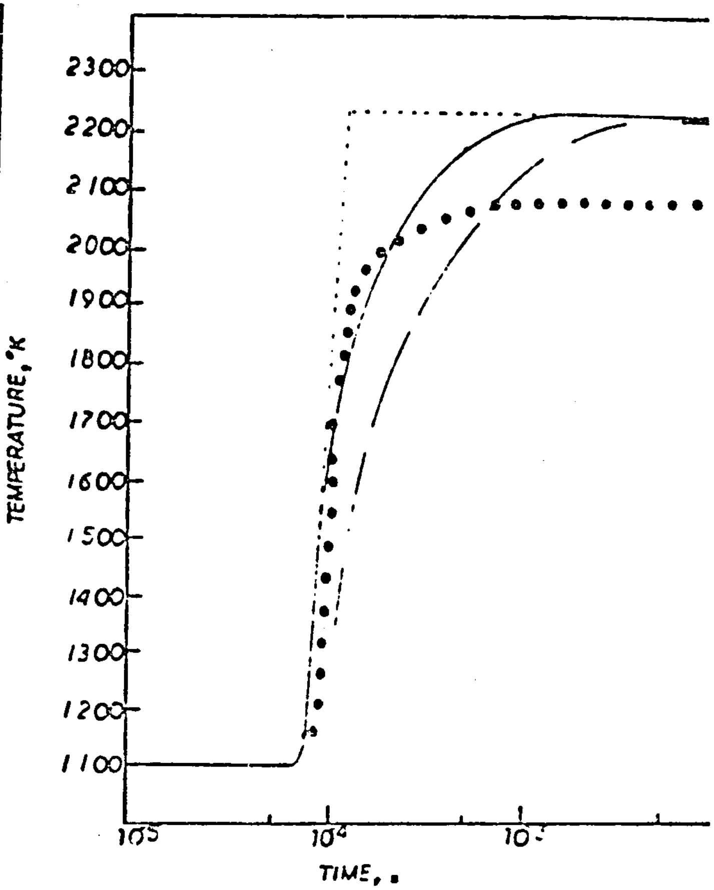

FIGURE 31 LAG FOR CASE NO. 11

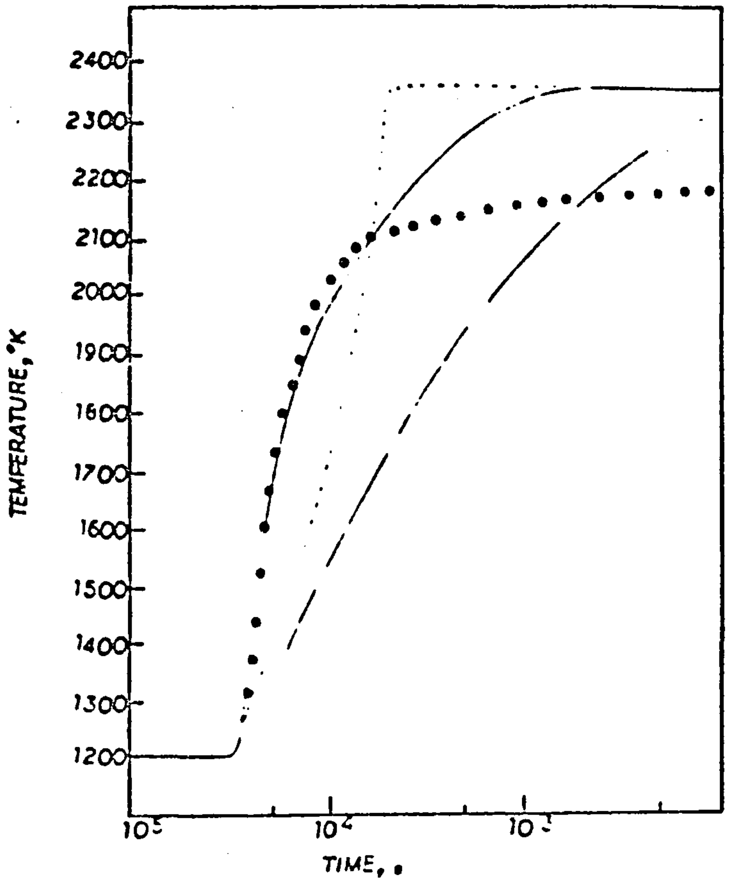

FIGURE 32 LAG FOR CASE NO. 15

5. APPLICATION OF THE CHARNAL CODE TO TURBULENT REACTION RATE MODELING

Work has been continuing dealing with the use of the CHARNAL computer code to assess and refine the turbulent reaction rate model discussed in previous status reports. At this time, three experiments are being examined using the code: (1) the Beach experiment (initial results are contained in a forthcoming NASA TM); (2) the Kent and Bilger experiment (see fig. 1); (3) the Northam experiment (see fig. 1). Some preliminary results obtained using the code in its non-finite-rate reaction modes are shown in figs. 2 - 5. In fig. 2, the experimental axial centerline temperature profile is shown along with CHARNAL results run as free jet with specified axial pressure gradient. As can be seen, the assumption of complete reaction results in too rapid a temperature increase and too high a maximum temperature. The eddy breakup assumption produces opposite results, indicating too slow a reaction rate. For purposes of comparison, the results of Edelman and Harsha (ref. 1) are shown and are seen to be relatively poor.

When the complete reaction and eddy breakup models are run assuming a confined jet, wherein the axial pressure gradient is computed by the code, both tend to lead to too rapid a temperature rise (fig. 3); however, in both cases, the predicted maximum temperature is only slightly too high. We plan to run this same case employing "turbulent" kinetics using the model developed under this grant.

Preliminary results for the Northam experiment are in figs. 4 and 5. Computer calculations involving this experiment will be made in close coordination with HPB personnel.

REFERENCE FOR SECTION 5

1. Edelman, R. B. and Harsha, P. T., "Laminar and Turbulent Gas Dynamics in Combustors - Current Status", Prog. Energy Combust. Sci., vol. 4, pp. 1 - 62.

Kent & Bilger

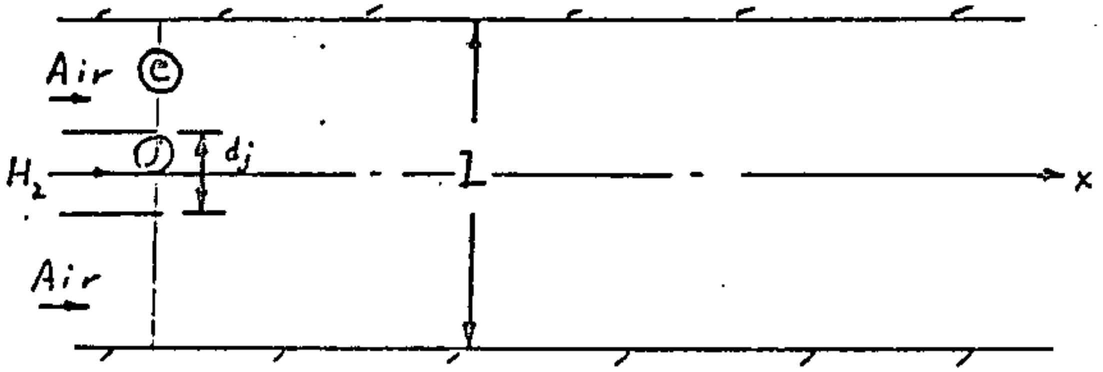
Air
ⓒ
ⓙ
d_j
H_2
L
x
Air

$\frac{\bar{U}_j}{U_e} = 10$, $p(x=0) = 1$ atm, $T(x=0) = 300$ K,

$d_j = 0.00762$ m, $L = 0.305$ m

Northam

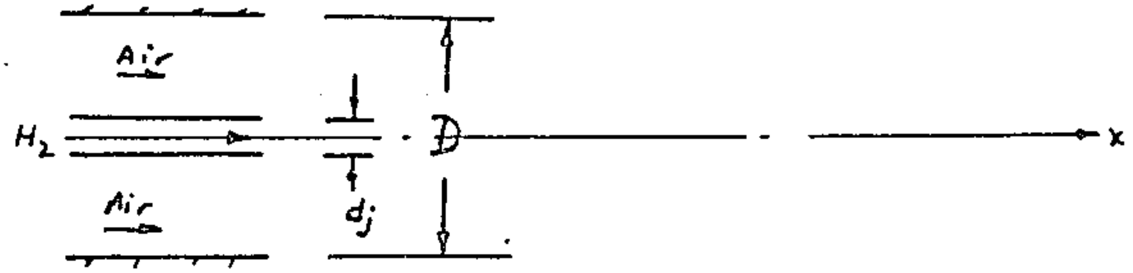
Air
H_2
Air
d_j
D
x

$\frac{\bar{U}_j}{U_e} = 5$, $p = 1$ atm, $T(x=0) = 300$ K,

$d_j = 0.001524$ m, $D = 0.007747$ m

FIGURE 1

NO. 340-10 DIETZGEN GRAPH PAPER
10 X 10 PER INCH
DIETZGEN CORPORATION
MADE IN U.S.A.

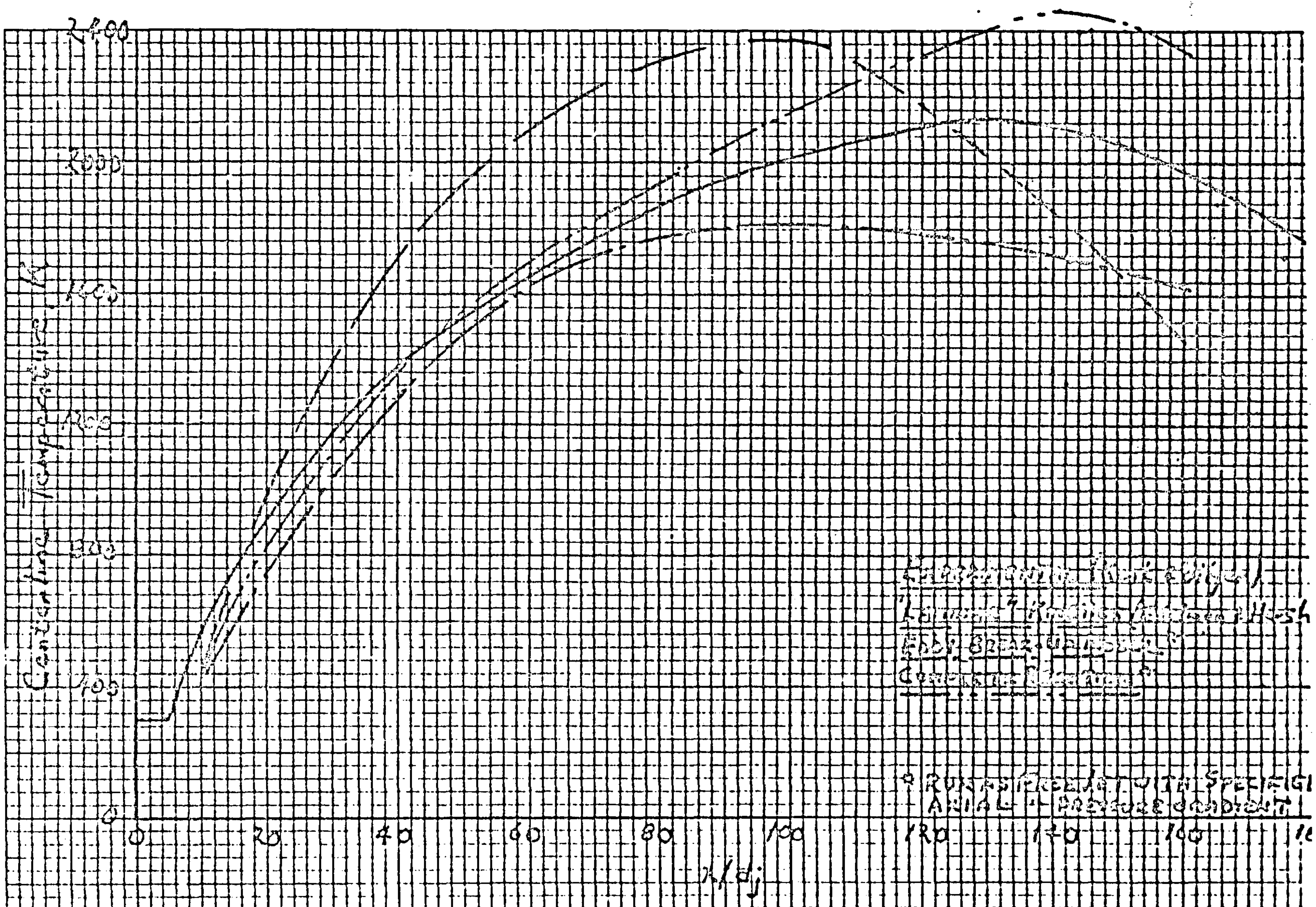

Figure 3. Axial profile of the centerline temperature in the Heat Exchanger Experiment. Part 1.

NO. 340-10 DIETZGEN GRAPH PAPER
10 X 10 PER INCH

DIETZGEN CORPORATION
MADE IN U.S.A.

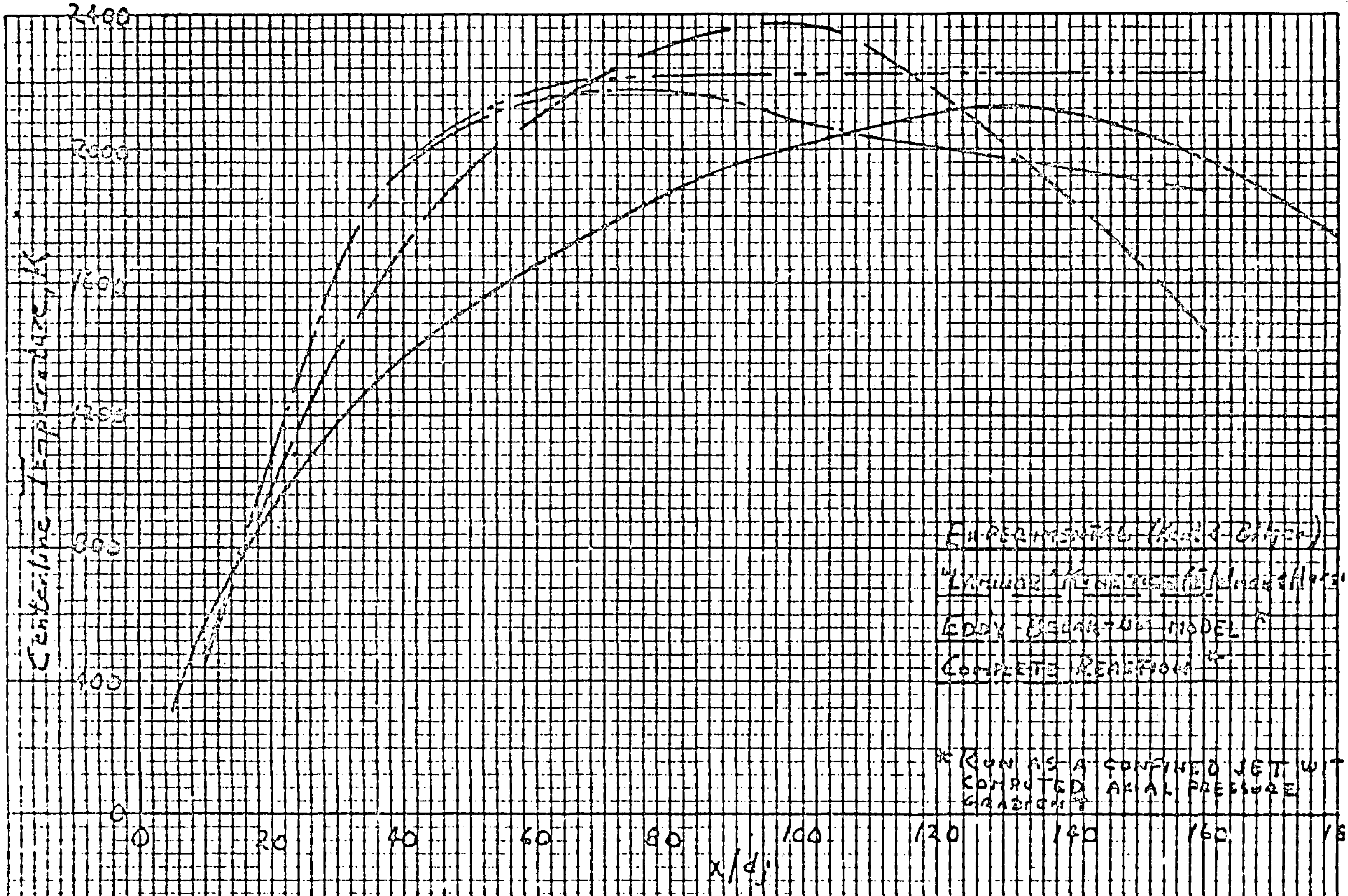

Figure 3 Axial profile of the centerline temperature in the Kent & Bilger Experiment Run 2

NO. 340-10 DIETZGEN GRAPH PAPER
10 X 10 PER INCH

DIETZGEN CORPORATION
MADE IN U.S.A.

Figure 4 Axial Centerline Temperature Profile in the Nocturn Experiment

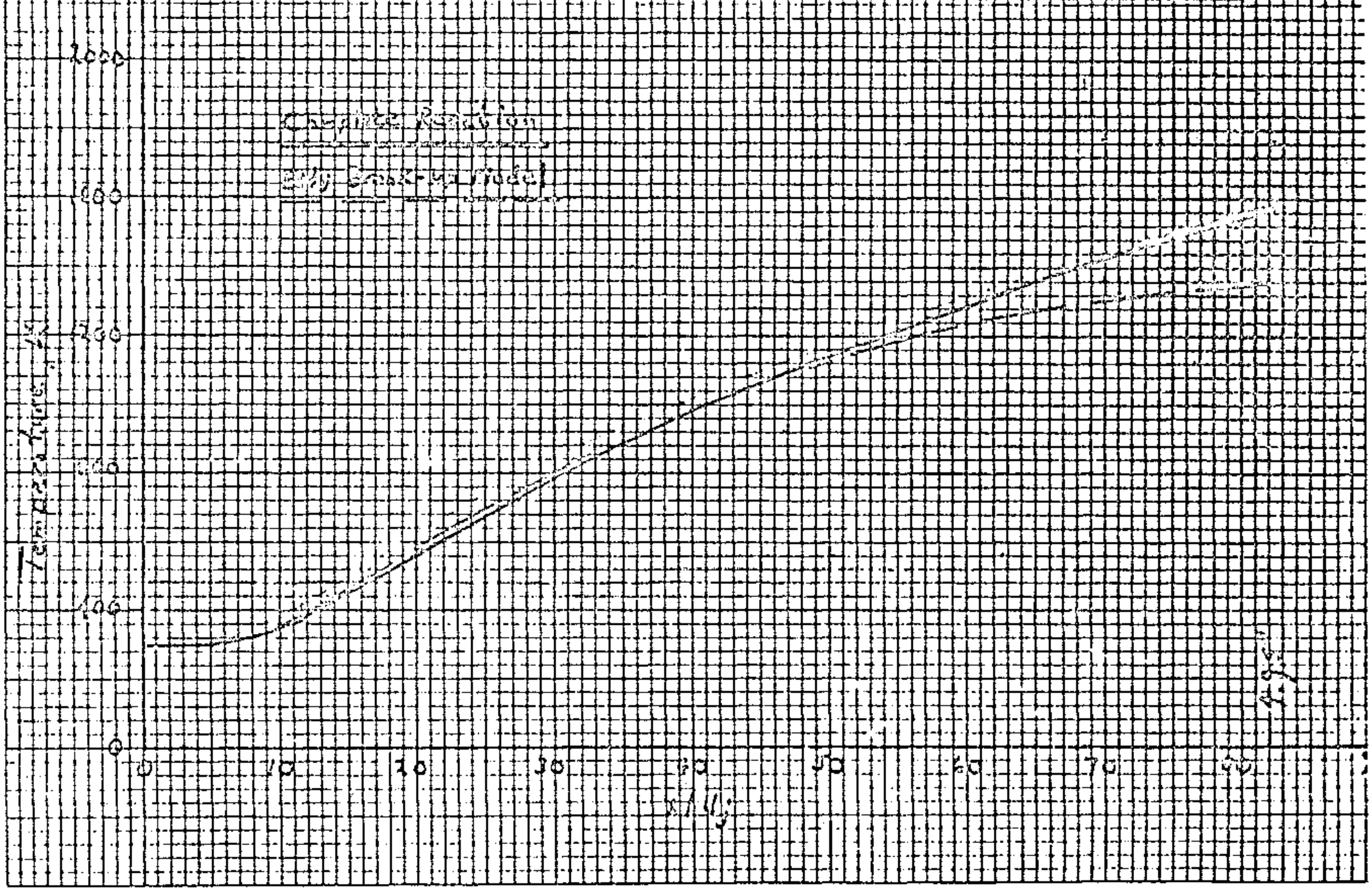

NO. 340-10 DIETZGEN GRAPH PAPER
10 X 10 PER INCH

DIETZGEN CORPORATION
MADE IN U.S.A.

Figure 5 Radial Temperature Profiles Predicted by the Eddy Break-Up Model in the Moriyan Experiment

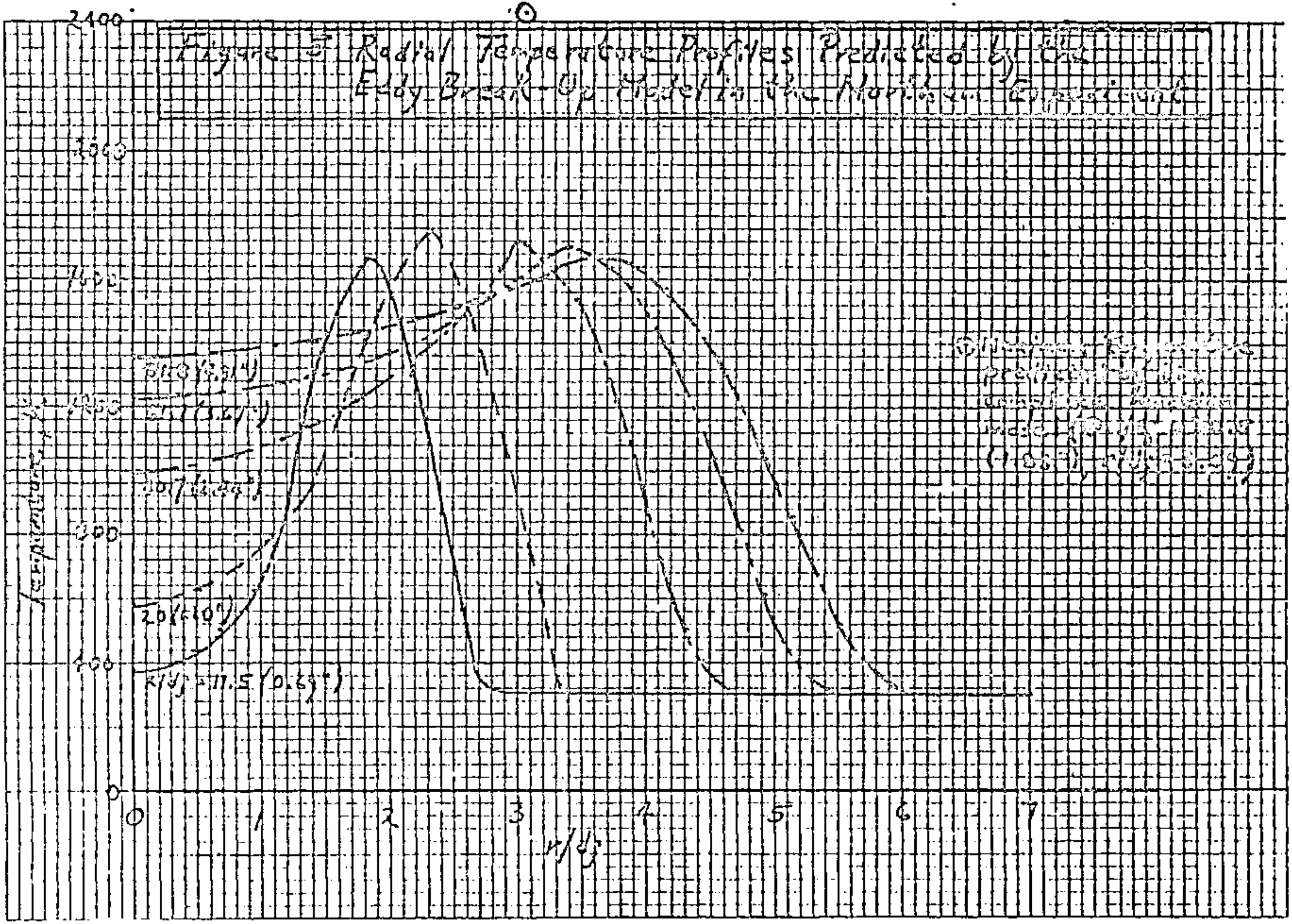

END

DATE

FILMED

APR 11 1984

LANGLEY RESEARCH CENTER
3 1176 00514 2360